Defining the role of the Golgi apparatus in juvenile NCL (Batten disease)

Davide Marotta

MRC Laboratory for Molecular Cell Biology
University College London
Dr. Sara E. Mole

A thesis submitted for the degree of Doctor of Philosophy in the University College London

October 2014

Declaration

I, Davide Marotta, confirm that the work presented in this thesis is my own. Where information has been derived from other sources, I confirm that this has been indicated in the thesis.

Abstract

The neuronal ceroid lipofuscinoses (NCLs) are a group of severe neurodegenerative lysosomal storage disorders characterised by accumulation of autofluorescent ceroid lipopigments in most cells. NCLs are caused by mutations in at least fourteen recessively inherited human genes. The NCL genes encode both soluble and transmembrane proteins localised to the endoplasmic reticulum, Golgi apparatus or endosomal/lysosomal organelles. Mutations in the *CLN3* gene result in juvenile neuronal ceroid lipofuscinoses (JNCL, Batten disease). JNCL represents the worldwide most common form of NCL. Currently more than 40 mutations have been characterised in the *CLN3* gene. However, the most common mutation causes a 1-kb deletion. *CLN3* encode a multi-pass type III transmembrane protein, which is conserved in single-celled eukaryotes such as the fission yeast *Schizosaccharomyces pombe*, suggesting a fundamental role for this protein in eukaryotic cells. CLN3 has been functionally linked to many different cellular processes, including lysosomal homeostasis, autophagy, lipid synthesis or modification, cytoskeleton organisation and trafficking. Despite these endeavours, the function of CLN3 remains unclear.

The main goal of this project was to investigate the role of the Golgi apparatus in the pathogenesis of juvenile CLN3 disease. The role of CLN3 at the Golgi apparatus was studied in mammalian cells and in fission yeast model. The morphology of the Golgi complex was studied in fibroblast cell lines from patients and in HeLa cells depleted for CLN3 using RNAi. The observed changes in morphology were accompanied by manganese dyshomeostasis within the Golgi complex, ER stress and apoptosis. The morphology of the Golgi complex was studied in *S. pombe* using electron microscopy in

order to confirm the changes observed in mammalian cells. Finally, drugs shown to ameliorate aspects of the yeast model of CLN3 disease were tested for their efficacy in mammalian cells as an early step in therapeutic development. In this study I have shown that both morphology and size of the Golgi apparatus result to be affected by the loss/depletion of *CLN3*. Moreover, the changes in Golgi complex morphology and size are accompanied by manganese dyshomeostasis within the Golgi complex with activation of ER stress and activation of the proapoptotic protein caspase 2. Together, these data suggest that the loss/depletion of *CLN3* activates secretory stress pathways and cell death. A dysfunctional Golgi apparatus may be the key to uncover the role of CLN3 and find new targets for therapeutic development.

Table of Contents

Figures

Tables

2.2.6.2.1 – Standard BSA preparation

2.2.12.2.2.1 – Dehydration steps in EtOH

Abbreviations

AFS – automatic freeze substitution

BME – β-mercaptoethanol

BSA – bovine serum albumin

Cacodylate – sodium cacodylate

Ca^{2+} - calcium

cm – centimetre

COPI – Coat protein I

COPII – Coat protein II

DAB – diamino benzedene

DDSA – dodecenyl succinic anhydride

dH_2O – distilled water

DMEM - Dulbecco's Modified Eagle's Medium

DMP-30 – 2,4,6 tri(dimethylamenomethyl)phenol

DMSO – dimethyl sulphoxide

DNA – deoxyribonucleic acid

EDTA – ethylene diamine tetraacetic acid

ER - endoplasmic reticulum

ERGIC – ER-Golgi intermediate compartment

ERES – ER exit site

FBS – foetal bovine serum

FOA – Fluoroorotic Acid

GA - Golgi apparatus

GFP – green fluorescent protein

HCl – hydrochloric acid

IF – indirect immunofluorescence

kDa – kilodalton

LC – lead citrate

min – minute(s)

mm – millimetre(s)

mM – millimolar

MNA – methylnadic aanhydride

Mn^{2+} - manganese

Mg^{2+} - magnesium

MRC-LMCB – Medical Research Council Laboratory for Molecular Cell Biology

mRNA – messenger RNA

NCL – neuronal ceroid lipofuscinosis

nm – nanometre(s)

nM – nanomolar

nt – nucleotide(s)

P. pastoris – *Pichia pastoris*

PBS – phosphate buffer saline

PFA – paraformaldehyde

pmol - picomole

qPCR – quantitative reverse transcription polymerase chain reaction

RNA – ribonucleic acid

RNAi – RNA interfering

RT – room temperature

S. pombe – *Schizosaccharomyces pombe*

S. cerevisiae – *Saccharomyces cerevisiae*

SDS – sodium dodecyl sulphate

siRNA – small interfering RNA

TEM – transmission electron microscope

TGN – trans Golgi network

TMD – trans membrane domain

UCL – University College London

WB – western blotting

µL – microliter

µm - micrometre

µM – micromolar

TA – tannic acid

OsO_4 – osmium tetroxide

UPR – unfolded protein response

Chapter one

Introduction

1.1 Overview

The neuronal ceroid lipofuscinoses (NCLs) are a group of lysosome storage diseases caused by mutations in known and unknown proteins with different cellular locations such as Golgi apparatus, endoplasmic reticulum (ER) and lysosomes. They are the most common childhood neurodegenerative disorders and most are inherited in an autosomal recessive manner. Mutations in the *CLN3* gene cause the juvenile form of NCL. The CLN3 protein localises at the Golgi complex, possibly also at the lysosome, and it is unclear how mutations in CLN3 lead to accumulation of storage material in the lysosomes.

The introduction is divided in five sections; the first includes a brief description of the lysosomal storage diseases, the second section focuses on NCLs and introduces the proteins involved, the third will discussed the juvenile form of NCL and the fourth will present the Golgi apparatus, in mammals and yeast, and its crucial role in manganese (Mn^{2+}) homeostasis along with its relation with neurodegenerative disease. The last section includes an introduction to the endoplasmic reticulum (ER) stress and unfolded protein response and their role in neurodegenerative disorders.

1.2 Lysosomal storage disorders

Inborn metabolic errors are a common cause of inherited diseases (Burton 1998), in which the lysosomal storage disorders (LSDs) are grouped. LSDs share the common phenomenon of accumulation of storage material in the lysosome accompanied by cellular pathology. Over 40 different LSDs have been described to date with different components of storage material and different affected cell types (Vellodi 2005).

They tend to be progressive, although the rate of progression is variable, and show almost exclusively recessive autosomal inheritance. Most LSDs result from a defect in a lysosomal hydrolase, leading to incomplete degradation of macromolecules and subsequent accumulation of these products (Winchester et al., 2000; Futerman and van Meer 2004). Furthermore, alterations in the lysosome degradation have been described in normal brain aging and in age-related neurodegenerative diseases such as Alzheimer (Oyama et al., 1998), Huntington (Dyer and McMurray 2001; Qin et al., 2004) and Parkinson's disease (Sevlever et al., 2008). Those findings highlight the central role of lysosomes during the cell homeostasis processes.

1.3 Neuronal ceroid lipofuscinoses

The neuronal ceroid lipofuscinoses (NCLs) were first described almost 2 centuries ago by Stengel (Stengel 1826; Stengel 1982). However, it was only in 1960 that Zeman and Dyken introduced the name NCL to distinguish them from the gangliosidoses (Zeman and Dyken 1969; Goebel 1999). The common characteristic of the NCLs is the presence of autofluorescent storage material resembling ceroid and lipofuscin lipopigments that also accumulate during the normal ageing process. This storage material is observed in many tissues and cell types. However, the pathological effect of the disease is most prominent in the central nervous system (CNS) and the eyes. There are several subtypes of NCLs, each of which is associated with a distinct gene and differs according to age of onset, disease progression and severity and the morphological appearance of the storage material (Goebel 1999; Wisniewski et al., 2001).

Historically, the classification of the NCLs has been clinically led, according to the age at onset of symptoms in: infantile, late infantile (LINCL), juvenile (JNCL) and adult (ANCL) NCLs. However, the NCLs are more genetically heterogeneous than initially thought. Mutations in the same gene may also lead to very different disease courses (Lebrun et al., 2011; Kousi et al., 2012) (*table* 1.3.1). An internationally developed new NCL nomenclature clearly identifies each NCL disease both genetically and clinically (*table* 1.3.1) (Mole 2011; Williams and Mole 2012). It classifies both the defective gene as well as the age at disease onset (congenital, infantile, late infantile, juvenile and adult). To date, fourteen different NCL genes have been described (*table* 1.3.1) (Kousi et al., 2012; Jalanko and Braulke 2009; Arsov et al., 2011; Noskova et al., 2011; Bras et al., 2012; Smith et al., 2012; Staropoli et al., 2012; Smith et al., 2013). More NCL genes

remain to be indentified as in some patients mutations cannot be demonstrated in any of the known NCL genes although they show the typical NCL symptoms and characteristic lysosomal storage material. Intracellular localisation and function (where known) (*table* 1.3.2) of the defective NCL proteins are different: four NCL types are caused by defects in lysosomal enzymes (CLN1; CLN2; CLN10; CLN13), others by defects in transmembrane proteins (CLN3; CLN6; CLN7; CLN8) (Jalanko and Braulke 2009). Mutations in an ATPase gene (CLN12) (Bras et al., 2012) and a potassium channel gene (CLN14) (Staropoli et al., 2012) also cause NCL disease. The recently identified *CLN4* gene (*DNAJC5*) codes for a protein with putative function in synapses (Noskova et al., 2011). How these genetic defects lead to neurodegeneration is still not clear. Clinically, the different NCL diseases have much in common despite their heterogeneity. This is important both for diagnosis and palliative care.

Common pathological characteristics of NCL diseases progression include progressive visual deterioration leading to blindness, epilepsy, intellectual and motor decline. Eventually all affected individuals die prematurely due to death of cortical neurons (Goebel 1999). The appearance of the storage material is characteristic for each type of NCL and has long been used as a diagnostic tool (Goebel 1999). There are four main types of storage with some additional variant forms: granular osmiophilic deposits (GRODs), curvilinear profiles (CL), rectilinear bodies (RL) and fingerprint bodies (FB) (Goebel 1999). In particular the RL and FB are typical features of CLN3 disease (Goebel 1999).

Phenotype		Gene and age of onset	
		Gene	Age of onset
Congenital		*CLN10/CTSD*	Before or around birth
Infantile		*CLN1/PPT1* *CLN14/KCTD7*	6-24 mo
Late Infantile (LINCL)	Classic	*CLN2/TPP1*	2-4 yrs
	Variant	*CLN5* *CLN6* *CLN7/MFSD8* *CLN8* *CLN10/CTSD* *CLN1/PPT1*	4-7 yrs 18 mo-8 yrs 3-7.5 yrs
Juvenile (JNCL)	Classic	*CLN3*	4-10 yrs
	Variant	*CLN1/PPT1* *CLN2/TPP1* *CLN9* *CLN12/ATP13A2*	
Northern epilepsy (NE) (progressive epilepsy with mental retardation [EPMR])		CLN8	5-10 yrs
Adult (ANCL) (Kufs disease)		*CLN10/CTSD*, *CLN1/PPT1*, *CLN3*, *CLN5*, *CLN6*, *CLN13/CTSF*, *CLN11/GRN*	15-50 yrs
Adult (ANCL) (Parry disease) autosomal dominant		*CLN4/DNAJC5*	

***Table* 1.3.1 -** NCL phenotypes and their known associated genes

Gene	Protein	Solubility and topology	Localisation
CLN1	PPT1 Palmitoyl protein thioesterase 1	Soluble	Lysosomes
CLN2	TPP1 Tripeptidyl peptidase I	Soluble	Lysosomes
CLN3	CLN3	Transmembrane	Golgi complex, Lysosomes
CLN4	DNAJC5	Soluble	Cytoplasm
CLN5	CLN5	Soluble	Lysosomes
CLN6	CLN6	Transmembrane	Endoplasmic reticulum
CLN7	MFSD8	Transmembrane	Lysosomes
CLN8	CLN8	Transmembrane	Endoplasmic reticulum
CLN9	Not known	Not known	Not known
CLN10	CTSD Cathepsin D	Soluble	Lysosomes
CLN11	Granulin GRN	Soluble	Secreted
CLN12	ATP13A2	Transmembrane (Mn transporter)	Lysosomes
CLN13	Cathepsin F	Soluble	Lysosomes
CLN14	KCTD7	Transmembrane (Potassium channel)	Plasma membrane

***Table* 1.3.2 -** Intracellular localisation of the NCL genes products

Changes in lysosomal pH have been reported as a result of mutations in NCL genes (Holopainen et al., 2001), although to date it has not been elucidated how this affects lysosomal function in NCL patients. Fibroblast cell lines from patients with mutations in *CLN1*, *CLN3*, *CLN5*, *CLN6* and *CLN8* showed increased lysosomal pH, with *CLN6* and *CLN1* being the most affected. A slight reduction in lysosomal pH was observed in fobroblast cells from patients with mutations in *CLN2*.

1.4 Juvenile NCL (JNCL)

The most common neuronal ceroid lipofuscinosis is the juvenile form of NCL (Consortium 1995), JNCL, more recently renamed as CLN3 disease. JNCL manifests the first symptom in children between the ages of 4-10 years old, as visual failure, caused by retinal degeneration, which leads to blindness within 2-4 years of onset. Learning difficulties become evident in early school years and epilepsy often develops around the age of 10. Motor symptoms become evident around puberty and clinically manifest as extrapyramidal and pyramidal signs, which gradually lead to loss of independent mobility. The movement disorder in JNCL is Parkinsonism that is sometimes responsive to L-DOPA. Usually, the motor impairment is accompanied by speech difficulties. There are also psychiatric and sleep problems. In addition to the neurological manifestations, the patients present cardiac abnormalities in the second decade of life. The disease leads to premature death, usually in the second or third decade of life (Consortium 1995; Jalanko and Braulke 2009). JNCL is one of the most prevalent types of NCL worldwide, and results from an autosomal recessive inheritance of mutations in the human gene *CLN3.*

1.4.1 CLN3

The juvenile NCL is caused by mutations in *CLN3* gene, mapping on chromosome 16p12.1 (Callen et al., 1991) and more than 40 disease-causing mutations have been identified in the *CLN3* gene (http://www.ucl.ac.uk/ncl) (Consortium 1995; Munroe et al., 1997; Lauronen et al., 1999; Bensaoula et al., 2000; Kwon et al., 2005; Leman et al., 2005; Sarpong et al., 2009; Drack et al., 2013). CLN3 is highly conserved across the species such as mouse, fruit fly as well as fission and budding yeast (Gachet et al., 2005) (Figure 1.4.1.1).

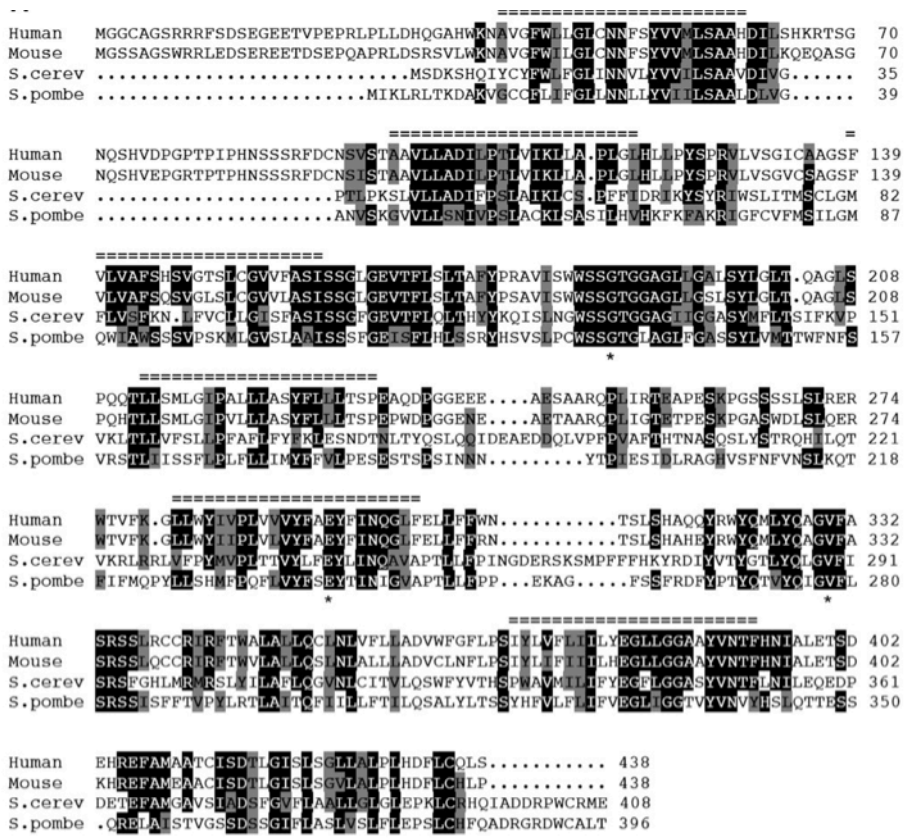

***Figure* 1.4.1.1** - Protein alignment between human CLN3 and its homologous proteins in mouse (Cln3) and two yeast species (Btn1), *S. cerevisiae* (*S.cerev*) and *S. pombe* (*S.pombe*). Shading indicates identical (dark) or similar (grey) residues. The position of residues mutated in *S. pombe* Btn1 during the course of this work that mimic those causing NCL are indicated by an asterisk (*). The likely transmembrane segments (TMS) in human CLN3 are indicated by ==. The positions of TMS are based on original predictions (Janes et al., 1996), recent work (Ezaki et al., 2003; Kyttälä et al., 2003; Mao et al., 2003) and the assumption that the sequence of TMS will be conserved between mammalian and yeast species. *(taken from Gachet et al., 2005).*

The majority of JNCL patients have a 1-kb deletion in common (Mole 2011) and around 74%, are homozygous for this mutation. However, about 22% of patients are compound heterozygous for the 1-kb mutations and one of the other rare mutations (Munroe et al., 1997) that comprise missense, nonsense and splice site mutations (http://www.ucl.ac.uk/ncl).

The breakpoints of the 1-kb mutation are in introns 6 and 8, resulting in loss of exons 7 and 8. This deletion leads to two different transcripts; one causes a frameshift and premature termination after aminoacid 153 and the second one comes from alternative splicing bringing the 3' end back into frame at residue 294 (Kitzmuller et al., 2008). In addition, it has been shown that the premature termination codon induced by the 1-kb deletion is recognized by nonsense-mediated decay, leading to the *CLN3* mRNA degradation and consequent decrease in protein synthesis (Miller et al., 2013). In addition, it has been shown that an uncommon 16p11.2 microdeletion cause an unusual 16p11.2 syndrome, with some feature resembling the JNCL, caused by the unmasking of a recessive mutation of CLN3 (Pebrel-Richard et al., 2014).

The *CLN3* gene encodes a highly hydrophobic type III transmembrane (TM), both N- and C-terminus facing the cytoplasm, protein of 438 aminoacids (Janes et al., 1996; Kaczmarski et al., 1999). The first empirical topological evidence described CLN3 as a type II transmembrane protein with five transmembrane spanning domains (Mao et al., 2003). However, further studies indicated that the N-terminus faces the cytoplasm that categorises CLN3 as a type III TM protein with six spanning domains (Kyttala et al., 2004). In addition, a computational approach confirmed the topology of CLN3 with an additional inclusion of a conserved luminal amphipatic helix (Nugent et al., 2008). The

CLN3 topology is shown in figure 1.4..1.2. Recently, a new CLN3 topology has been proposed. The new topology model for CLN3 agrees with the previous proposed CLN3 topology. However, it differs from the precedent model in terms of position of the transmembrane domains (TMDs) and the length of luminal and cytosolic loops (Ratajczak et al., 2014).

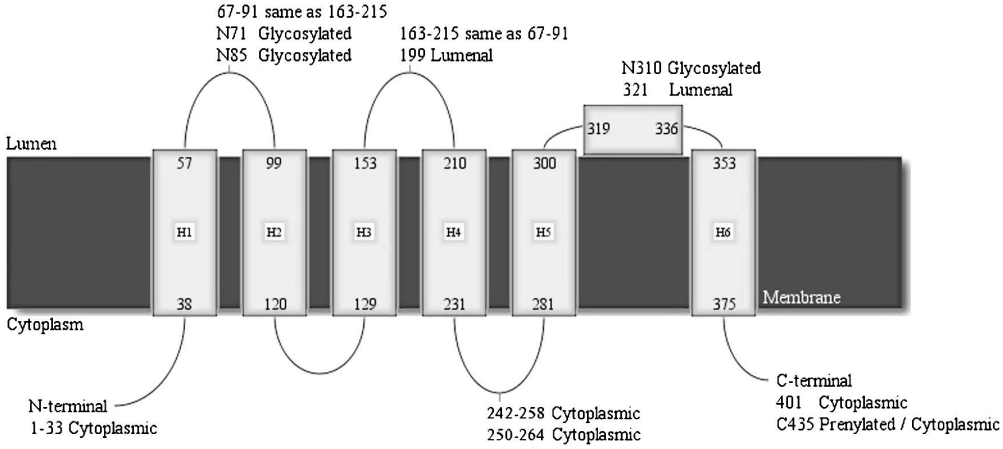

***Figure* 1.4.1.2** - CLN3 is a type III TM protein with six transmembrane domains, N- and C-terminus facing in the cytoplasm and the amphipathic helix in the third luminal loop *(taken from Nugent et al., 2008).*

Interestingly, all the known disease-causing mutations are lodged in or adjacent to a predicted transmembrane helix, or in the conserved luminal loop or in the C-terminus (Nugent et al., 2008). Indeed, mapping the missense and nonsense mutations on CLN3 reveals that most of these mutations are in the luminal side of the protein. In particular, the common 1-kb deletion cause the loss of the second luminal loop, which is one of the most conserved across the species (Gachet et al., 2005; Muzaffar and Pearce 2008; Ratajczak et al., 2014) (Figure. 1.4.1.1 and figure 1.4.1.3).

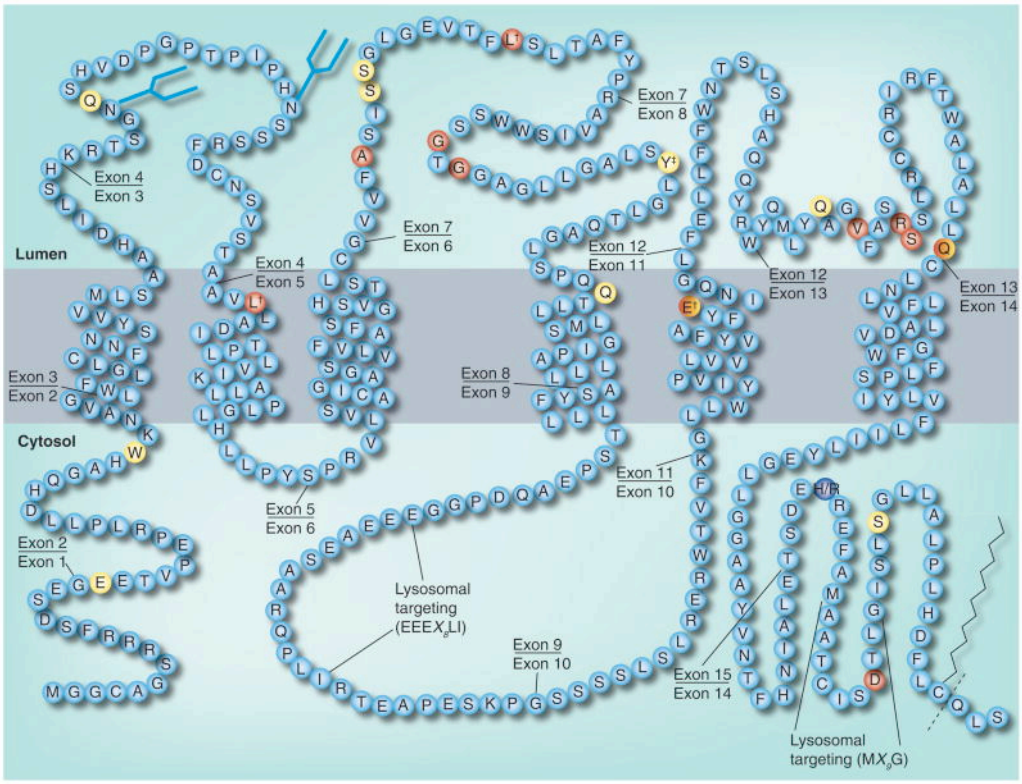

***Figure* 1.4.1.3 - CLN3 topology and juvenile-onset neuronal ceroid lipofuscinosis mutations**
The predicted topology of CLN3 is depicted. Sites for post-translational modifications are shown (blue forked lines represent N-glycosylation, zigzag represents prenylation and dotted line represents a possible cleavage site following prenylation), and point mutations are marked by red (missense) and yellow (nonsense) colored circles. A reported polymorphism at residue 404 (H/R) is shown (dark blue). Residues E295 and Q352 are both red and yellow as they are sites for both missense and nonsense mutations. †A residue that has been associated with slower disease, in compound heterozygosity with the common 1-kb deletion mutation. ‡A residue that has been associated with slower disease in homozygosity (*taken from Cotman, S.L. and Staropoli, J.F., 2012*).

Sequence analysis of CLN3 predicts different potential sites for posttranslational modifications. There are four putative N-glycosylation sites and consensus sequences for phosphorylation, farnesylation and myristoylation. Studies, done using CLN3 overexpressed, have shown that CLN3 is present in two different forms; the non glycosylated and a N-glycosylated form (Jarvela et al., 1998). In particular, CLN3 has two glycosylation site at Asn71 and Asn85 (Storch et al., 2007) and also, it might be glycosylated at Asn310 (Mao et al., 2003) In addition, it has been shown that the glycosylation of CLN3 varies in different tissue (Ezaki et al., 2003). The membrane proteins involved in neuronal function often have lipid modifications. CLN3 is showing different putative sites for lipid modifications. An N-myristoylation site at N-terminus

and a prenylation/farnesylation motif at the C-terminus have been suggested (Pullarkat and Morris 1997; Kaczmarski et al., 1999). Indeed, at the C-terminus is present a CaaX farnesylation motif which is modified by farnesyl groups (Kaczmarski et al., 1999). This is a particular C-terminal sequence, with a cysteine residue (C) followed by two aliphatic residues ad a carboxyl-terminal "X" residue, which can be cysteine, serine, methionine, glutamine or alanine (Ma et al., 1992). Proteins containing this motif undergo farnesylation of the cysteine residue, proteolytic removal of the three amino acids distal to cysteine and methilation of the C-terminus (Ma et al., 1992).

CLN3 has been reported to be located in many different intracellular compartments. However, variable results have been obtained by different groups probably due to the low expression level of CLN3 in mammalian cells, the overexpression modifies the location of CLN3 and the lack of a sensitive antibody able to detect CLN3 at basal level. Studies have shown that CLN3 localise at endosomes/lysosomes and is able to traffic through ER and Golgi complex (Jarvela et al., 1998; Kida et al., 1999; Haskell et al., 2000; Kyttala et al., 2004). In addition, CLN3 localises at early endosomes in neuronal cells (Luiro et al., 2001; Kyttala et al., 2004; Storch et al., 2007). Furthermore, the protein has been noticed in lipid rafts preparation (Rakheja et al., 2004). Recently, has been shown in both fission and budding yeast a significant localisation of the CLN3 orthologue at the Golgi complex (Codlin and Mole 2009; Kama et al., 2011) that it has been previously reported, also, for CLN3 in mammalian cells (Kremmidiotis et al., 1999). CLN3 is able to traffic to the lysomes. Indeed, two lysosomal target motifs have been identified (Kyttala et al., 2004). The first motif, presents in the large cytosolic loop of CLN3, comprises a dileucine motif (aa253-aa254) (Kyttala et al., 2004; Storch et al., 2004; Storch et al., 2007) . However, controversial data has been shown about the bond between the dileucine motif of CLN3 and the main adaptor protein involved in the

trafficking of lysosomal proteins from the trans-Golgi network (TGN) to the lysosomes (Storch et al., 2004; Kyttala et al., 2005). The second lysosomal targeting motif is localised at the C-terminus of CLN3. This unusual motif consists of methionine and glycine residues separated by nine aminoacids [M(X)9G] (Kyttala et al., 2004). None of the reported CLN3 mutations directly affect the lysosomal targeting motif (Kyttala et al., 2004).

Recently, algorithms such as the structural classification of proteins (SCOP) and Pfam suggested that most of the CLN3 protein (aa 11-433) has a domain structure similar with members of the major facilitator superfamily (MFS). The MFS is one of the two largest families of membrane transporters that include small-solute uniporters, symporters and antiporters found across bacteria, archaea and eukaryotes (Pao et al., 1998). MFS proteins are single polypeptide chains that contain, in most of the case, 12 transmembrane domains. CLN3 has six transmembrane domains (Nugent et al., 2008) and one study showed that myc-tagged and non-glycosylated overexpressed CLN3 is able to form homodimers (Storch et al., 2007). However, whether the endogenous CLN3 also forms stable homodimers has not been yet confirmed.

Despite the fact that the *CLN3* gene and protein have been identified more than a decade ago, the function of this highly conserved protein remain elusive. Due to its extreme hydrophobicity, the generation of a specific and sensitive CLN3 antibody has turned out to be difficult (Kyttala et al., 2004). In addition, it is unclear if the epitopes used to generate peptide-specific antibodies are accesible in an intact cellular milieu (Janes et al., 1996) To date, proposed functions of CLN3 include lysosomal acidification, lysosomal arginine import, membrane fusion, vescicular transport, cytoskeletal linked functions, autophagy, apoptosis and proteolipid modifications. CLN3 may have multiple roles, or exert a primary role able to influence multiple pathways.

1.4.2 The CLN3 orthologue in fission and budding yeast

The homologue of *CLN3* in *Schizosaccharomyces pombe*, *btn1* encodes a 396aa transmembrane protein that is 30% identical and 48% similar to the human CLN3 (Gachet et al., 2005) (Figure. 1.4.1). Study of *btn1,* the *CLN3* orthologue, in both the fission yeast *Schizosaccharomyces pombe* (*S. pombe*) and the budding yeast *Saccharomyces cerevisiae* (*S. cerevisiae*) have provided unique insights into CLN3 protein function. Most importantly, in both yeast species, Btn1p and CLN3 have been demonstrated to be functional orthologues of human gene (Gachet et al., 2005; Codlin et al., 2008a; Codlin et al., 2008b). Btn1p was proposed to localise and act at vacuole level (Croopnick et al., 1998; Pearce et al., 1999a; Pearce et al., 1999b); (Kim 2005; Wolfe et al., 2011) with a pre-vacuolar function indicated by Gachet et al., (2005). However, many of these studies used ectopic expression of Btn1p from a plasmid, which can result in protein overexpression that could alter localization. Recent studies suggest that Btn1p is located to the Golgi apparatus in *S. pombe* (Codlin and Mole 2009) and later in *S. cerevisiae* (Vitiello et al., 2010; Kama et al., 2011). All yeast studies reveal multiple effects of complete loss of Btn1p in *btn1*Δ cells. For example, Btn1p is required for vacuole homeostasis (Pearce et al., 1999a), cytokinesis (Gachet et al., 2005) growth regulation (Codlin et al., 2008b) response to oxidative stress (Osorio et al., 2007) and Golgi function (Codlin and Mole 2009). In *S. pombe* loss of Btn1p affects the number of the Golgi stacks, their morphology and location within the cell (Figure 1.4.2.1). In addition, it has been shown, in mammalian cells, that loss of CLN3 prevents exits from the TGN of the mannose-6phosphate receptor playing a role in TGN-endosome trafficking (Metcalf et al., 2008). In S. *pombe,* deletion of *btn1* affects the trafficking of the vacuole hydrolase carboxipeptidase Y (Cpy1p) to the vacuole,

probably by its effect on the trafficking of its receptor, vacuole protein sorting 10 (Vps10) from the endoplasmic reticulum through the Golgi to the trans-Golgi network (TGN) (Codlin and Mole 2009). In contrast, in *S. cerevisiae btn1*Δ cells, Vps10 and CPY trafficking is normal (Kama et al., 2011). In addition, it has been demonstrated that in this budding yeast Btn1p overexpression and/or deletion affects the assembly of Golgi SNAREs. Indeed, It has been proposed that Btn1p could modulate the phosphorylation state of Sed5, an essential SNARE involved in Golgi transport and morphology, through the modulation of Yck3 (Kama et al., 2011), a palmitoylated-protein kinase involved in Sed5 regulation (Banfield et al., 1994). These findings of a role for Btn1 at the Golgi are consistent with the multiple downstream effects of loss of Btn1 on other intracellular pathways that affect vacuole size and pH, cell wall structure and deposition, and polarised growth (Gachet et al., 2005; Codlin et al., 2008b), all of which are rescued by expression of CLN3. However, a role for CLN3 at the Golgi apparatus has not yet been explored in detail.

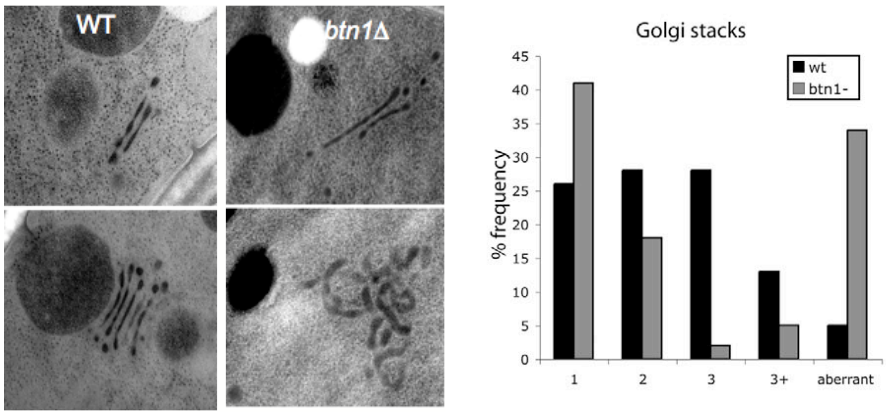

***Figure* 1.4.2.1 -** Btn1 affects Golgi morphology. Electron micrographs of recognisable Golgi with stacked cisternae, and examples of larger aberrant Golgi structures. Scale bar: 0.5 µm. Graph) *btn1*Δ cells have many atypical Golgi and fewer Golgi with multiple stacked cisternae. Bar chart of % frequency of Golgi complexes with defined numbers of stacks *(taken from Codlin et al., 2008).*

1.4.3 Phenotypes in *btn1*Δ cells

To date, efforts to elucidate CLN3 or Btn1 function have mainly relied on comparing the effects on yeast cells of complete deletion of the *btn1* gene. Expression of the wild type yeast Btn1p and, importantly, the human CLN3 protein rescues the resultant phenotypes, which has allowed the effect of some disease-causing mutations to also be examined. The vacuole pH in *S. pombe btn1*Δ cells is less acidic than normal, suggesting an imbalance in pH homeostasis. Moreover, the vacuoles in cells where *btn1* is deleted are larger than wild type cells (Gachet et al., 2005). Similarly, lysosomes in cells depleted for CLN3 by RNAi are larger (Kitzmuller et al., 2008) and the lysosomal pH of JNCL cells is less acidic (Holopainen et al., 2001). In contrast, in the *S. cerevisi*ae model Btn1p has been linked to vacuolar arginine transport, ion homeostasis and nitric oxide synthesis (Pearce et al., 1999a; Kim et al., 2003; Kim 2005; Osorio et al., 2007).

The vacuolar pH is more acidic in yeast cells lack Btn1p. It could be the result of an inability to regulate the coupling of ATP hydrolysis and proton pumping activities of the V-ATPase (Padilla-Lopez and Pearce 2006). The acidification of vacuoles may be linked to, and modulated, by the actin cytoskeleton, which in turn, affects the activity of the membrane v-ATPase. Btn1p has been shown to have an effect on actin, and therefore in the trafficking of v-ATPase and other membrane transporters (Codlin et al., 2008b). *btn1*Δ cells are viable under normal laboratory growth conditions (30°C) but they are slower growing and have a higher septation index, that leads to a higher number of binucleate cells and suggests an abnormal cell cycle (Gachet et al., 2005) Codlin et al., 2008). However, the presence of Btn1p is essential for growth of yeast

cells at 37°C. At this temperature, *btn1*Δ cells struggle to establish growth at new ends following division, resulting first in a pear-like shape, and later swelling and lysing.

In the same study, it was also shown that the endocytosis process is defective in *btn1*Δ cells, both in uptake and trafficking to the vacuole route. A similar defect in neurons could affect the movement, release and uptake of neurotransmitter, leading to neurodegeneration. There are also changes in the metabolism of *btn1*Δ cells, such as an increase in glycolytic flux and amino acid changes (increase in glutamate and decrease in basic amino acids) (Pears et al., 2010). There is an interaction between various glycolytic enzymes and v-ATPase components, suggesting a link between glycolysis and the v-ATPase activity. Therefore, metabolic changes occurring in those cells could be due to the vacuolar defects that occur in those cells, which up-regulates v-ATPase in order to compensate for the increased vacuolar pH. This up-regulation would lead to an increase in the glycolytic flux. If these defects occur in neuronal cells, they could lead to brain dysfunctions and neurotransmitter impairment (Pears et al., 2010). In addition, glycolysis in neurons has recently been suggested to be tightly coupled to glutamatergic neurotransmission with an anti-oxidant role as well as energy production. In fact about 80% of the energy produced by the cortical glucose is destined for the glutamatergic neurotransmission (Magistretti et al., 1999), which plays a key role during the conversion of glutamate to glutamine. Astrocytes take up the glutamate, from the synaptic space, via a specific transporter that uses the electrochemical gradient of Na^+, as a driving force. The Na^+ gradient is maintained by ATP, which is required to drive the Na^+/K^+-ATPase. The hypothesis of Magistretti et al. is that glycolysis is tightly coupled to the Na+, K+-ATPase (Magistretti et al., 1999), reminiscent of the proposed coupling of glycolysis to the v-ATPase in yeast. In addition, the increased glycolytic

flux, which has been proposed to be a characteristic of NCLs, may be associated with a glutamate–glutamine cycling defect, as it was reported in the CLN3 mouse (Pears et al., 2005). Thus, the glutamate present in the synaptic space could lead to neuronal excito-toxicity.

Four different phenotypes that have been characterised in *btn1*Δ cells were selected as marker phenotypes to further understand the effect of mutations in Btn1. These phenotypes were: enlarged vacuoles and the cytokinesis delay with an increased septation index at 25°C, and monopolar growth and cell curving at 37°C (Gachet et al., 2005; Codlin et al., 2008b; Haines et al., 2009). All these phenotypes can be rescued by expression of Btn1p and CLN3. Only the first phenotype can be rescued by Btn1p mutant protein equivalent to the 1-kb deletion. That is, a mutant protein corresponding to this common mutation is functional for vacuole size but not for the other three phenotypes. This suggests that this mutation does not completely abolish Btn1p function, since mutants are able to restore the vacuole size. This data was confirmed by Kitzmuller et al. This study showed that the expression of mutant CLN3, equivalent to that present in JNCL cells (1-kb deletion) in normal fibroblast and fibroblast cells from JNCL patients, causes a decrease in size of lysosomes. The cell curving phenotype was the only one rescued by a mutant protein carrying the yeast equivalent to the p.Glu259Lys mutation, which is known to cause a very mild form of JNCL (Haines et al., 2009). Despite the studies done on CLN3 its function remain elusive.

1.5 Golgi apparatus

The Golgi apparatus (GA) is named after Camillo Golgi, who first described the complex *apparato reticolare interno* in 1898 (Golgi 1898a; Golgi 1898b). However, only after the electron microscopic confirmation of the existence of the GA in cells by Dalton in 1951, did scientists start to believe in its reality. The Golgi apparatus, or Golgi complex, is an intracellular organelle in which proteins received from the ER are further processed and sorted for transport to their eventual destinations, such as lysosomes, plasma membrane or for secretion. The Golgi complex is a multifunctional organelle. Its primary role is the processing of newly synthesized proteins and lipids moving through the secretory pathway. The processing events taking part in the Golgi complex are glycosylation, sulfation and proteolytic processing. Those modifications play roles in protein localisation, stability, activation and specificity of interactions. A secondary function is sorting. Exit routes from the Golgi complex for newly processed protein and lipids are distinct and depend on whether the cargo is destined for constitutive or regulated secretion or for trafficking toward lysosomes (Keller and Simons 1997). Furthermore, in polarised cells additional exit routes target specialised membranes (Keller and Simons 1997; Folsch et al., 2009; Weisz and Rodriguez-Boulan 2009). Another important aspect of sorting is the retrieval of proteins to endoplasmic reticulum (ER) to ensure their localisation (Lee et al., 2004). Golgi complex components, such as the Golgi-resident enzymes, are also subject to sorting to ensure their correct localisation (Tu and Banfield 2010). Another important function of the Golgi complex is its size control and its role in supporting the plasma membrane (Gauthier et al., 2009). The Golgi complex is also involved in ion homeostasis, mainly calcium (Ca^{2+}) and manganese (Mn^{2+}) (Missiaen et al., 2007; Mukhopadhyay and

Linstedt 2011). Finally, the membranes of the Golgi complex serve as platform for different signalling pathways (Saini et al., 2009).

1.5.1 Morphology of the Golgi complex

The Golgi complex is known for its stacked morphology, which is evident in most eukaryotic cells. In many animal and plant cells the Golgi complex appears as a series of associated flattened membrane-enclosed sacks, so called cisternae, aligned in parallel to form a stack called the dictyosome (Polishchuk and Mironov 2004). In mammalian cells, the Golgi complex is present as a network of stacked membranes called the Golgi ribbon. Along the ribbon network there are zones of fenestration where adjacent stacks appear to connect with each other through dynamic tubular contacts (Rambourg 1997; Ladinsky et al., 1999).

The number of cisternae per stack varies. However, they are comprised in three functionally distinct compartments: *cis, medial* and *trans* Golgi compartments (Figure 1.5.1.1). *cis*-localised enzymes act on cargo first followed by *medial* and *trans* enzymes (Mellman and Simons 1992). The *trans*-Golgi network (TGN) is a fourth compartment specialised for packaging cargo into carrier vesicles as it leaves the Golgi complex (Griffiths et al., 1985). Both the *cis*- and the *trans*- are mainly tubular (Figure 1.5.1.1). It is the *medial*-Golgi that has the typical dictyosome or flattened cisternae structure (Rambourg 1997; Polishchuk and Mironov 2004), which can vary in number from one cell type to another. Within the same cell type, the number of cisternae can be similar (Ladinsky et al., 1999) or vary depending on the functional state.

A striking feature of the Golgi apparatus is its distinct polarity in both structure and function. Several gradients exist within Golgi stacks: a gradient in the cisternae fenestration, in the cisternae thickness, in the localizations of the Golgi enzymes (which show a polarised distribution in which early-acting enzymes are concentrated in *cis* while late-acting enzymes are concentrated in *trans*), in the lipid bilayer thickness, in the pH and a gradient in concentration of cholesterol. Proteins from the ER enter at the *cis* face of the Golgi, which is convex and oriented toward the nucleus, and serves primarily to receive transport vesicles from the ER and to sort their contents and proteins. Those cargoes are marked for residence within the ER are recognised and returned to the ER by the recycling pathway, in COPI coated vesicles. Others are transported through the Golgi and exit from its concave *trans* face, where the final stages of the protein processing are completed. However, the secretory pathways of plants and animals are not identical. In plants, the organization of the organelles that make up the secretory pathway differs greatly from that of mammals and yeast (for yeast Golgi complex see paragraph 1.5.2). Despite the identification of plant homologues of proteins that are known to be involved in vesicular transport in other systems, the mechanisms in plants have not yet been fully characterized. Given the differences in the features of the secretory pathway of plants compared with those of other organisms, it seems likely that plants have evolved unique characteristics for achieving efficient protein transport between organelles. The localisation of the Golgi complex can vary between species. Indeed, the mammalian Golgi apparatus remains relatively stationary in the peri-nuclear region of the cell and is much larger than the plant Golgi. It has been reported that in various plant cellular systems the Golgi apparatus is present as multiple stacks that are distributed throughout the cytosol and are

capable of rapid movement (Boevink et al., 1998; Nebenfuhr et al., 1999; Takeuchi et al., 2000). In addition, the mammalian secretory pathway contains an additional organelle known as the ER-Golgi intermediate compartment (ERGIC), which does not exist in plants, although the cis-Golgi may play a similar role. Despite these differences in the secretory pathways, proteins in both plants and animals are generally transported in the anterograde direction from the ER to the Golgi apparatus, at which point they are sorted for further transport, either forward, in the direction of the cell surface and organelles in the later secretory pathway, or back towards the ER.

Golgi cisternae are the smallest functional unit of the Golgi apparatus and their morphology strongly contributes to the overall morphology of the organelle. All cisternae are fenestrated and the large openings in cisternae can form wells (Ladinsky et al., 1999), necessary for the movement of secretory granules (Rambourg 1997). In particular, critical features in cisternal size are surface area and shape. The surface area of the Golgi cisternae depends on the ratio of membrane input and output to the compartment along different trafficking routes. One example of this is that the inhibition of Golgi complex-to-ER transport, a Golgi efflux pathway, increases the size of the Golgi complex (Burman et al., 2010). The total surface area of *cis*, *medial* and *trans* cisternae is similar (Ladinsky et al., 1999), which suggests that the flux is uniform across the Golgi stacks at steady state. However, an altered trafficking can drastically change the surface area. Cisternal shape refers mainly to the degree to which the membranes are flattened. The resulting high surface to volume ratio increase the concentration of the Golgi complex enzymes (Mellman and Simons 1992). The dilation of the cisternae is observed in different pathological conditions such as cancer and neutralisation of the normal slightly acidic luminal pH (Kellokumpu et al., 2002; Maeda

and Kinoshita 2008). The mechanisms that contribute to cisternal flattenig are mainly three. The first is the interactions in trans of the Golgi-resident enzymes. Binding in trans hold the membrane in close contact, thereby flattening the shape. One of the first identified interactions was between the *medial* Golgi complex enzymes *N*-acetylglucosaminyltransferase I and mannossidase II (Nilsson et al., 1994; Hassinen et al., 2010). A second mechanism depends on actin assembly at the Golgi complex. Actin depolymerisation induces cisternal swelling (Egea et al., 2006). The *trans* Golgi-localised protein Golgi phosphoprotein 3 (GOLPH3), yeast Vps74, links the Golgi membranes to an actin-based motor by simultaneously binding the phosphoinositide-4-phosphate in the membrane and the unconventional myosin MYO18A (Dippold et al., 2009). Depletion of the GOLPH3 dilates Golgi cisternae, suggesting that the motor exerts pulling forces on Golgi membranes that contribute to their flattened shape. The third possible mechanism is induced by membrane curvature. The edges of the flattened cisternae, the rims, have high membrane curvature. Energy imparted to the membranes to maintain this curvature could rise from local changes in lipid composition or interaction with curvature-inducing proteins (Graham and Kozlov 2010).

Golgi complex forms stacks through proteinaceous elements that cross link adjacent cisternae (Mollenhauer 1965; Franke et al., 1972). These cross-linking proteins are the Golgi Reassembly And Stacking Proteins (GRASPs). In vertebrates two GRASPs, GRASP65 and 55, localise to *cis* and *medial* cisternae respectively, while lower eukaryotes only have one GRASP protein (Barr et al., 1997; Shorter et al., 1999; Kondylis et al., 2005; Behnia et al., 2007; Levi et al., 2010). In addition, it has been shown that the deletion of both GRASPs abolishes stack formation and that the re-expression of both can partially rescue the phenotype (Xiang and Wang 2010).

Vertebrate GRASPs form homo-oligomers (Wang et al., 2003; Tang et al., 2010; Xiang and Wang 2010). The oligomerisation of the GRASPs is mediated by its PDZ domain (Sengupta et al., 2009; Tang et al., 2010). The PDZ domain is able to cross link membrane. For this to occur efficientely, the PDZ domain needs to be correctly oriented through a dual anchoring mechanism in which the PDZ domain is flanked by upstream and downstream membrane attachment sites (Bachert and Linstedt 2010). The first of these sites is a N-terminal myristoylation site while the other is a second PDZ domain which in GRASP65 stably binds the C-terminus of the golgin GM130 (Barr et al., 1997; Barr et al., 1998; Bachert and Linstedt 2010). GM130 is a predicted elongated coiled-coil protein that extends from the membrane. GM130 binds the vesicle docking protein p115 at its N-terminus and has been implicated in different tethering events at *cis*-Golgi (Ramirez and Lowe 2009). However, when it comes to Golgi complex stacking the GRASPs cannot be the only responsible factor. Indeed, in the fruit fly the loss of the single GRASP has a minor effect on Golgi stacking (Kondylis et al., 2005), while in *S. cerevisiae* the cisternae are unstacked despite the presence of a GRASP known as Grh1p (Behnia et al., 2007; Levi et al., 2010). Plants have stacked Golgi complex yet they lack a GRASP altogether (Staehelin and Kang 2008; Faso et al., 2009). These studies suggest that other factors are involved in Golgi complex stacking and that the GRASPs must have further roles in addition to cisternal stacking. Indeed, GRASPs are involved in linking Golgi cisternae in order to form ribbons (Puthenveedu et al., 2006; Feinstein and Linstedt 2008), and play a role in the tethering of transport vesicles (Behnia et al., 2007). GRASPs can also have a role in the trafficking of certain cargoes (Kuo et al., 2000; D'Angelo et al., 2009). Finally, GRASPs have a role in an unconventional secretion, that is transport to the cell surface avoiding the typical secretory route through the Golgi complex (Kinseth et al., 2007; Schotman et al., 2008).

In most vertebrates the Golgi stacks are connected to form a ribbon (Mogelsvang et al., 2004) which is located in juxtanuclear position around the centrosome, suggesting a functional link with the microtubule cytoskeleton. Indeed, it is well known that an intact microtubule network and the minus end-directed microtubule motor cytoplasmic dynein are essential to maintain the Golgi ribbon (Burkhardt 1998). Furthermore, Golgi complex *per se* can act as microtubule organiser (Chabin-Brion et al., 2001; Efimov et al., 2007; Rivero et al., 2009). Golgi-derived microtubules form an asymetric network that extends towards the leading edge of migrating cells that is important for the polarised delivery of Golgi carriers to this region of the plasma membrane (Efimov et al., 2007; Miller et al., 2009; Rivero et al., 2009). The formation of microtubules at the *trans*-Golgi is dependent of the regulator CLASP, which is recruited to the membrane through interaction with the golgin GCC185 (Efimov et al., 2007). Furthermore, it requires active dynein as is the case for centrosomal microtubules. Microtubules can also form at the *cis*-Golgi via a distinct mechanism involving AKAP450, a well known interactor of the γ-tubulin ring complex found at the centrosome (Rivero et al., 2009). AKAP450 is recruited to the *cis*-Golgi through binding with GM130 and microtubules generated by this complex are important for polarised secretion. CLASP-dependent Golgi-nucleated microtubules are required also for assembly of the Golgi ribbon (Miller et al., 2009). During Golgi assembly they act in a "search and capture" fashion to bring together individual Golgi stacks which are transported from the periphery to the cell centre via dynein- mediated trafficking along the centrosomal microtubule network. Although, Golgi ribbon formation requires two sets of independently nucleated microtubules acting in concert. Furthermore, the Golgi-derived microtubules are important in the maintanance of the ribbon.

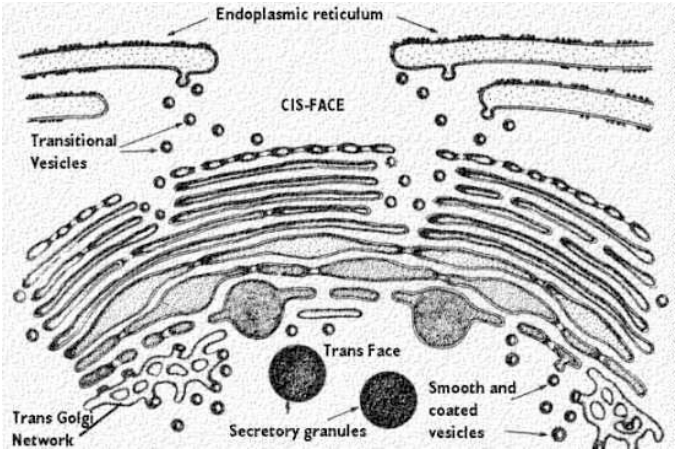

Figure 1.5.1.1: Golgi complex and its compartment *(taken from Bannykh, S., et al., 1997).*

1.5.2 The Golgi complex in yeast

The structural organisation of the Golgi varies among different species. In yeast the Golgi complex is composed of tubular networks and isolated discs, which was first described in budding yeast *S. cerevisiae sec* mutants in 1980 by Novick (Novick et al., 1980). Each compartment can be observed by electron microscopy (EM) as individual disk-shaped or fenestrated cisternae that rarely associate with one another. Indeed, the Golgi in this organism has an unusual structure, consisting of individual cisternae that are scattered throughout the cytoplasm. In contrast, the fission yeast *S. pombe* has multiple Golgi organelles, which form stacks.

Recent evolutionary study suggests that ancestral unicellular eukaryotes had stacked Golgi (Mowbrey and Dacks 2009). The yeast *S. pombe* and *P. pastoris*, still have stacked Golgi, while *S. cerevisiae* has lost the stacked organisation and developed a dispersed Golgi complex instead. The organisation of the Golgi complex might be

related to the generation of this organelle (Rossanese et al., 1999). In particular, the COPII transport carrier is formed on the endoplasmic reticulum (ER) at specialized domains, the transitional-ER (tER) sites or ER exit site (ERES) (Farquhar and Palade 1981). Because the COPII vesicles can form a pre-Golgi complex by themselves, the ERES is thought to be the site of Golgi generation (Bevis et al., 2002). Indeed, the Golgi structure in *P. pastoris* is suggested to depend on the organisation of ERES (Connerly et al., 2005). The organisation of the ERES differs among yeast species, as in *P. pastoris* and *S. pombe* appear as 2-5 discrete spots, whereas in *S. cerevisiae* appear as numerous small spots that appear to be detected all over the ER (Mowbrey and Dacks 2009). ERES are dynamic structures, and it might be the difference in the size and number of ERES that affect the morphology of the Golgi complex in yeast.

1.5.3 ER-Golgi intermediate compartment (ERGIC)

After its synthesis, folding and quality control, cargo exits from the endoplasmic reticulum exit site and moves to the Golgi complex through the ER-Golgi intermediate compartment. The ERGIC is a complex membrane system between the rough ER and the Golgi complex that was defined following the identification of a 53kDa membrane protein (ERGIC-53) (Schweizer et al., 1988; Hauri et al., 2000). It consists of vesicular-tubular clusters (VTC), defined as clusters of a few small vesicles and tubular-saccular elements associated with the rough ER (Bannykh et al., 1996; Mironov et al., 2003). Within the ER-Golgi interface, several post-translational modifications are performed: O-glycosylation (Tooze SA 1988), acylation (Rizzolo et al., 1985), generation of mannose-6-phosphate signal

for lysosomal protein targeting (Pelham et al., 1988), protein palmytoilation, retrieval of misfolded proteins (Hammond and Helenius 1994) and segregation of secretory cargoes, regulatory secretory proteins, constitutive secretory proteins, protein destined for the apical plasma membrane and basolateral, endosomal and lysosomal proteins by enzymatic cleavage of the retention signal in the ER.

1.5.4 *Cis*-Golgi network (CGN)

The *cis*-Golgi network is an extensive tubular-vesicular network bound to the *cis* face of the Golgi stacks, which functions to receive the cargo from the ER. The CGN is composed mainly of three domains. The first domain represents the highly perforated disk, similar in shape with the cisternae. It is attached to the Golgi stacks and is named as the attached CGN or the *cis*-perforated cisternae of the intermediate compartment or CGN (CISCIC). CISCIC appears as a disk with 30 nm perforations. The second part of the CGN is a small tubular part that appears as the three dimensional tubular network near to the dictyosomes. This area of the CGN is called the free CGN. Indeed, it produces tubules moving towards the ER-exports site (Marra et al., 2001; Mironov et al., 2003). Another part of the CGN is connected with the CISCIC by tubules and has similar shape with the CGN. It localizes out of the organelle and appears as the late intermediate compartments (Marra et al., 2001) that could be rather a stable compartment (Bonifacino and Lippincott-Schwartz 2003). It has been shown that the CGN contains early processing enzymes such as α-mannosidases that trim high mannose N-linked oligosaccharides added to the nascent chain in the ER. The CGN receives newly synthesized or recycled polypeptides from the ER, which are then post-

translationally modified such as glycosylation, sulphatation, phosphorylation, palmitoylation, myristoylation or methylation (de Graffenried and Bertozzi 2004).

1.5.5 *Trans*-Golgi Network (TGN)

The Trans-Golgi network (TGN) is a unique compartment located at the exit side of the Golgi stacks (Griffiths and Simons 1986) and is typically associated with a large amount of vesicles and tubular membrane. The morphology of TGN varies between cell types, due to a different secretory activity (Gu et al., 2001). Like the other Golgi cisternae, the TGN contains different resident enzymes involved in the processing of the cargo molecules, such as glycosyltransferase involved in addition of terminal sugars, several protein convertase such as Furin, and tyrosine sulphatation enzymes (Rabouille et al., 1995; Thomas 2002). For example, glycosaminoglycan chains are synthesized and sulphated in TGN (Velasco et al., 1988). However, unique functions clearly distinguish the TGN from the other Golgi cisternae. Firstly, the TGN sorts various mature cargo proteins and lipids into membrane carriers destined for the plasma membrane, endosomes, secretory granules or earlier Golgi cisternae or the ER (Velasco et al., 1988; Young et al., 2005). Secondly, the TGN receives cargo from various endosomal locations (Shewan et al., 2003). Sorting is one of the main functions of the TGN and recent studies have shown that depleted CLN3 affects the correct protein sorting between TGN and lysosomes (Metcalf et al., 2008).

1.5.6 Transport machinery at Golgi apparatus

Vesicular transport provides a dynamic communication network between the subcellular compartments that define the structure and identity of membrane bound organelles (Bonifacino and Glick 2004). The mechanisms that direct this cargo flow involve specialised multi-protein machineries. One of them is assembled to form a protein complex called coatomer that coats membrane-bound vesicles. The different types of coatomer that are involved in ER-Golgi trafficking are: Coat protein I and II (COPI, COPII) (Figure 1.5.6.1).

1.5.6.1 Coat protein I

The coat protein I is considered the most characterised coat complex, and represents the core machinery by which vesicle formation and cargo sorting are coupled to initiate vesicular transport (Bonifacino and Lippincott-Schwartz 2003). COPI vesicles have been implicated in both intra-Golgi transport and retrograde transport from the Golgi to the ER. COPI is an ADP-ribosylation factor-dependent adaptor protein. ARF belongs to the family of small GTPases involved in vesicular trafficking, acting as a regulator of COPI transport, and is post-translationally modified at its N-terminus by the addition of the fatty acid myristate. Like all small GTPases, guanine nucleotide exchange factors (GEFs) are required to catalyse the activation of Arf (Casanova 2007) and GTPase-activating proteins (GAPs) are required to catalyse its deactivation (Inoue and Randazzo 2007). In this way Arf switches between GTP and GDP-bound conformations, which cause different effects. In the GTP-bound form the myristate and the hydrophobic N-

terminus are more exposed. In the GDP bound conformation, Arf become less hydrophobic and dissociates from the membrane. For cargo sorting the coatomer recognizes two types of di-basic sequence on cargo proteins. These sorting signals - KKXX (Lys-Lys-X-X) and KDEL (Lys-Asp-Glu-Leu) are both carboxyl terminal motifs important for protein retention in the ER. However, despite the presence of one of these sequence signals proteins do leak from the ER towards the Golgi complex (Munro and Pelham 1987; Pelham et al., 1988), and so these signals also determine retrieval from the Golgi back to the ER. Thus retrograde transport is COPI mediated. KDEL is recognised by its receptor (KDELR) and so KDEL interacts indirectly, via the transmembrane KDELR, with the cytosolic COPI coatomer structures (Lewis and Pelham 1990), whereas the KKXX signal binds directly COPI protein (Cosson et al., 1996).

1.5.6.2 Coat protein II (COPII)

The coat protein II (COPII) are vesicle coat proteins that contribute to transport proteins from the ER to the Golgi, anterograde transport. COPII coat is composed of different proteins such as Sec23/24 (Hicke et al., 1992), Sec13/31 (Salama et al., 1993) and Sar1 regulator Sec12 (Nakano and Muramatsu 1989). These COPII components generate COPII vesicles through a sequence of events. The first step is initiated by conversion of the small GTPase Sar1-GDP to Sar1-GTP, mediated by GEFs. Sar1 activation occurs in the ER, which triggers the exposure of the N-terminal amphipatic α-helix and its insertion into the ER membrane. Activated Sar1 recruits the heterodimer Sec23/Sec24 by binding Sec23, forming the pre-budding complex (Kuehn et al., 1998). Subsequently

the pre-budding complex recruits the Sec13-Sec31 heterotetramer onto the pre-budding complex (Lederkremer et al., 2001). The Sar1-Sec23/24-Sec13-Sec31 complex present on the membrane layer deforms the membrane enough to bud a vesicle off. There is a negative control on the pre-budding complex, since the Sec23 subunit of Sec23/24 is a GAP protein that causes hydrolysis of GTP in Sar1, which leads to the loss from the membrane of the Sar1-Sec23/24 complex (Yoshihisa et al., 1993; Antonny et al., 2001). However, kinetically stable Sec23/24-Sar1 complexes are maintained on the membrane by the presence of the GEF Sec12, which counteracts the action of Sec23 by constantly charging Sar1 with GTP (Futai et al., 2004). COPII vesicles lose their coats before binding and fusion with the Golgi complex and this uncoating reaction is mediated by Sar1 GTP hydrolysis (Oka and Nakano 1994). The COPII vesicles, in mammalian cells, do not fuse directly with the Golgi complex but rather they appear to fuse to each other, that is, homotypic fusion, to form carrier intermediates that lie close by the ER. COPII vesicles continue to fuse with these intermediates, which become larger and eventually fuse with the Golgi. Different names have been given to that compartment, such as ER-Golgi intermediate compartment (ERGIC), or pre-Golgi intermediate and vesicular tubular complex (VTC).

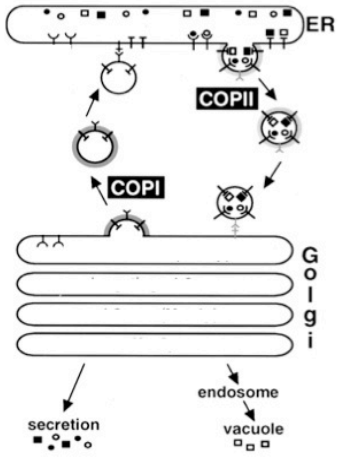

Figure 1.5.6.1 **-** Vesicular trafficking mediated by COPI and COPII *(Gaynor et al., 1997)*

1.5.7 Golgi complex in neurodegenerative disorders

Golgi complex is a highly dynamic organelle and the typical ribbon structure of the Golgi complex can change profoundly. Under pathological conditions, overexpression of Golgi-related proteins and pharmacological agents can cause changes in the organisation of the Golgi complex. Furthermore, during mitosis the Golgi complex fragments reversibly into vesicles and tubules that are distributed equally to the daughter cell (Warren and Malhotra 1998).

The Golgi complex undergoes fragmentation, also during apoptosis. The caspases cause the fragmentation of the Golgi cleaving a Golgi-associated matrix protein (Mancini et al., 2000; Sutterlin et al., 2005). The most well known drug able to induce the fragmentation of the Golgi complex is the fungal metabolite brefeldin A, which induces the Golgi to collapse into tubules and vesicles that fuse with the ER (Klausner et al., 1992).

In particular, fragmentation is a classical feature of the organelle observed in neurodegenerative diseases. Golgi complex, in neuronal cells, shows morphological changes in many neurodegenerative disorders, such as lost the normal network configuration, which is replaced by disconnected small elements (Fujita et al., 2000; Sakurai et al., 2000; Sakurai et al., 2002). A fragmented Golgi complex has been observed in different neurodegenerative diseases such as Alzheimer's disease (AD) (Baloyannis et al., 2004), amyotrophic lateral sclerosis (ALS) (Stieber et al., 1998), Creutzfeldt-Jacob disease (CJD) (Sakurai et al., 2000), multiple system atrophy (Takamine et al., 2000; Sakurai et al., 2002), Parkinson's disease (PD) (Fujita et al.,

2006), spinocerebelar ataxia type 2 (SCA2) (Huynh et al., 2003) and Niemann-Pick disease type C (NPC) (Lin et al., 2007).

The fragmentation of the Golgi in neurodegenerative diseases is probably caused by mechanisms involving the interaction between mutant proteins and any of the proteins involved in the maintenance of the Golgi complex. Many studies have described that Golgi is fragmented in anterior horn cells of patients with sporadic ALS (Stieber et al., 2004). The copper/zinc superoxide dismutase (SOD1) is an abundant enzyme with an essential role in antioxidant defense and its mutant form may be one of the causes for ALS. Indeed, SOD1 mutant acquire a toxic property that kills motor neurons (Xia et al., 2005). Membranes of the Golgi complex or key proteins mediating the anchorage of Golgi membranes with microtubules, may be targets of the toxic function of SOD1 mutant (Karecla and Kreis 1992). Indeed, it has been shown that there is a direct gain-of-interaction between the SOD1 mutant and dynein (Zhang et al., 2007).

α-synuclein is a 140aa protein that is enriched in presynaptic terminals of neurons (Goedert 2001). Neurological disorders such as PD, MSA and dementia with Lewy bodies are characterised by amyloid-like fibrillar aggregates of α-synuclein. Mutant or overexpressed α-synuclein could cause damage by interfering with particular steps of neuronal membrane traffic. The microtubule system seems to be a potential target of α-synuclein (Lee et al., 2006). Indeed, the α-synuclein aggregates cause an overload of the microtubules that could lead to the fragmentation of the Golgi complex.

Phosphoproteins of the stathmin family are important regulators of microtubule dynamics, in particular in the developing and mature nervous system. Stathmin, a

ubiquitous cytosolic phosphoprotein and generic element of the protein family that includes the neural specific proteins SCG10, SCLIP, RB3 and its splice variant RB3' and RB3'' are associated with the Golgi complex and vesicular membranes, through their palmitoylated N-terminal A domain (Gavet et al., 2002; Charbaut et al., 2005). Stathmin proposed to be a small regulatory protein, interferes with microtubule dynamics by inhibiting the formation of microtubules and favoring their depolymerisation. Stathmin has the ability to interact with soluble tubulin inducing the formation of tubulin complexes, which sequester soluble tubulin and therefore impedes microtubule formation (Curmi et al., 1999). Microtubules are essential for the structural integrity of the Golgi complex, and stathmin, the microtubule depolymerizing protein, is confirmed in the pathogenesis of ALS (Ozon et al., 2002). Fragmented Golgi complex suggests a link between the disruption of the structure of the microtubules and stathmin accumulation.

Tau, a microtubule- associated protein enriched in either Golgi complex or ER membranes, is know to stabilize and promote the formation of microtubules during axonal outgrowth. In several neurodegenerative disorders including Alzheimer's disease, hyperphosphorylated Tau accumulates in the somatodendritic compartment, self-aggregates, and forms neurofibrillary tangles. They may be classified as taupathies (Croisier and Graeber 2006). Tau can inhibit kinesin-dependent transport of peroxisomes, neurofilaments and Golgi-derived vesicles into neurites. Loss of peroxisomes makes cells vulnerable to oxidative stress and leads to degeneration (Stamer et al., 2002).

The Golgi complex undergoes fragmentation during apoptosis, in part as result of caspase-mediated cleavage of several Golgi-associated proteins. For example, it has been shown that clusters of vesicles pinching off from the Golgi cisternae were reduced in size in apoptotic cells (Sesso et al., 1999). In response to FAS receptor activation or staurosporine treatment, several Golgi proteins, p115 and golgin-160, underwent to caspase-mediated cleavage and occurred independently of major changes to the actin and tubulin cytoskeleton (Mukherjee et al., 2007). In addition, GM130, an integral membrane protein, contribute to the maintenance of the Golgi complex structure and facilitates membrane fusion with secretory vesicles, was reduced during FAS-mediated apoptosis associated with Golgi fragmentation (Walker et al., 2004). The Golgi fragmentation is a downstream apoptotic event due to the caspase activation and cleavage. However, cells expressing non-cleavable golgin-160 showed a delayed response to apoptotic stimuli that cause ER stress or ligate death receptors (TNF1 and FAS) (Maag et al., 2005). Importantly, the delay of the apoptosis is observed with all pro-apoptotic stimuli. The cells can normally respond to a DNA damaging agents, protein inhibitors and a broad-spectrum kinase inhibitor. Therefore, the cleavage of golgin-160 appears to be required for the progression of apoptosis induced by specific stimuli. In addition, the caspase-cleavage fragments of some Golgi structural protein may actively regulate apoptosis (Chiu et al., 2002). Therefore, the Golgi complex fragmentation plays a pivotal role during neurodegenerative processes regulating, also, the apoptotic events that lead to neuronal loss.

1.5.8 Golgi complex and manganese homeostasis

Manganese (Mn) represents an essential trace element that is accumulated and utilised by all form of life. It is required for normal growth, development and cellular homeostasis (Erikson et al., 2005). Mn exists in various chemical forms including oxidation states (Mn^{2+}, Mn^{3+}, Mn^{4+}, Mn^{6+}, Mn^{7+}), salts (sulfate and gluconate), and chelates (aspartate, fumarate, succinate). Specifically, Mn is important in bone formation, fat and carbohydrate metabolism, and blood sugar regulation. This redox active metal is a key cofactor for a wide range of metalloenzymes, including oxidases and dehydrogenases, DNA and RNA polymerases, kinase, decarboxylases and sugar transferases (Crowley 1999). Furthermore, Mn is a required cofactor of several enzymes involved in neuronal and glial function, as well as enzymes involved in neurotransmitter synthesis and metabolism (Butterworth 1986; Hurley 1987; Erikson and Aschner 2003). It has been shown that, in yeast, there are roles for both ions within the Golgi, including roles in protein modification, in regulation of sorting and vesicular traffic and in removal of toxic levels of ions. Mannosyltransferases present in the Golgi complex require Mn as a metal cofactor (Lisman et al., 2004; Lobsanov et al., 2004). Crystal structures of several glycosyltransferases show Mn binds to a conserved DXD motif in the catalytic site (Gastinel et al., 2001; Persson et al., 2001; Lobsanov et al., 2004). In addition to serving as an essential nutrient, manganese can also be toxic. In humans, exposure to manganese can cause severe neurological damage, leading to a Parkinsonian-like disorder known as manganism (Barbeau 1984; Barceloux 1999; Pal et al., 1999; Uversky et al., 2001). Because manganese is potentially toxic, the ions are not free to diffuse in the cell unattended, but rather are handled in a very high controlled fashion by manganese homeostasis proteins. Such homeostasis factors include cell

surface and intracellular manganese transporters and putative manganese chaperones that guide the metal to a designated trafficking pathway, ending in the activation of manganese enzymes. The factors involved in manganese homeostasis discovered so far, have been revealed through studies done with *S. cerevisiae*.

In *S. cerevisiae* two members of the natural resistance-associated macrophage proteins (NRAMP) family (Smf1p and Smf2p) act in the uptake and intracellular trafficking of manganese (Cellier et al., 1995). They are localised at the cell surface and provide uptake of manganese from the extracellular milieu. In particular, some of the Smf2p-transported manganese reaches the Golgi complex and the mitochondria for activation of sugar transferase (STase) enzymes and SOD2, respectively. Such model is analogous to what has been shown for the mammalian Nramp transporter DMT1 (Edwards and Hoke 1975; Canonne-Hergaux et al., 1999; Andrews 2000). The Golgi complex, in yeast, acquires its manganese through the action of Pmr1p, a P-type Ca^{2+} and Mn^{2+} transporting ATPase (Rudolph et al., 1989). The calcium and manganese transported by Pmr1p facilitates the processing and trafficking of polypeptides that move through the secretory pathway (Rudolph et al., 1989; Antebi and Fink 1992; Durr et al., 1998; Rutherford and Bird 2004). Pmr1p is the prototype of a family of transporting ATPases known as SPCA (secretory pathway Ca^{2+} -ATPases) found in various fungi, *C. elegans*, *D. melanogaster* and mammals (human SPCA1 and SPCA2) (Ton et al., 2002; Missiaen et al., 2004; Xiang et al., 2005). The Golgi-localised SPCA molecules are members of a large superfamily of Ca^{2+} -ATPases that also includes calcium pumps at the cell surface and sarco/endoplasmic reticulum (Sorin et al., 1997; Missiaen et al., 2004); however, the SPCA transporters are unique in that they function in manganese and calcium transport (Missiaen et al., 2004).

Yeast cells respond to manganese starvation by increasing levels of the Smf1p and Smf2p transporter. The transporters then accumulate at the cell surface (Smf1p) and intracellular sites (Smf2p) to increase the uptake of manganese (Liu and Culotta 1999a; Liu and Culotta 1999b; Portnoy et al., 2000; Luk and Culotta 2001). However, manganese starvation does not increase the level of *SMF1* and *SMF2* mRNA (Liu and Culotta 1999b; Luk and Culotta 2001). The response of manganese starvation occurs at the posttranslational level. Manganese starvation leads to enhanced stability of the Smf1p and Smf2p polypeptides and a shift in the cellular localisation of these transporter (Liu and Culotta 1999a; Liu and Culotta 1999b; Portnoy et al., 2000; Luk and Culotta 2001). Indeed, upon manganese starvation these transporters fail to reach the vacuole for degradation and their localisation is shifted either to cell surface (Smf1p) and intracellular vesicles (Smf2p). Smf1p and Smf2p are largely absent under manganese-replete or manganese toxicity conditions, cells can still accumulate the metal by other transport mechanisms. The phosphate transporter Pho84p has been proposed as a manganese transporter, in yeast. *PHO84* encode a cell surface phosphate transporter in yeast (Wykoff and O'Shea 2001). Pho84p also act as low affinity manganese transporter. When cells are exposed to high manganese concentrations, in excess of 10 μM, they accumulate the metal and deletion of *pho84* eliminates the uptake of excess manganese (Jensen et al., 2003). Unlike Smf1p and Smf2p, there is known down-regulation of Pho84p in response to manganese. Therefore, the cell becomes vulnerable to manganese toxicity. Fortunately, much of the accumulated manganese is eliminated from the cell through the action of Pmr1p at the Golgi complex, which exerts a pivotal role in manganese detoxification. The excess manganese is either sequestered in the vacuole or eliminated from the cell by Pmr1p and the secretory pathway. Indeed, Pmr1p not only plays a role in supplying Golgi STase enzymes with manganese but also

is the major route for eliminating toxic manganese from the cell. Mutants lacking Pmr1p are sensitive to manganese toxicity and accumulate very high levels of it, largely in the cytosol (Lapinskas et al., 1995; Ton et al., 2002). The excess of manganese pumped into the Golgi complex by Pmr1p exits the cell via secretory pathway vesicles that fuse with the cell surface and release the manganese contents back to the extracellular environment. Humans express two Pmr1p homologues: SPCA1 functions in both calcium and manganese transport of diverse cell types (Ton et al., 2002; Fairclough et al., 2003; Missiaen et al., 2004) and SPCA2 is expressed specifically in the brain (Xiang et al., 2005). In particular, SPCA2 does not function in calcium transport but has specifically evolved for manganese homeostasis (Xiang et al., 2005). The central nervous system is particularly vulnerable to manganese toxicity and SPCA2 has been implicated as a major player in manganese detoxification in the brain (Xiang et al., 2005). The role of the secretory pathway in manganese homeostasis and detoxification is conserved among eukaryotes and is of particular relevance in cases of manganese neurotoxicity in humans.

1.5.9 Role of manganese in neurodegenerative disorders

Enzymes in both neurons and glia function only in presence of manganese. These manganese-binding proteins, referred to as manganoproteins, include glutamine synthase, superoxide dismutase 2 (SOD2), arginase, pyruvate decarboxylase and serine/threonine phosphatases (Christianson 1997; Takeda 2003; Bowman 2010). In particular, glutamine synthetase (GS), the most abundant manganoprotein, is predominantly expressed in astrocytes where it converts glutamate to glutamine. GS

contain manganese and this metal is able to regulate the GS activity (Wedler and Denman 1984). Indeed, insufficient manganese increases glutamate trafficking, glutamatergic signalling and excitotoxicity (Maciejewski and Rothman 2008). In addition, individuals with manganese deficiency are more susceptible to seizures due in part to decreased GS levels and/or activity (Eid et al., 2008). Arginase regulates elimination of ammonia from the body by converting L-arginine, synthesised from ammonia, L-ornithine and urea as part of the urea cycle. Moreover, in the brain, L-arginine is converted to nitric oxide by neuronal nitric oxide synthetase. Proper regulation of arginase promotes neuronal survival by impairing nitric oxide signalling (Ash et al., 2000; Estevez et al., 2006). Pyruvate carboxylase is an essential enzyme required for glucose metabolism that interacts with manganese to generate oxaloacetate, a precursor of the tricarboxylic acid (TCA) cycle (Mildvan et al., 1966). Interestingly, in the brain, pyruvate carboxylase is predominantly expressed in astrocytes in order to support the high-energy demand of the neurons (Yu et al., 1983; Zwingmann et al., 2003).

Manganese can cross the blood-brain barrier (BBB) and blood-cerebrospinal fluid barrier (BCB) through several carriers and in different oxidation states. Given the essential functions of manganese and the neurotoxicity associated with manganese overload, the absorption and transport of this metal is stringently regulated.

Several manganese transporters, at the BBB have been characterised. Manganese can be transported via the divalent metal transporter 1 (DMT1), the transferrin receptor (TfR) that mediate trivalent Fe uptake, the divalent metal/bicarbonate ion symporter ZIP8 and ZIP14, various calcium channels, the solute carrier-39 (SLC39), park9/ATP13A2, the

magnesium transporter hip14 and the transient receptor potential melastatin 7 (TRPM7) channels/transporters (Murphy et al., 1991; Rabin et al., 1993; Aschner and Gannon 1994). The divalent metal transporter 1 (DMT1) is a member of the family of natural resistance-associated macrophage proteins (NRAMP) and play a crucial role for the maintenance of essential metal homeostasis in the brain (Gunshin et al., 1997; Garrick et al., 2003; Mackenzie and Hediger 2004). DMT1 is also known as the divalent cation transporter (DCT1) due to its ability to transport divalent metals including Zn^{2+}, Mn^{2+}, Co^{2+}, Cd^{2+}, Cu^{2+}, Ni^{2+}, Pb^{2+} and Fe^{2+} across the plasma membrane into the cytoplasm (Gunshin et al., 1997; Forbes and Gros 2003). In addition, two different isoforms of DMT1 are present and both localise at the plasma membrane; however, one of them localises also to late-endosomes and lysosomes and the other localises to early-endosomes (Au et al., 2008).

In the last decade there has been an increasing interest in the identification of novel Mn transporters including Hip14 and the product of *park9* gene. The huntingtin-interacting protein 14 and 14L (Hip14 and Hip14L) mediates the transport of Mn^{2+} and other divalent metals across the cell membrane (Goytain et al., 2008; Gitler et al., 2009). Hip14 is involved in the palmitoylation of several neuronal protein including huntingtin (Au et al., 2008). In addition, it is required for endo- and exocytosis, as well as targeting of cysteine string protein (CSP) and synaptosomal-associated protein 25 (SNAP25) to the synapse (Singaraja et al., 2002; Ohyama et al., 2007). Hip14 localises in the presynaptic terminal, Golgi complex and vesicular structure localised in the axon, dendrites and soma of neurons (Stowers and Isacoff 2007). The *park9* gene responsible for the Kufor-Rakeb syndrome (KRS), a rare parkinsonian phenotype with juvenile onset, also transports Mn (Gitler et al., 2009). The *park9* gene encodes a putative P-type

transmembrane ATPase (ATP13A2) protein. Although the exact function of *park9* is unknown, it is generally thought to be a shuttle for cations, including Mn, across the cell (Ramirez et al., 2006). Recently, in a family with a typical NCL pathology exome sequencing has been performed revealing a single homozygous mutation in ATP13A2. NCL and KRS may share etiological features and implicate the lysosomal pathway in Parkinson's disease (Bras et al., 2012). Furthermore, manganese has been shown to be involved in the pathogenesis of CLN6 disease. In particular, the expression level and activity of the manganese-dependent superoxide dismutase (MnSOD) were increased in the sheep CLN6 model as well as humans affected by CLN6 disease (Heine et al., 2003). Recently, studies conducted on ovine CLN6 model revealed and increase in Zn and Mn concentrations in the brain. The regions most affected are those where neuroinflammation and neurodegeneration occur. In addition, synaptic proteins, the metal-binding protein metallothionein, and the Akt/GSK3 and ERK/MAPK cellular signalling pathways were also altered (Kanninen et al., 2013a). The metals accumulation has been detected also in the CLN6 mouse model. Furthermore, increased expression of the ER/Golgi-localized cation transporter protein, Zip7, was detected in cerebellar Purkinje cells and whole brain fractions. Further analysis revealed biometal accumulation in CLN6 brain fractions expressing markers for ER, Golgi, endosomes and lysosomes. These data link CLN6 expression and biometal homeostasis in CLN6 disease, and support altered cation homeostasis regulation as a key factor in NCL pathogenesis (Kanninen et al., 2013b).

In the last few years there has been a growing interest in understanding the metabolism of neurotoxic metals and their influence on different neurodegenerative diseases, including manganism, Wilson’s disease, PD and AD. These metals also contribute to

Huntington's disease though fewer studies have investigated the link. Occupational and environmental exposure to neurotoxic metals including Zn^{2+}, Mn^{2+}, Hg^{2+}, As^{2+}, Cr^{2+}, Ni^{2+}, Pb^{2+} and Al^{3+} have been associated with neurodegeneration and modulation of the age of onset and severity in neurodegenerative diseases. The brain is able to regulate the homeostasis of these metals in physiological conditions; however, excessive exposure can cause their accumulation in the brain. The distribution of metals in the brain is not uniform, and accumulation in specific brain regions reflects neurotoxicity. For example, Mn accumulation and neurotoxicity in the globus pallidus cause manganism (Robison et al., 2012). Alterations in metal homeostasis have been suggested to cause neurodegeneration via association of metals with proteins and induction of aggregates formation (Tamas et al., 2014). Moreover, metals can cause neurodegeneration through a vicious cycle by disrupting mitochondrial function (Perier and Vila 2012), which deplete ATP, induces ROS production leading to cell death by apoptosis and/or necrosis.

1.6 Endoplasmic reticulum (ER) stress response

The ER is the first compartment in the secretory pathway, which is responsible for the synthesis, modification and delivery of active proteins to their targets. As with other biochemical pathways, flux through the secretory pathway is controlled at its early steps. The ER is the entrance site for most of the proteins processed in the secretory pathway. Within the ER the early steps of the protein maturation process are taking place, such as: the folding of the nascent polypeptide chains and posttranslational modifications important for the correct folding and function of the protein. If the influx of nascent unfolded polypeptides exceeds the folding and processing capacity of the ER the homeostasis of the ER would be perturbed. Under these ER stress conditions a signalling pathway is active, known as the unfolded protein response.

The ER has a fine mechanism to ensure that only properly folded proteins exit the ER, a process termed ‘quality control’. Therefore, an important aspect of this control is the ability to discriminate between folded, misfolded and unfolded polypeptides. The protein folding status is relayed to the cytosol and nucleus by the UPR. In case of stress, in order to bring the folding capacity of the ER in line with the folding demand on the ER, the folding demand is decreased and the folding capacity of the ER increased. To decrease the folding demand, the transcription of genes encoding secretory proteins (Harding et al., 1999) is downregulated and the misfolded protein cleared through the ER-associated degradation (ERAD) is increased (Travers et al., 2000). To increase the folding capacity of the ER, the synthesis of the chaperones is increased (Kozutsumi et al., 1988) and the ER increases in size to dilute the increased unfolded protein load and to host more chaperone machineries (Dorner et al., 1989; Schuck et al., 2009).

Upon ER stress, three independent branches sense stress, with the inositol-requiring

enzyme 1 (IRE1) branch being the most highly conserved among eukaryotes. In yeast only the IRE1 pathway is found while metazoans use two additional pathways: double stranded RNA-activated protein kinase-like ER kinase (PERK) and activating transcription factor 6 (ATF6). These ER-localised proteins are able to sense ER stress resulting in the activation of different pathways. Translational depletion and activation of UPR genes are the most common outputs. However, the UPR can lead to apoptosis if the cells fail to reach homeostasis and undergo prolonged stress. Early work on the UPR was performed in cells where the expression of ER-resident chaperones, such as Bip/GRP78, GRP94, PDI/ERp59 and Erp72, were shown to be induced by different treatments causing the accumulation of unfolded proteins in the ER (Kozutsumi et al., 1988; Dorner et al., 1990).

1.6.1 The UPR in fission and budding yeast

In *S. cerevisiae* ER stress is monitored by the transmembrane sensor protein Ire1. Ire1 is activated by either direct binding of unfolded proteins or from the release of the molecular chaperone Bip/GRP78 from the luminal domain of Ire1. After its activation, Ire1 oligomerises followed by *trans*-autophosphorylation through its cytosolic kinase domain (Shamu and Walter 1996). When Ire1 is activated, its cytosolic ribonuclease domain cleaves the intron of the pre-mRNA *HAC1* to initiate the synthesis of Hac1 transcription factor (Cox et al., 1993; Mori et al., 1993; Cox and Walter 1996). The UPR can alleviate stress by reversing severe dysfunctions through the upregulation of nearly 400 genes (Thibault et al., 2011). These target genes include ER chaperones, lipid biosynthesis enzymes and ER associated degradation (ERAD) machinery. The

UPR program is adaptable and might be remodeled according to the needs of the cells. This differential regulation of the UPR, from different stressors, suggests the involvement of additional unknown regulatory factors (Thibault et al., 2011). The UPR protein Ire1 is conserved also in *S. pombe* (Wood et al., 2002) and despite having no *HAC1* orthologue, Ire1 still plays a crucial role in alleviating ER stress (Frost et al., 2012; Kimmig et al., 2012). In *S. pombe* Ire1 degrades ER-localised mRNAs to alleviate the protein load in a pathway known as regulated Ire1-dependent decay (RIDD). This pathway was first identified in metazoa where Ire1 degrades mRNAs (Hollien and Weissman 2006; Hollien et al., 2009). Moreover, certain mRNAs cleaved by Ire1 in *S. pombe*, are stabilized instead of being degraded (Kimmig et al., 2012). Indeed, *Bip1* mRNA, which encodes an HSP70 family protein, is cleaved by Ire1 and it remains stable and its translation is increased. Other players are likely to work in synergy with Ire1 to regulate the UPR pathway. In particular the UDP-glucose-glycoprotein glucosyltransferases (UGT) and a calnexin orthologue (*cnx1*) have been identified and they can recognise only misfolded protein and are essential under extreme ER stress in *S. pombe* (Sousa and Parodi 1995; Fanchiotti et al., 1998). Those findings helped to better understand the ER stress response in yeast and elucidate the similar pattern in higher organisms.

1.6.2 The UPR in mammals

The ER is a major protein-folding compartment in eukaryotic cells and is second only to the cytosol. Many principles governing the protein folding in the cytosol apply to the ER. However, the protein folding in the ER is more complex than protein folding in the cytosol because proteins are posttranslationally modified by N-glycosylation and

disulphide bond formations. The protein folding in the ER has to fulfill thermodynamic and kinetic requirements (Dobson et al., 1998).

The protein folding machinery of the ER consists of three classes of proteins, foldases, molecular chaperones and the lectins (Calnexin [CNX], Calreticulin [CRT]). Foldases catalyse steps in protein folding and molecular chaperones facilitate protein folding by shielding unfolded regions from surrounding proteins. The ER-resident chaperones are the HSP70 chaperones Bip/GRP78, LHS1/GRP170 (Lin et al., 1993), their co-chaperones of the DnaJ (Feldheim et al., 1992) and GrpE families (Boisrame et al., 1998) and the HSP90 chaperone GRP94 (Steel et al., 2004). In particular, the GRP94 recognises partially folded proteins, which are recognized as being unfolded by Bip/GRP78 (Argon and Simen 1999). Bip/GRP78 bound to an unfolded protein does not facilitate protein folding indeed it maintains the protein in a folding-competent state. Bip/GRP78 has an N-terminal ATPase and a C-terminal binding domain. In the ATP-bound state, Bip/GRP78 binds substrates with low affinity. Substrate binding triggers the ATPase activity of Bip/GRP78 to generate ADP. The ADP-bound state of Bip/GRP78 has high affinity for the bound peptide (Gething 1999). In particular, Bip/GRP78 preferentially binds the short hydrophobic peptides such as those forming β-strands that are deeply buried in the protein core (Gething 1999). Therefore, the exposure of hydrophobic regions is the thermodynamic hallmark of an unfolded protein. Exchange of ADP with ATP releases the substrate from Bip/GRP78, which is free to progress on its folding pathway.

Prolonged interaction of a folding protein with the chaperone machinery activates three ER-resident transmembrane proteins; three different ER stress transducers that facilitate the activation of the UPR (Walter and Ron 2011). Those transducers are activating

transcription factor 6 (ATF6), the inositol requiring kinase 1 (IRE1) and double-stranded RNA-activated protein kinase (PKR)-like ER kinase, which then transduce an unfolded protein signal across the ER membrane and eventually Ca^{2+} is released from the ER to activate apoptotic signalling pathways.

Two forms of IRE1 are present in mammals where IRE1α is expressed ubiquitously while IRE1β is expressed only in the intestinal and lung epithelium (Bertolotti et al., 2001; Martino et al., 2013). In humans, IRE1α and IRE1β are encoded by *ERN1* and *ERN2* respectively. The transcription factor downstream of IRE1α, XBP1, has variance in its primary aminoacid sequence with Hac1 but shares the common Ire1-mediated splicing activation of its mRNA and the basic leucine zipper motif. XBP1 activates similar downstream target genes as Hac1 in yeast (see paragraph 1.6.1), with the induction of genes involved in protein folding (Yoshida et al., 2001). In addition, IRE1-XBP1 pathway is important for the activation of major chaperones as Bip/GRP78 and GRP94 (Ozcan et al., 2004).

PERK, which is an ER transmembrane kinase, mediates transcriptional and translational control of the UPR (Harding et al., 1999). Upon ER stress, PERK oligomerises and phosphorylates itself together with eIF2α. eIF2α phosphorylation results in temporary attenuation of the overall protein translation and upregulation of the transcription factor ATF4. This translation inhibition decreases the influx of proteins entering the ER, reducing ER protein folding load and alleviating ER stress. Certain mRNAs are translated when eIF2α when is limiting, one of which is transcription factor ATF4. Subsequently, ATF4 upregulates C/EBP homologous protein and DNA damage-inducible 34 (GADD34). CHOP promotes ER stress-induced apoptosis (Zinszner et al., 1998) and GADD34 is involved in a negative feedback loop to counteract PERK by

dephosphorylation of eIF2α, which resumes protein synthesis and trigger apoptosis (Marciniak et al., 2004). Interestingly, PERK inhibits also ER-stress induced apoptosis through the induction of cellular inhibitors of apoptosis protein (cIAPs) (Hamanaka et al., 2009), and is a critical cross-talk regulator to influence the UPR in determining the cell fate under ER stress (Brewer 2014). In addition, the activation of PERK could lead to downregulation of anti-apoptosis protein XIAP, which could lead to increase in apoptosis (Hiramatsu et al., 2014). Upon accumulation of unfolded proteins, ATF6 is packaged into vesicles and transported to the Golgi complex (Schindler and Schekman 2009). The cleavage of both ATF6 luminal and transmembrane domains occurs subsequently by SP1 and SP2 proteases, liberating the N-terminal cytosolic fragment, ATF6(N), for localisation into the nucleus to activate the UPR target genes (Yoshida et al., 2000). Many different genes are activated downstream of ATF6(N). In particular, ATF6(N) activate the transcription of Bip/GRP78, protein disulphide isomerase (PDI) and glucose-regulated protein 94 (GRP94). Moreover, ATF6(N) is a major inducer for downstream response of ER chaperones and ERAD components (Okada et al., 2002; Adachi et al., 2008).

If the aforementioned pro-survival mechanisms fail to rescue the cell then apoptosis can occur. It is not clear at which point the switch between pro-survival and pro-apoptotic signalling occurs, nor are the mechanisms underlying cell death fully explained. It is well known that the apoptotic signals generated from excessive activation of the UPR converge on the mitochondria resulting in opening the permeability of the transmembrane pores and loss of mitochondrial membrane potential ($\Delta\psi_m$) with consequent release of pro-apoptotic factors and activation of apoptosis through the apoptosome which is formed by the apoptotic protease activating factor 1 (Apaf-1) with pro-caspase 9 and cytochrome *c* (Olson and Kornbluth 2001; Szegezdi et al., 2009).

1.6.3 ER stress and UPR in neurodegenerative disorders

Death of neurons, like that of other cells, is regulated by two pathways (Mattson 2000; Yuan et al., 2003). The extrinsic pathway is triggered by the activity of cell membrane death receptors through activation of caspase 8 that cleaves downstream substrate including other caspases (Degterev et al., 2003; Danial and Korsmeyer 2004). The intrinsic pathway is activated by different stressors, the signals triggered by the intrinsic pathway converge on the mithocondria causing changes in the membrane potential and release of pro-apoptotic factors (Olson and Kornbluth 2001; Szegezdi et al., 2009). In particular, in neuronal cells the extrinsic pathway plays a less prevailing role compared with other cell types.

To contrast cell death, neurons express a variety of anti-apoptotic factors that counteract cell degeneration caused by both environmental and genetic insults (Mattson 2000; Yuan et al., 2003). The Bcl-2 family consists of both anti-apoptotic proteins such as Bcl-2 and Bcl-xL, and pro-apoptotic factors such as Bax, Bak and Bik (Danial and Korsmeyer 2004). Bcl-2 controls the integrity of the mitochondrial membrane under normal conditions (Danial and Korsmeyer 2004). The pro-apoptotic protein Bik is largely localised to the ER (Germain et al., 2002). In addition, Bim translocates to the ER membrane and is important for ER stess-mediate cell death (Morishima et al., 2004). However, little is known, so far, about the roles of those pro-apoptotic proteins in ER stress-induced neuronal death or in human neurodegenerative disorders. However, studies have confirmed a pathogenetic role of ER stress in neurodegenerative disorders. Indeed, ER stress in conjuction with abnormal protein degradation can contribute to the pathophysiology of Parkinson's disease (Kuang et al., 2014) as well as in Alzheimer's disease together with disturbed calcium homeostasis (LaFerla 2002; Katayama et al., 2004; Verkhratsky 2005), and also in the Amyotrophic lateral sclerosis (Wootz et al.,

2004).

In lysosomal storage disease (LSD) ER stress has been shown to play a role in pathophysiology. There are at least 45 different disorders classified as LSD. In G_{M1}-gangliosidosis, the ER stress and the UPR response were shown to accompany the disease (Tessitore et al., 2004). Indeed, there is an upregulation of Bip/GRP78, CHOP and the activation of caspase 12 and JNK2 pathaways causing cell death.

In LINCL and progressive epilepsy with mental retardation (EPMR) caused by mutations in *CLN8* gene, which encode a protein that localises to the ER, ER stress plays a crucial role in the pathogenesis. Indeed, it has been shown that Bip/GRP78, CHOP, ATF6 are upregulated and caspase 12 activation in CNS and retina of the $CLN8^{mnd}$ mouse model, suggesting that ER-stress combined contribute to the progression of the disease in CNS structures (Galizzi et al., 2011).

In view of this, it is important to know more about the role of the ER stress in neurodegenerative disorders. In particular, which step of the ER stress is peculiar to each neurodegenerative disease and which step of the ER stress response to target and at what particular stage of the disease.

1.7 Project aims

CLN3 is a multi-pass transmembrane protein, which is conserved in single-celled eukaryotes such as the fission yeast *S. pombe*, suggesting a fundamental role for this protein in eukaryotic cells. CLN3 has been functionally linked to many diverse cellular processes, including lysosomal homeostasis, autophagy, lipid synthesis or modification and cytoskeleton organisation. Despite these endeavours, the function of CLN3 remains elusive. However, recent works have shown that Btn1p, in yeast, localises at the Golgi complex and its deletion affects trafficking of the vacuolar sorting protein 10 (Vps10p) and depletion of CLN3 affects the trafficking of mannose 6-phosphate receptor in mammalian cells. Since the Golgi complex play a pivotal role in the cellular homeostasis maintenance and regulation. The lack of Golgi homeostasis regulation would explain most of the aforementioned phenotypes observed in CLN3/Btn1p models. In particular the topology of CLN3 suggests a role as ions transporter, either calcium or manganese, which both play a fundamental role within the Golgi complex. Therefore, the aim of this project is to clarify the role of CLN3 and Btn1p at the Golgi complex in yeast and mammalian cells and how this is affected in CLN3 disease. My results will be directly relevant for the understanding of JNCL and may have a wider impact on the identification of new targets suitable for therapeutic intervention in JNCL as well as uncover new roles of the Golgi complex within the cell. Furthermore, they also may be relevant to understanding the molecular basis of NCLs caused by mutations in CLN6 and CLN8 proteins, which are located upstream of the Golgi apparatus, in the endoplasmic reticulum.

Chapter two

Materials and Methods

2.1 Materials

2.1.1 List of reagents

Listed here are frequently used reagents, including information about the manufacturer and whether they were stored as a stock solution.

Acrylamide (30% acrylamide/ 0.8% bis-acrylamide): Sigma

Agar: Sigma

Alloxazine: Sigma

Ammonium chloride: Sigma

Ampicillin: Sigma

APS (ammonium Persulphate): Sigma

Beta-mercaptoethanol (BME): Sigma

Bromophenol blue: Sigma

Albumin fraction V from bovine serum (BSA): VWR

Complete, Mini, EDTA-free: Roche

DAB (TAAB):

DDSA: TAAB

DMEM: GIBCO® Life Technologies

DMP-30: TAAB

DMSO: Sigma

DNA marker: 1-kb ladder (Promega)

DNA marker: 100 bp ladder (Promega)

DO mix: Formedium

DO supplements: Formedium

E64: Sigma

Enhanced Chemo-luminescence (ECL): Pierce® ECL, Thermo Scientific

ECL+: SuperSignal® west femto, Thermo Scientific

Foetal bovine serum (FBS): Sigma

Fluoroorotic Acid (FOA): Sigma

Glucose: Formedium

Glycine: Sigma

Hydrochloric acid (HCl): Sigma

Isopropanol: Fisher Scientific

Manganese chloride ($MnCl_2$): Sigma

Metafectene®Pro: Biontex Laboratories, GmbH

Methanol: Fisher Scientific

MNA: TAAB

Osmium tetraoxide: TAAB

PFA (paraformalaldehyde): Sigma

Penicillin/streptomycin: Sigma

Phenylmethanesulfonylfluoride (PMSF): Cell Signalling

Ponceau red: Sigma

Potassium ferricyanide:

Prochlorperazine dimaleate: Sigma

Propylen oxide (PO): Sigma

Protease inhibitor mix: Roche

PVDF: BioRad

Rainbow protein marker: Thermo Scientific

RIPA buffer 10X: Cell Signalling

Saponin: Sigma

SDS: BDH

SOC media: Invitrogen

Sodium Cacodylate: Sigma

Sodium chloride (NaCl): Sigma

Sodium hydrogen phosphate (Na_2HPO_4): Sigma

Sodium hydroxide (NaOH): Sigma

SYBR green: Thermo Scientific

TAAB resin: TAAB

Tannic acid: TAAB

TEMED: Sigma

Tris base: Sigma

Triton-X: Sigma

Trypsin: Sigma

Tween-20: Sigma

Yeast extract: Formedium

2.1.2 Mammalian cells culture

2.1.2.1 Cell type/lines used

Cell line	Species	Transformed/primary	Source
HeLa	Human	Transformed	Mole lab stock
Fibroblasts	Human	Primary	Mole lab and others

***Table* 2.1.2.1.1 –** cell lines used

2.1.2.2 Fibroblast cell lines used

Code	Diagnosis	Gene	Mutation	Source
HF523N	Healthy control	-	Cell line established 5.7.05	Elaine Aegius, Mole Lab
HF524N	Healthy control	-	Cell line established 5.7.05	Elaine Aegius, Mole Lab
HF526N	Healthy control	-	Cell line established 5.7.05	Elaine Aegius, Mole Lab
HF527N	Healthy control	-	Cell line established 5.7.05	Elaine Aegius, Mole Lab
HF470Pa	JNCL	CLN3	1-kb/1-kb	GOS
HF478Pa	JNCL	CLN3	1-kb/1-kb	Kohlschutter
HF480Pa	JNCL	CLN3	1-kb/1-kb	Kohlschutter
HF481Pa	JNCL	CLN3	1-kb/1-kb	Kohlschutter
HF338Pa HF338Pb	vJNCL	CLN3	Deletion exons 9-15	Isabella Carreira, Portugal
HF423Pa HF423Pb	vLINCL	CLN6	c.316insC/c.316insC p.[Arg106fs]+[Arg106fs]	France/GOS Sent to Simonati.
HF471Pa	VLINCL	CLN6	E72X/E72X p.[Glu72X]+[Glu72X]	Costa Rica/Boustany
HF170Pb	cLINCL	CLN2	IVS5-1G>C/IVS5-1G>C	GOS
HF532Pa	LINCL	CLN2	Q509X/Q509X	Santorelli. Italy
HF467Pa	vLINCL	CLN7	c.881C>A p.Thr294Lys homoz	Elleder Sent to Gasnier
HF474Pa	vLINCL	CLN7	c.1393C>T p.Arg465Trp homoz	Greece Sent to Gasnier
HF469Pa	INCL	CLN1	R151X/R151X	GOS

HF530Pa	INCL	CLN1	L222P/L222P	Santorelli. Italy
HF534Pa	vLINCL	CLN8	A30P/A30P	Santorelli. Italy
HF535Pa	vLINCL	CLN8	Y158C/c.66delG	Santorelli. Italy, Cannelli et al neurogenetics 2006
HF484Pa HF484Pb	vLINCL	CLN5	c.35G>A p.Arg112His; c.619T>C p.Trp207Arg	Guys Hospital/ Ruth Williams
HF546Pa	VLINCL	CLN5	homozygous for c.1072-1073delTT	Mewasingh, Leicester, line made by CK

***Table* 2.1.2.2.1-** Human fibroblasts used in this project

2.1.2.3 Cell culture media

Growth medium composition	
DMEM	500ml
Penicillin/streptomycin	5ml
Foetal bovine serum	50ml
Freezing medium	
DMSO	10ml
FBS	80m

***Table* 2.1.2.3.1 –** cell culture media used

2.1.3 siRNA, plasmids and qPCR primers

2.1.3.1 Primers, siRNA and plasmid used

Primers (qPCR)		
CLN3	F	GTACCAGGCTGGCGTCTTT
	R	AGGAACACCAGGTTGAGGC
CLN6	F	CAGCACCTGGGAGCGAC
	R	AGAACCAGAGGTCGAGGTGG
GAPDH	F	AAGGTGAAGGTCGGAGTCAAC
	R	GGGGTCATTGATGGCAACAATA
siRNA		
CLN3	sense	GGUCGGAGAGGGAAGCCCUUdTdT
	Anti-sense	AAGGGCUUCCCUCUCCGACCdTdT
CLN6-1	sense	CCGGUCUCUUCCUCGGAAAdTdT
	Anti-sense	UUUCCGAGGAAGAGACCGGdTdT
CLN6-2	sense	CCAGAGACCGAGAGCAUGAdTdT
	Anti-sense	UCAUGCUCUCGGUCUCUGGdTdT
Plasmids		
Btn1		pREP42GFP-Btn1
NatMX		pFA6a
Genomic integrants		pSL1180

***Table* 2.1.3.1.1 –** primers used for qPCR and siRNA sequences used for gene depletion and plasmids used.

2.1.4 qPCR reaction and FastStart PCR

qPCR (20 µL total volume for each reaction)	
SYBR green master mix	10 µl
Primer pairs (1.2 µM)	5 µl
cDNA	10 µl
Filter-sterile ddH_2O	3 µl

***Table* 2.1.4.1 –** reagents added for each qPCR reaction

FastStart PCR	
10X buffer + Mg^{2+}	10µl
DMSO	1.5µl
dNTPs	2µl
Sense primer	4µl
Antisense primer	4µl
DNA	1µl
FastStart polymerase	0.3µl
H_2O	81.5µl

***Table* 2.1.4.2 –** reagents added for each Fast Start PCR reaction

2.1.5 Protein extraction and SDS-page

2.1.5.1 List of antibodies used

Name	Description	Application	Dilution	Source
GM130	Anti-GM130, cis-Golgi marker	IF	1:700	BD Transduction laboratories
GRP78	ER stress marker	WB	1:1000	Abcam
GPP130	Anti-GPP130, protein Mn^{2+}, monoclonal mouse	WB	1:1500	Santa Cruz
CHOP/GADD153	ER-stress marker, monoclonal mouse	WB	1:1500	Santa Cruz
Giantin	Medial-Golgi marker	IF	1:1000	Abcam
TGN46	TGN marker sheep	IF	1:1500	AbD Serotec
ϒ-adaptin	Mouse	WB	1:1000	BD Transduction laboratories
Caspase 2	Monoclonal rabbit	WB	1:1000	Abcam
β-tubulin		WB	1:1000	Santa Cruz
EGFR	monoclonal rabbit	WB	1:1000	Santa Cruz

***Table* 2.1.5.1.1 -** Primary antibodies. WB: western blot, IF: indirect immunofluorescence.

Name	Tag	Application	Dilution	Source
Goat anti-mouse	HRP	WB	1:1000	Santa Cruz
Goat anti-rabbit	HRP	WB	1:1000	Promega
AlexaFluor488	Mouse, rabbit, sheep	IF	1:700	Invitrogen
AlexaFluor534	Mouse, rabbit, sheep	IF	1:700	Invitrogen

***Table* 2.1.5.1.2 -** Secondary antibodies. WB: western blot, IF: indirect immunofluorescence.

2.1.5.2 Mammalian cells lysis buffer

Lysis buffer
RIPA 1X (50mM Tris pH7.8; 150mM NaCl; 1% NP40; 0.5% Na deoxycholate; 0.1% SDS) Protease inhibitor cocktail (Complete, Mini, EDTA-free)(1 tablets every 10mL of RIPA 1X) PMSF 200mM (working concentration 1mM)

***Table* 2.1.5.2.1 –** Lysis buffer composition

2.1.5.3 Laemmli buffer

2X (50mL)	
1M Tris-HCl pH6.8	25 ml
10% SDS	15 ml
0.8% BME	10.4g
Bromophenol blue	
Aliquots and store at -20°C	

***Table* 2.1.5.3.1 –** Sample buffer composition

2.1.5.4 Protein gel buffers

Running Buffer (per litre)	
Tris-base	3g
Glycine	14.4g
10% SDS	10 ml

***Table* 2.1.5.4.1 –** Running buffer composition

Half Towbin transfer buffer (per litre)	
Tris-base	1.45g
Glycine	7.2g
Methanol	100 ml
10% SDS	500 µl

***Table* 2.1.5.4.2 –** Transfer buffer composition

2.1.5.5 Protein gels

Resolving gel	**7.5%**	**12%**
30% acrylamide/bis-acrylamide	2.5 ml	4 ml
1.5M Tris-HCl pH8.8	2.5 ml	2.5 ml
10% Ammonium Persulphate (fresh)	0.05 ml	0.05 ml
10% SDS	0.1 ml	0.1 ml
TEMED	0.02 ml	0.02 ml
Water	4.84ml	3.34ml
Stacking gel		
30% acrylamide/bis-acrylamide	1.3 ml	
0.5M Tris-HCl pH6.8	2.5 ml	
10% Ammonium Persulphate (fresh)	0.05 ml	
10% SDS	0.1 ml	
TEMED	0.02 ml	
Water	6 ml	

***Table* 2.1.5.5.1 -** Gel casting

2.1.6 *S. pombe* strains and maintenance

2.1.6.1 *S. pombe* strains used

Standard nomenclature has been used in this thesis to describe all the *S. pombe* used. SP23 is an auxotrophic wt strain, lacks adenine, leucine and uracil (Obtained from Kazu Tomita). This strain has been used to create SP29, in which *btn1* has been replaced with the NatMX cassette in order to generate the *btn1* deleted strain.

Strain	Genotype
SP23	*h-, Leu1-31, ura4-D18, ade6-M210*
SP29	*h-, btn1::NatMX, Leu1-31, ura4-D18, ade6-M210*

Table* 2.1.6.1.1 –** Fission yeast strains. **::** replacement, ***h- mating type (M type), **-** fusion.

2.1.6.2 Growth media

Yeast Extract with supplements (YES) liquid media (500 ml)	
Yeast extract	2.5g
Glucose	12.5g
Leucine	250mg
Adenine	250mg
Uracil	250mg
Histidine	250mg

***Table* 2.1.6.2.1 –** Liquid rich medium composition

Yeast Extract with supplements (YES) solid media (500 ml)	
Yeast extract	2g
Glucose	10g
Bacto agar	8g
Leucine	200mg
Adenine	200mg
Uracil	200mg
Histidine	200mg

***Table* 2.1.6.2.2 –** Solid rich medium composition

AA plates	
Bottle 1:	
Water	250ml
DO mix	750mg
Do supplements	250mg
Yeast nitrogen base	850mg
Ammonium sulphate	2.5g
Bottle 2:	
Water	300ml
Glucose	12g
Bacto Agar	8.5g
Sonicate bottle 1 and autoclave both bottles	
Pour bottle 2 down to 250ml and add bottle 2 to bottle 1, mix and pour	

***Table* 2.1.6.2.3** – AA plates composition.

FOA plates	
Bottle 1:	
FOA	437mg
Uracil	50mg
AA supplements	250mg
Yeast nitrogen base	850mg
Ammonium sulphate	2.5g
DO mix	750mg
Water	250ml
Bottle 2:	
Water	300ml
Glucose	12g
Bacto Agar	8.5g
Sonicate bottle 1 and warm to 50°C, autoclave bottle 2	
Pour bottle 2 down to 250ml and add bottle 2 to bottle 1, mix and pour	

***Table* 2.1.6.2.4** – FOA selective plate composition.

Minimal Medium (MM) (500ml)	
Water	440mL
NH_4Cl	l2.5g
Na_2HPO_4	1.1g
Potassium hydrogen phthalate	1.5g
Adenine	250mg
Uracil	125mg
Leucin	125mg
Autoclave and cool and add:	
20% Glucose	50mL
Stock salts[1]	10mL
Stock vitamins [2]	500µL
Stock minerals[3]	50µL

***Table* 2.1.6.2.5 –** Minimal medium composition

Stock salts[1] (50X) 500mL	
$MgCl_2.6H_2O$	26.25g
$CaCl_2$.$2H_2O$	367mg
KCl	25g
Na_2SO_4	1g
Autoclave and store at 4°C	

Table 2.1.6.2.6 – 50X stock salts solution

Stock vitamins[2] (1000X) 100mL	
Pantothenic acid	100mg
Nicotinic acid	1g
Inositol	1g
Biotin	1mg
Filter sterilized and store at 4°C	

***Table* 2.1.6.2.7 –** 1000X vitamins stock solution

Stock minerals[3] (10000X) 100mL	
Citric acid	1g
Boric acid	500mg
$MnSO_4 .H_2O$	500mg
$ZnSO_4 .H_2O$	400mg
$FeCl_3 .6H_2O$	200mg
Molybidic acid	305mg
KI	100mg
$CuSO_4 .5H_20$	40mg
Add in order shown, filter sterilized and store at 4°C	

***Table* 2.1.6.2.8 –** 10000X minerals stock solution

2.2 Methods

2.2.1 Cell culture and maintenance

HeLa cells and Human fibroblast cell lines (tables 2.1.2.1.1 and 2.1.2.2.1) were cultured in Dulbecco's Modified Eagle's Medium (DMEM) supplemented with 10% complete foetal bovine serum (FBS), 1X penicillin-streptomycin (see Table 2.1.2.3.1). All cells were grown in incubators at 37°C in 5% CO_2. All cell cultures were passaged when they reached ~90% of confluence. Cells were washed twice in sterile PBS and detached from flasks using 5ml of 1X trypsin/EDTA per 75 cm² culture flask for 5 minutes at 37°C.

Cell lines were frozen and stored by re-suspending aliquots of $4x10^6$ cells in 1ml of freezing medium (see Table 2.1.2.3.1) in cryo-vials (1 ml/vial). Vials were slowly frozen (–80°C overnight) in isopropanol using a freezing container (Nalgene® Sigma), which provides the critical 1°C/min cooling rate required for successful cryo-preservation of cells, and transferred to liquid nitrogen after 24 hours.

2.2.2 siRNA Transfection of HeLa cells using Metafectene®Pro

The day before transfection HeLa cells were seeded in the culture vessel of choice in DMEM without FBS, so they would reach 80% confluency on the day of transfection. Cells were transfected with CLN3 or CLN6 siRNA (sequence table 2.1.3.1.1) using Metafectene®Pro (Biontex Laboratories GmbH). Before transfection, growing medium was removed and replaced with 0.8 ml of transfection medium (DMEM, serum and pen/strep free). A total of 5 µl of siRNA (Dharmacon, 20pmol/ µL) was added to 95 µl of transfection medium, and 6µl of Metafectene®Pro was added to 96 µl of transfection

medium in separate tubes. The two solutions were then combined together and incubated at room temperature for 30 min. For the control cells only Metafectene®Pro was added with no siRNA in order to check that the Metafectene®Pro is not toxic and any observed results are due to the depletion of the gene of interest. The 200 µl of siRNA- Metafectene®Pro complexes were added to the cells and, after gentle mixing, were incubated at 37°C with 5% CO_2 for 4 hours. Transfection medium was then replaced with normal growth medium and cells were allowed to recover for 72 hours before further experiments were performed.

2.2.3 Quantitative PCR (qPCR)

In order to assess the efficiency of gene knockdown by siRNA a qPCR was performed. In the following paragraph every step has been described.

2.2.3.1 RNA extraction from HeLa

RNA extraction was done with Qiagen Kits according to the manufacturer's instructions. Cells were lysed and passed through a QiaShredder and RNA extracted using an RNeasy mini kit. RNA was then eluted in RNase free water and stored at -20°C.

2.2.3.2 RNA reverse transcription

The extracted RNA was retro-transcribed using the QuantiTect reverse transcription kit (QIAGEN). Once the reverse transcription reaction was set up, the reaction tubes were incubated at 42°C for 15 minute. The reverse transcriptase was inactivate at 95°C for 3 minute. The cDNA was then stored at -20°C or kept on ice if being used immediately after the retro-transcription.

2.2.3.3 Endpoint PCR using FastStart polymerase

A total reaction volume of 50µl was used, containing 1µg of sense and antisense oligonucleotide primer each, and 10-50ng of template DNA. Deoxyribonucleoside triphosphates (dNTPs) (dATP, dCTP, dGTP and dTTP) were used at a final concentration of 0.2mM. The PCR cycle consisted of a denaturation step of 94°C held for 30 seconds, followed by an annealing step of between 40 and 60°C held for 60 s. The extension step (72°C) was held for 60 seconds per kilobase of product. 30 cycles of amplification were used per reaction. Reactions were concluded with 7 minutes incubation at 72°C to allow complete product extension.

2.2.3.4 qPCR calibration curve

The qPCR technique was used to quantify the amount of target template in a sample. In order to check the primer efficiency and sensitivity a qPCR on serially diluted samples (1:10) must be performed.

A PCR (40 cycles) was performed in order to generate a considerable amount of specific amplicons. Using the FastStart PCR protocol an end-point PCR was performed using the primers listed in table 2.1.3.1.1 using the cDNA made from the RNA extracted from the HeLa. The PCR product was separated in a 1% agarose in TAE gel against a 100bp DNA ladder. A unique band of the expected size has been cut and purified. The concentration of the amplicons was determined using the Nanodrop. Once the concentration in ng/µl was determined it was converted to copy number. The amplicon was diluted at $1x10^6$ and six 10X dilutions were made. So, the final dilution

contained only template copies. A qPCR was performed using the amplicon as template and the CLN3/CLN6 primers (Figure 2.2.3.4.1).

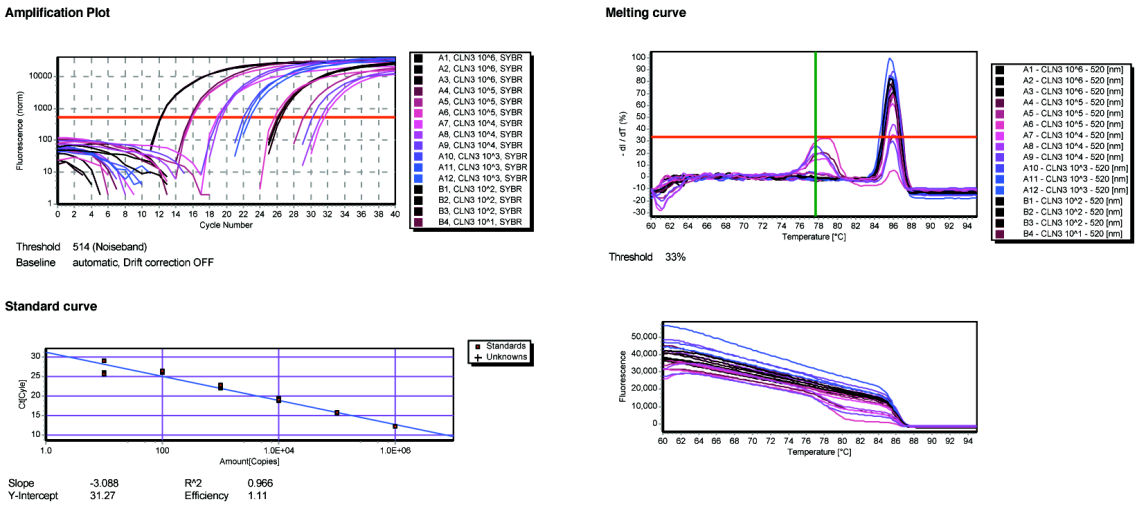

***Figure* 2.2.3.4.1** – qPCR calibration curve. Both primers (CLN3 and CLN6) efficiency and sensitivity were tested. qPCR was performed on serially diluted samples (1:10).

2.2.3.5 qPCR

The qPCR was performed (Eppendorf) with the reaction mixture shown in table 2.1.4.1. Knockdown efficiency was quantified in triplicate samples from each transfection experiment compared with the housekeeping gene GAPDH. Furthermore, Data have been analysed using the $2^{-\Delta\Delta C(T)}$ method (Livak and Schmittgen 2001). Samples were done in triplicates. The conditions are shown in figure 2.2.5.5.1.

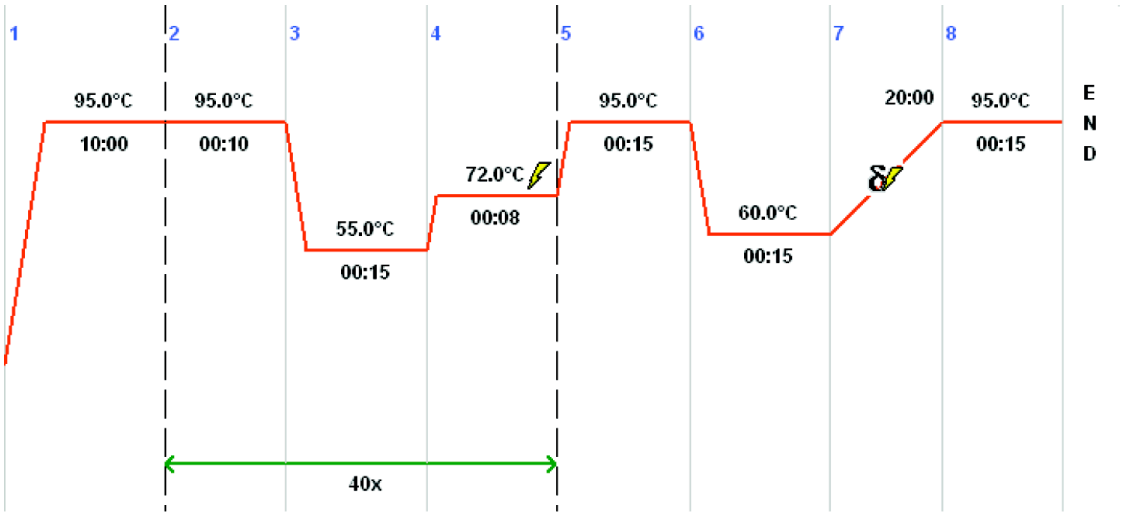

***Figure* 2.2.3.5.1** – qPCR conditions. The figure shows the qPCR set up, with melting curve (65-95°C) read every 0.5°C.

2.2.4 Manganese (Mn^{2+}) exposure

HeLa depleted for CLN3 and fibroblast cells were plated in 6 well plates for protein assessment and 24 well plate for indirect immunofluorescence and exposed to 500 uM Mn^{2+}. The cells exposed to Mn^{2+} were incubated at 37°C in 5% CO2 for 0, 1, 8 hours. After the time course the cells destined for protein assessment were harvested.

2.2.5 Indirect Immunofluorescence (IF)

The cell lines used for this project were observed using the confocal light microscope (LEICA SPE scanning confocal microscope) and fixed and stained using the following protocol.

The day before immunofluorescence (IF) HeLa depleted for CLN3 and CLN6 and the human fibroblast cell lines were seeded onto 20 mm diameter coverslips in complete DMEM, so they would reach 75% confluence on the day of the IF, and left overnight at 37°C in 5% CO_2. The next day the DMEM was removed and the coverslips washed 3 times in PBS 1X and fixed for 20 minute at room temperature (RT) with 4% PFA in PBS 1X solution. The fixed cells were washed 3 times in PBS 1X and incubated for 10 minute in Perm solution (0.1% Triton X-100 in PBS 1X). Once the cells had been permealised, the coverslips were rinsed in PBS 1X and incubated in the blocking solution (1% BSA, 0.025% Saponin in PBS 1X) for 30 minute at 4°C. Meantime, the solution containing the primary antibody was prepared in Blocking solution and after the blocking step the coverslips have been washed 5 times with PBS 1X and flipped onto 40ul of primary antibody (AbI) solution. The coverslips were incubated in AbI for 1 hour at RT. After 1 hour the coverslips were washed 5 times in PBS 1X and incubated, for 1 hour at RT in the dark, with the secondary antibody dilute in 1% BSA in PBS 1X. The nuclei were stained with Hoechst diluted 1:10000 in PBS 1X and incubated for 2 minute. The coverslips have been post-fixed, in 2% PFA for 10 minute to prevent any dissociation of the secondary antibody. The coverslips were mounted onto a drop of mountant solution (90% glycerol, 3% N-propyl-galate in PBS 1X) and sealed with nail varnish. Specific dilutions for all primary and secondary antibodies used for IF are stated in table 2.1.3.1.1 and 2.1.3.1.2.

2.2.6 Mammalian protein extraction and quantification

2.2.6.1 Protein harvesting and lysis

For the assessment of protein expression such as GPP130, CHOP/GADD153, EGFR, caspase 2 and GRP78 HeLa cells were grown to confluence in 6 well tissue culture plate washed with 10 ml ice-cold PBS and incubated for 5 minute with trypsin and then harvested. The cells were centrifuged at 800 revolutions per minute (rpm) for 8 minute and then lysed. The pellets were suspended in 50µl of lysis buffer (table 2.1.3.2.1) and placed on ice for 30 minutes. The suspension was centrifuged at 12,000 rpm for 20 minutes at 4°C and the supernatant transferred to a clean tube.

2.2.6.2 Protein quantification

Protein concentration was determined using the PIERCE™ BCA protein assay kit and following the instructions given by the supplier. The 1:10 dilution of the stock solution containing the proteins was made (45µl of PBS 1X plus 5µl of protein stock solution). Each standard (table 2.2.6.2.1) and unknown samples (1:10 dilution) were pipetted (25µl) in replicate into a 96 well plate and 200µl of the working reaction (WR) was added. The final volume of the working reaction, made with reagent A and B in ratio 50:1, was calculated using the following formula:

(9 standards + number of unknown) x (number of replicate) x (volume of WR for each sample)

i.e. (9 +6) x (2) x (200µl) = 6ml

Once the standards, samples and working reaction were added the 96 well plate was covered in foil and incubated at 37°C for 30 min. The plate was cooled at room temperature and the absorbance read at 562nm on an ELISA plate reader (machine).

Vial	PBS 1X (µl)	BSA (µl)	Final [BSA] µg/ml
A	0	300 of stock	2000
B	125	375 of stock	1500
C	325	325 of stock	1000
D	175	175 of vial B solution	750
E	325	325 of vial C solution	500
F	325	325 of vial E solution	250
G	325	325 of vial E solution	125
H	400	100 of vial F solution	25
I	400	0	0=Blank

Table 2.2.6.2.1 – Standard BSA preparation

2.2.6.3 Sodium dodecyl sulphate polyacrylamide gel electrophoresis

Sodium dodecyl sulphate polyacrylamide gel electrophoresis (SDS-PAGE) was used to separate proteins according to their electrophoretic mobility, which is dependent on the molecular weight of proteins.

The separation of the proteins was performed in polyacrylamide gels that consist of "stacking" and "resolving" gels. The reagent concentration of the resolving gel was chosen according to the molecular weight of the proteins to be separated. A 7.5% resolving gel was used for the detection of GPP130. For detection of CHOP/GADD153 12% resolving was used. Both resolving gels and stacking were prepared following the conditions shown in table 2.1.5.5 (2.1 Materials) and cast using the 1.5 mm thick glass plate (BioRad, MiniPROTEAN® electrophoresis system).

The resolving gel was poured to within 2 cm of the top of the glass plates and overlaid with isopropanol. The resolving gel was left to polymerise before the isopropanol was removed and the stacking gel poured on the top. Combs were immediately added to the

stacking gel to create sample wells. Once the stacking gel had polymerised the combs were removed and the gel was placed into an electrophoresis chamber (BIORAD Mini) (50mA for the stacking and 70mA for the resolving gel). Before loading onto the gel, protein samples were diluted 5-fold with 2X Laemmli loading buffer (table 2.1.7.1) and denatured using a heating block for 5 minutes at 100°C. The gel was run in running buffer (table 2.1.8.1) for ~1 hour (till the loading dye had reached the bottom of the gel) at 50mA for the stacking and 70mA once they had reached the resolving gel. A rainbow protein ladder (Thermo Scientific) was loaded on the same gel to evaluate the correct size of the protein bands.

2.2.7 Western Blotting

2.2.7.1 Electrophoretic Transfer to PVDF Membrane

The resolved proteins were transferred from the SDS-PAGE gel (section 2.3.2.1) to a polyvinylidene difluoride membrane (PVDF, BioRad) for detection of proteins by Western blot. The PVDF membrane was first activated in methanol before the blotting sandwich was prepared in 1X Half Towbin transfer buffer (table 2.1.8.2) in the following order: fibre pad, filter paper, PVDF membrane, gel, filter paper, fibre pad.
The sandwich was placed into the transfer device in order to allow the electrotransfer of proteins from the gel to the PVDF membrane. The transfer was performed in 1X Half Towbin transfer buffer at 250 mA, constant amperage, for 1.5 hours in the cold room, to avoid the overheating of the apparatus.

2.2.7.2 Western Blot detection

Prior to the detection process the membrane was first blocked in 5% BSA in TBS-T 1X, on a shaker, for 1 hour at room temperature (or alternatively overnight at 4°C). The membrane was then incubated with the primary antibody diluted in 1% BSA solution for 1 hour at room temperature (or overnight at 4°C). Specific dilutions for all primary antibodies used for Western blotting in this thesis are reported in table 2.1.5.1.1. The membrane was then washed three times on a shaker (~200 rpm) with TBS-T 1X, for 10 minutes each time. Next, the membrane was blocked with diluted secondary antibody (table 2.1.5.1.2) in 1% TBS-T and incubated at room temperature for 1 hour. Membrane washes were repeated as above. The secondary antibodies were all conjugated to Horse

Radish Peroxidase (HRP) which allows detection once the membrane is incubated with the enhanced chemo-luminescence (ECL) western blotting detection system reagents (Pierce® ECL, Thermo Scientific) at a ratio of 1:1 for reagent A:B. The membrane was exposed and developed using the ImageQuant 2000 using 10 seconds incremental exposure. The western blot were analised comparing the density of each band. The band intensity was then normalised with the intensity of the loading control's band. The western blot analysis was performed using the open source software FIJI. Statistical analysis was performed using GraphPad Prism software version 6.0b for mac (GraphPad Software Inc. San Diego, CA, USA).

2.2.8 Lysosome function assay

HeLa cells *CLN3* depleted have been tested for lysosomal function using the VIVAprobe™ lysosome assay kit. The kit use the photostable red fluorophore cresyl violet (CV), bi-substituted via amide linkage to the peptide sequence Arg-Arg to give the cathepsin B substrate CV-$(RR)_2$. The cathepsin B substrate diluted in 52µl DMSO to constitute the stock concentrate. The working solution was made in PBS1X, 1:10 ratio.

The HeLa cells were collected (concentration of $2x10^6$ cells/ml) in a falcon tube and incubated for 1 hours at 37°C with the cathepsin B substrate working solution (20µl every 300µl of cell sample). 100µl of cells were pipetted in each well of a 96 well plate and the fluorescence intensity was measured in ELISA plate reader. Cathepsin B substrate has an optimal excitation and emission wavelength of 592nm and 628nm.

2.2.9 Image processing and analysis

To quantify the morphology of the Golgi complex, in these cells, the immunofluorescence was recorded as a digital 8-bit gray-scale, 1024X1024 pixels image (Confocal images were acquired using a Leica TCS SPE confocal imaging system with plan-Apochromat 63X 1.25 NA oil objective and recorded using Leica LAS AF software. Images were opened and analysed in ImageJ). The threshold of the images was set at ~90 for GM130 and at ~45 for both Giantin and TGN46 (all pixels with a value under 90 and/or 45 are excluded from the quantification) to remove background pixels from measurements. The region of interest was defined for each cell and the corresponding area measured. All image processing and analysis, IF and WB, was performed using the open source software FIJI (http://imageJ.nih.gov/ij).

2.2.10 *S. pombe* mutant strains

2.2.10.1 *S. pombe btn1* deleted strains

The fission yeast *btn1* deleted strain was made by Dr. Michael Bond and Mariana Vieira using the long primer method. Essentially, a new yeast strain was made for the Hermes project (not explained in this thesis). For this project it was needed to use a strain that was auxotrophic for leucine. The previous strain used by Codlin (Codlin et al., 2009) used leu2 to replace *btn1*. Once the new strain was made we start to use it in order to obtain consistent results with one another. In this method long primers (100nt) are designed in which the first 80nt are homologous to the flanking regions of the gene of interest and the last 20nt are homologous to a generic plasmid, in this case pFA6a. When these primers are used to amplify from pFA6a a product is generated with the flanking regions of *btn1* either side of a cassette. There are a number of versions of this plasmid, but in this case the one containing the NatMX cassette was used (Figure 2.2.10.1.1).

The NatMX cassette is a simple resistance cassette and it confers resistance to the anti-fungal nourseothricin sulfate, also called ClonNat. Following transformation, cells were plated onto YES. After 24h they were replica plated onto ClonNat (this gives the cells a chance to express the resistance gene before selection), and resistant colonies selected. To check if the integration occurred at the right place a PCR was performed (Bähler et al., 1998).

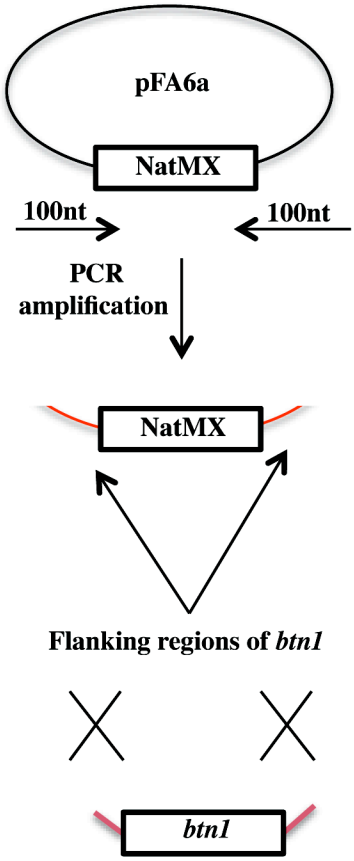

***Figure* 2.2.10.1.1** – *S. pombe btn1* deleted strain. Long primers (100nt) are designed in which the first 80nt are homologous to the flanking regions of *btn1* and the last 20nt are homologous to a generic plasmid, in this case pFA6a.

2.2.11 *S. pombe* transformation

S. pombe was transformed with plasmid DNA or linear DNA fragments using the lithium acetate method described by Okazaki *et al*. (1990) (Okazaki et al., 1990).

2.2.12 Transmission Electron Microscopy (TEM)

2.2.12.1 High-pressure freezing (HPF) and freeze substitution (FS) of *S. pombe* for TEM

The aim of the high pressure freezing is to preserve the biological samples and minimise artifacts related to conventional aldehyde fixation and room temperature dehydration.

2.2.12.1.1 Rapid freezing in Electron Microscopy sample preparation

The freezing of biological samples at a rapid rate allows the formation of vitreous ice so that ice crystals formed cannot be detected by the electron microscope. Mainly, there are four method of cryo-fixation: a) plunge freezing, b) propane jet freezing, c) cold metal block freezing and d) high pressure freezing (HPF) (Gilkey and Staehelin 1986). However, for samples thicker than 0.6 mm the HPF is the technique most suitable. Indeed, the other three methods are suitable for very thin samples such as monolayer of cells. This is because only thin samples can reach, at atmospheric pressure, a freezing ratio of 10000°C/sec. The high pressure (~2050 bar) applied immediately before the freezing step is able to change the properties of the water avoiding the formation of ice crystals (Gilkey and Staehelin 1986; Moor, 1987 #1940).

2.2.12.1.2 *S. pombe* growth preparation for HPF and FS

To ensure a successful HPF in *S. pombe* it is important to filter and prepare the yeast at the mid log phase (0.4-1.0×10^7 cells/mL). A start culture was prepared two days before the filtration process. *S. pombe* strains (table 2.1.3.1.1) were inoculated in 10 ml YES medium (table 2.1.3.2.1) and incubated for 17 hours at 30°C.

After 17 hours a larger volume culture was set up using both minimum (table 2.1.3.2.3) and rich (table 2.1.3.2.1) media. The optical density (OD_{600}) of the start cultures was measured to calculate the cell concentration. The cell concentration together with the doubling time of *S. pombe* (~2.5 hours) allows us to calculate the volume of start culture to inoculate in100 ml culture using the following equation:

$$[V(Y/X)] / [2(T/DT)]$$

Y is the target OD 600; X is the current OD 600; T is the number of hours of growth; V is the culture volume in ml; DT is the doubling time in hours. The large culture (100 ml) was then incubated for 17 hours at 30°C in order to reach the mid log phase.

2.2.12.1.3 *S. pombe* filtration and HPF

The *S. pombe* filtration and HPF was performed following the protocol (Murray 2008) with some adjustment. The yeast was collected by filtration using cellulose acetate filters (25mm diameter, pore size 0.45µm, Sartorius Stedim) mounted on a Whatham filter holder (25mm×50ml, Scientific laboratory supplies) connected to a vacuum pump. The filter was allowed to equilibrate for 2 minute in appropriate yeast medium, before being inserted. Yeast culture (10 ml) was poured into the filter holder. This filtration step is critical, if the filter is either too wet or too dry, the freezing will be unsatisfactory. The filtered yeast on the membrane filter should have a consistency of apple sauce (Murray 2008). In order to reach the right consistency the vacuum pump was turned off prior to the meniscus of the medium reached the filter membrane at the bottom of the filter system and the pump released. The filter membrane was plated on a drop of 40µl medium spotted on a petri dish lid, to keep the yeast humid, avoiding to drying out. A portion of the yeast paste was scraped from the filter using a pipette tip and loaded into the specimen carrier (100 nm deep, Leica). The scraping and loading is a critical step, drying out of the sample must be avoided so, it is recommended to proceed quickly and with the help of a colleague. The specimen carrier, filled with the yeast paste, was mounted in the specimen rod and clamped into position in the HPF EMPACT (Leica). The specimen was inserted into the HPF and locked. Once all the samples had been frozen, they were transferred to the automatic freeze substitution unit (Leica) and the remaining samples stored in liquid nitrogen.

2.2.12.1.4 *S. pombe* freeze substitution (FS) and embedding

Freeze substitution is the process that allows the dissolution of vitreous ice by an organic solvent in the presence of a secondary fixative (Steinbrecht and Muller 1987). *S. pombe* AFS was carried out using the FS Leica system according to the conditions showed below in the figure 2.2.12.1.4.1.

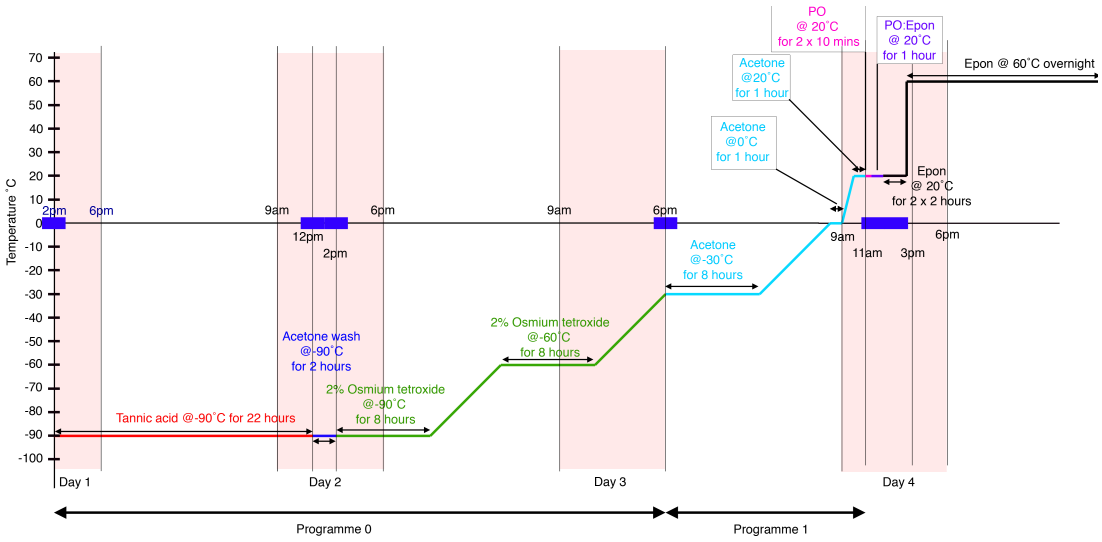

***Figure* 2.2.12.1.4.1 -** Automatic freeze substitution program. The AFS was carried out according to the program showed in the figure and the solutions and temperature steps are explained in the text.

The freeze substitution was carried out in Leica AFS. The samples were kept in 0.1% of tannic acid in 98% acetone for 22 hours at -90°C. After the aforementioned time the specimens were washed with 98% acetone for 2 hours at the same temperature. The samples once were washed in acetone were incubated in 2% osmium tetraoxide (OsO_4) solution in acetone for 8 hours at –90°C, the temperature then shifted from -90°C to -60°C (6 hours step, 5°C /hour). The samples then were kept for 8 hours at -60°C before the temperature start to increase from -60°C to -30°C (6 hours, 5°C /hour). After 28

hours in 2% in OsO4, this was replaced with 98% acetone and incubated for 15 hours (8 hours at -30°C) after 8 hours the temperature increased (5°C /hour) till 0°C. The samples then, were incubated in acetone for 1 hour, from 0°C to 20°C, followed by a second incubation with acetone at 20°C for 2 hours. The specimens kept at 20°C were incubated twice in PO (2x10mins) and then incubated in PO-Epon for 1 hour. After that the sample were incubated in Epon twice (2x2 hours) embedded and baked overnight at 60°C

2.2.12.2 Fixation and embedding of mammalian cell lines for TEM

2.2.12.2.1 Fixation

Human fibroblast and HeLa cell lines were plated in 20mm diameter coverslips and fixed, for 30 minute at room temperature, using a solution of 1.5% glutaraldehyde and 2% PFA in 0.1M of Na^{2+} Cacodylate. Fixative was removed and the coverslips washed 3X with 0.1M of Na^{2+} Cacodylate. In order to make the cells electron dense and improve contrast the cells were incubated for 1 hour at 4°C in the presence of 1%OsO_4 and 1.5% $K^{+}Fe_2$cyanide. The working solution was made from 2% OsO_4 and 3% $K^{+}Fe_2$cyanid in H_2O stock solution and mixed in 1:1 ratio to obtain the final concentration. After 1 hour the solution was removed and the coverslips washed 3X with 0.1M of Na^{2+} Cacodylate. If necessary the coverslips could be left in 0.1M of Na^{2+} Cacodylate for a week.

2.2.12.2.2 Mammalian cells embedding for EM

In order to proceed with embedding, the 0.1M Na^{2+}Cacodylate was removed and the coverslips incubated for 45 minute in the dark with 0.1% tannic acid (TA) in 0.05M of Na^{2+} Cacodylate. After 45 minutes, the 0.1% TA was removed and the coverslips were rinsed and incubated for 5 minute in 1% Na^{2+}sulphate in 0.05M Na^{2+}Cacodylate. The coverslips were rinsed and incubated for 3 minute in dH_2O. The coverslips have been dehydrated in ethanol (EtOH) following the conditions illustrated in table 2.2.12.2.2.1.

EtOH dehydration
2X wash in 70% EtOH (5min each) 2X wash in 90% EtOH (5min each) 2X wash in 100% EtOH (5min each)

Table 2.2.12.2.2.1 – Dehydration steps in EtOH

After dehydration the coverslips were incubated in propylene-oxide EPON (PO-EPON), 1:1 solution, for 1 hour at room temperature. The PO-EPON was removed and substituted with EPON for 2 hours at RT. After 2 hours the EPON was replaced with fresh EPON and incubated for 2 more hours at room temperature. Finally, the coverslips were mounted on the top of EPON stabs and baked overnight at 60°C.

2.2.12.3 Sectioning

Sections were cut with a Leica Ultracut UC7 microtome onto formvar-coated slot grids, stained for 10 minutes with lead citrate (Lead nitrate 133g, Sodium citrate 1.76g and 0.8ml of 10N NaOH in 30ml of deionised water), and viewed with a transmission electron microscope (TECNAI12: Philips, Eindhoven, The Netherlands). Images were acquired using a Morada digital camera (Olympus-SIS).

2.2.13 Bacterial Strains and transformation

Cloning was performed using the *Escherichia coli* (*E. coli*) strain DH5α (Stratagene, Cambridge, UK). 1 μL of plasmid (stated in table 2.1.3.1.1) was added to 100μL of DH5α *Escherichia coli* competent cells and incubated on ice for 30 min. Cells were subjected to heat shock at 42 °C for 45 seconds and immediately placed on ice for 2 minutes. Cells were then allowed to grow by adding 500μL of SOC medium (Invitrogen) and incubating in an orbital shaker at 37°C for 30 minute at 220 rpm. Subsequently, 200 μl were spread onto LB agar plates supplemented with the appropriate antibiotic. Plates were incubated overnight at 37°C.

2.2.14 Plasmid DNA Purification, Miniprep

Plasmids were extracted from overnight bacterial cultures using the QIAGEN mini-prep kit. 5 ml of bacterial cultures were pelleted by centrifugation at 3,200 rpm for 5 minutes. The resulting pellet was resuspended in 250 μl of Buffer P1 and transferred to

a 1.5 ml micro-centrifuge tube before addition of 250 μl of Buffer P2 to allow cell lysis. The tube was carefully inverted several times. Subsequently 350 μl of the alkaline Buffer N3 was added, and the solution was immediately mixed by inversion. The mixture was then centrifuged at 13,000 rpm for 10 minutes to pellet cellular debris, including genomic DNA. The supernatant, which contained the plasmid DNA, was transferred to a QIAprep spin column and centrifuged for 1 minute at 13,000 rpm. The column, with bound plasmid DNA, was washed with 750 μl of Buffer PE and centrifuged as above. The flow through was discarded and the column was centrifuged for a further 1 minute at 13,000 rpm to wash away any residual buffer. The QIAprep column was then placed into a clean 1.5 ml tube and 50 μl of elution buffer was added to the centre of the column and left to stand for 1 minute. The column was then centrifuged at 13,000 rpm for 1 minute to elute the plasmid DNA and the concentration was determined by NanoDrop® (Spectrophotometer, *ND-10000*).

2.2.15 Agarose Gel Electrophoresis

1% agarose gel was prepared by dissolving 1 % w/v agarose in 1X TBE buffer (90 mM tris-base, 90 mM boric acid, and 2 mM EDTA, pH=8.0) and heating, then supplemented with 5 µl of ethidium bromide (EtBr, 10 ng/ml). 6X DNA loading buffer (2 mM EDTA, 50% glycerol and 0.1% orange G) was added to the sample before loading on the agarose gel. A DNA ladder (Promega) was loaded on the same gel as a size standard. The electrophoresis was run at 120 Volts for ~45 minute.

2.2.16 Analysis of data

Statistical analysis was performed using GraphPad Prism software version 6.0b for Mac (GraphPad Software Inc. San Diego, CA, USA). Statistical significance was determined using either unpaired t-student test or ANOVA. All images were downloaded to either Microsoft Excel for analysis, or to Adobe Photoshop 4 and Illustrator 4 for assembly into montages.

2.2.17 Stereology

The streological approach was used in order to estimate the ER and yeast Golgi complex volume fraction, using a point counting grid and the square array (Hally 1964). In the square array the points lie at the vertices of adjacent squares (Figure 2.2.17.1). The unit 'cell' is a square of side d unit long, d = 0.1. The grid of choice was superimposed on the images in question.

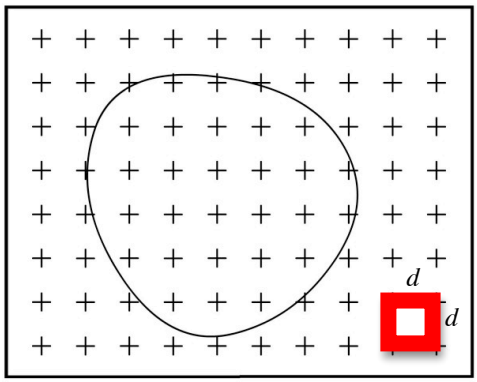

***Figure* 2.2.17.1** - Square array. Point counting grid with the points arranged in a square pattern. In this pattern the unit cell is also a square with d = 0.1

Points that fall within the contour at each of the superimpositions were counted. Finally, the area A enclosed by the profile was calculated from:

$$A = n\,a$$

Where n is the number of points counted and a is the area of the unit cell as defined above.

To estimate the volume of the ER the fractional area occupied by the ER within the general containing transection was calculated. This is illustrated in figure 2.2.17.2.

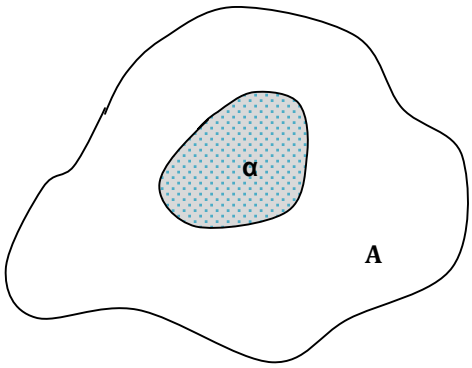

***Figure* 2.2.17.2** - Fractional area. The fractional area enclosed by the inner (shaded) contour α is estimated by the number of grid points which fall on it, in relation to the total number of grid points which fall on the area A as a whole.

The area of the whole is A and the area of the inner object α. The fractional area (A_A) of α is calculated from:

$$A_A = \alpha/A$$

In addition, the fractional area (A_A) and the fractional volume (V_V) of these objects are estimated by quotients, in short:

$$V_V = A_A$$

Result

Chapter Three

Chapter Three

Effects of *CLN3* loss/depletion in mammalian cells

3.1 Loss/depletion of *CLN3* affects Golgi complex morphology

This section details the effects of *CLN3* gene depletion by siRNA on the morphology of the Golgi apparatus in HeLa cells. In addition, it examines the morphology of the Golgi apparatus in fibroblast cell lines generated from biopsies of patients homozygous for the common 1-kb deletion.

3.1.1 Golgi complex morphology in *CLN3* depleted HeLa cells

Previous work in our laboratory investigated the connection between Golgi apparatus morphology and *btn1* mutations in yeast (Codlin et al., 2009). Here, I investigate the correlation between Golgi morphology and CLN3 in mammalian cell lines. An observation of Golgi morphological changes in the cells from patients with CLN3 disease would give further indication as to whether Golgi defects are likely to play a role in the human pathology.

As a step towards addressing the role of CLN3 at the Golgi complex, the morphology of this organelle was monitored in CLN3-depleted HeLa cells, by immunostaining with antibodies against GM130, Giantin and TGN46 (table 2.1.5.1.1), proteins that localise at the *cis*, *medial* and *trans* Golgi network (TGN) respectively (Prescott et al., 1997; Marra et al., 2001; Rudell et al., 2014). Since the depletion experiments are performed in the same cell line, any differences in Golgi morphology should be a consequence of CLN3 depletion.

In HeLa cells 48 hours after gene depletion (Figure 3.1.1.1, D), the Golgi complex undergoes significant morphological changes, which are more evident in the *cis* and *trans*-Golgi network. A 26% increase in area was observed for both *cis*-Golgi (Figure 3.1.1.1, Panel A [i, i', ii, ii'], Graph B) and TGN (Figure. 3.1.1.3). However, the medial compartment does not show a significant increase in its area (Figure 3.1.1.2). To confirm that the morphological changes in the Golgi complex are specific to *CLN3* depletion, the Golgi morphology was also analysed in *CLN6*-depleted HeLa cells (Figure 3.1.1.1, panel A [iii, iii'], graph C). CLN6 is a transmembrane ER-resident

protein (Heine et al., 2004; Mole et al., 2004). Mutations in CLN6 generally cause disease with onset in late infancy (CLN6 variant late infantile disease) (Sharp et al., 1997). The Golgi apparatus of HeLa cells depleted for *CLN6* (stained for GM130) was relatively normal and similar to the Golgi complex of mock-treated cells (Figure 3.1.1.1, panel A [iii, iii'], graph C). This suggests that changes of the Golgi apparatus are striking features of *CLN3* depletion.

Since the morphology of the Golgi complex is strictly correlated to its organisation (Sens and Rao 2013), the latter was also studied. Compactness was used as a parameter to study the organisation of the Golgi complex. The compactness known also as coefficient of circularity is an adimensional number comprised between 1.0 (a perfect circle) and 0.0 (a less circular, more polygonal geometrical object (Figure 3.1.1.4, A and B). In order to calculate the compactness of the Golgi complex the area of the organelle was factored with the square value of its perimeter and multiplying it by 4π. Because the Golgi apparatus is generally formed of several clusters of Golgi stacks, we adapted the equation by using the sum of the areas of the clusters and the sum of their perimeters to calculate the "compactness" of the whole structure (Figure 3.1.1.4, graph C). The equation used to calculate the compactness is showed below (Bard et al., 2003):

$$4\pi(\Sigma \text{ area})/(\Sigma \text{ perimeter})^2$$

Using this method we verified that the Golgi complex is bigger and less compact/organised in *CLN3* depleted cells (Figure. 3.1.1.4, C). These results are consistent with observations in *S. pombe* lacking all *btn1* function, published by Codlin et al., (2009) (see figure 1.4.2.1, introduction).

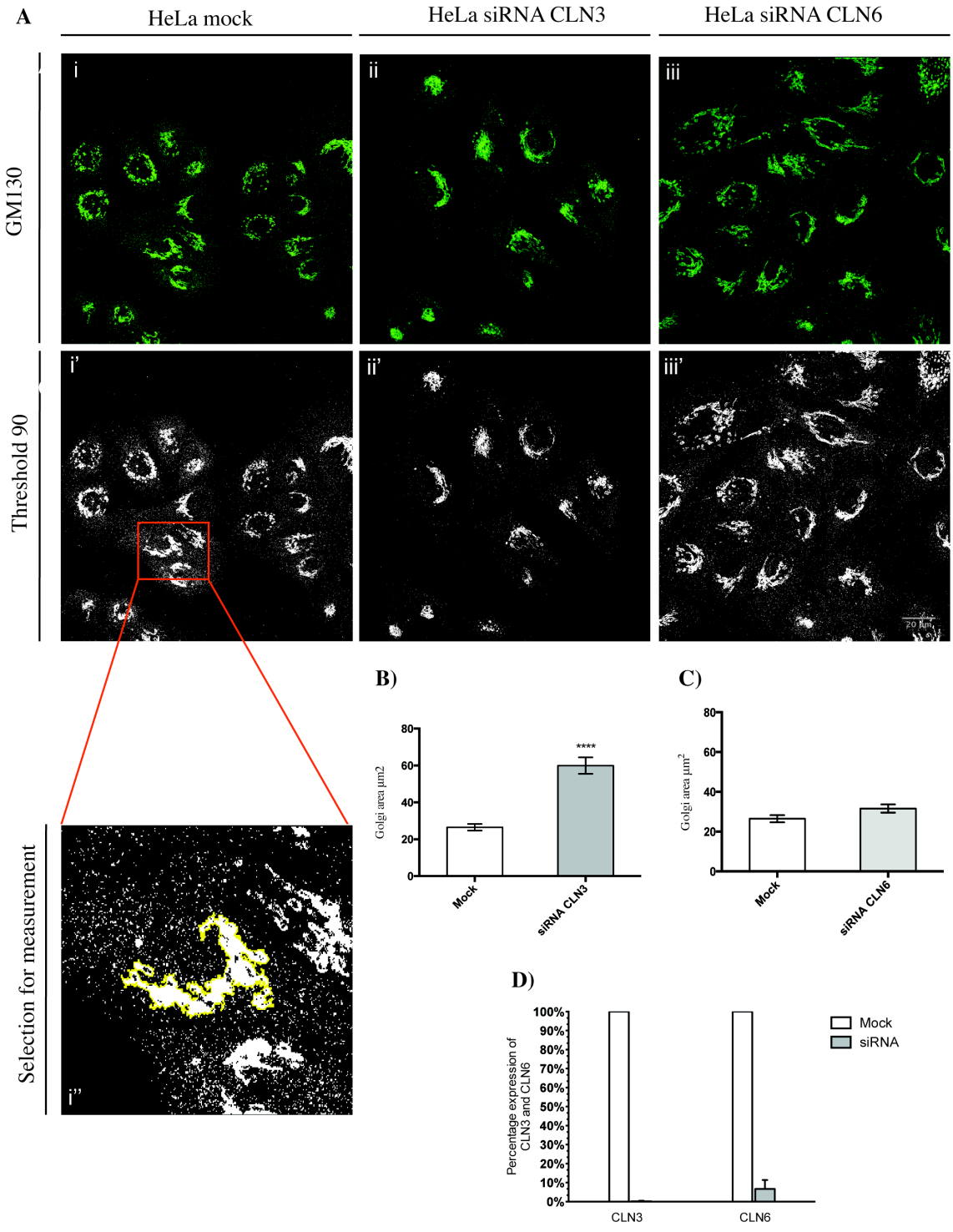

***Figure* 3.1.1.1** - CLN3 siRNA dependent changes in *cis*-Golgi morphology. **A)** Immunofluorescence images of HeLa cells, control and CLN3 depleted, stained for GM130 (**i** and **ii**). To quantify the GA area the images were set at a threshold of ~90 (**i'** and **ii'**) and the region of interest selected (**I''**), images were taken using a Leica SPE scanning confocal microscope (Scale Bar 20 µM). **B)** The graph depicts the increase in GA area upon CLN3 depletion. **C)** The graph shows the Golgi complex in CLN6 depleted cells. **D)** The graph shows the knockdown efficiency for CLN3 and CLN6 compared with mock treated cells were any siRNA was added but only the transfection reagent. (The experiment was done in triplicate, and the data shown are mean±SEM shown in *Appendix A*).

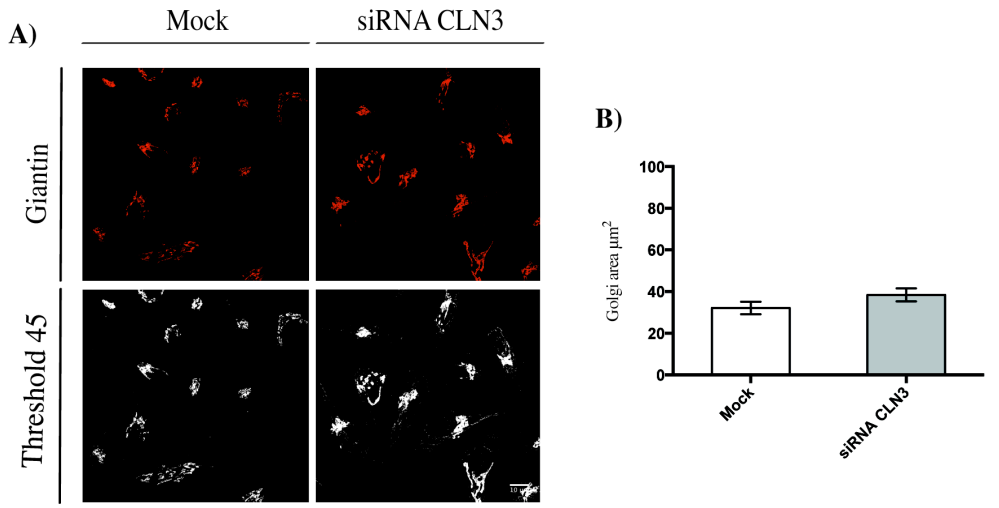

***Figure* 3.1.1.2** – CLN3 depletion does not affect the *medial*-Golgi area. **A**) Images show the immunostaining of the *medial*-Golgi using Giantin as a marker (upper panel) and the thresholded images for the quantification (Scale Bar 10 µM). **B**). The graph shows the mean of the *medial*-Golgi area upon CLN3 depletion (The experiment was done in triplicate, and the data shown are mean±SEM shown in *Appendix A*).

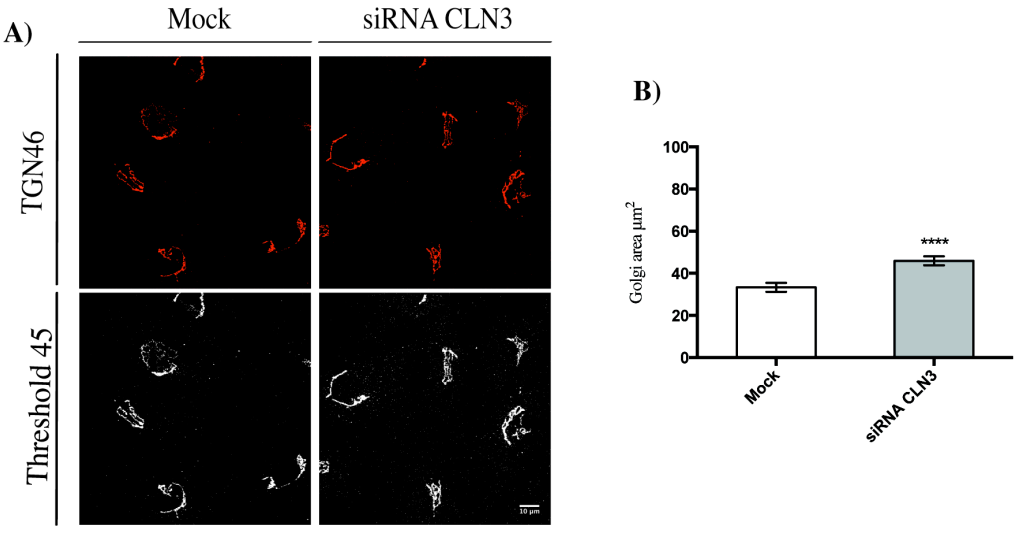

***Figure* 3.1.1.3** – CLN3 depletion affects the TGN area. **A**) The images show the immunostaining of the TGN using TGN46 as a marker (upper panel) and the thresholded images for the quantification (Scale Bar 10 µM). **B**). The graph shows the mean of the TGN area upon CLN3 depletion (The experiment was done in triplicate, and the data shown are mean±SEM shown in *Appendix A*).

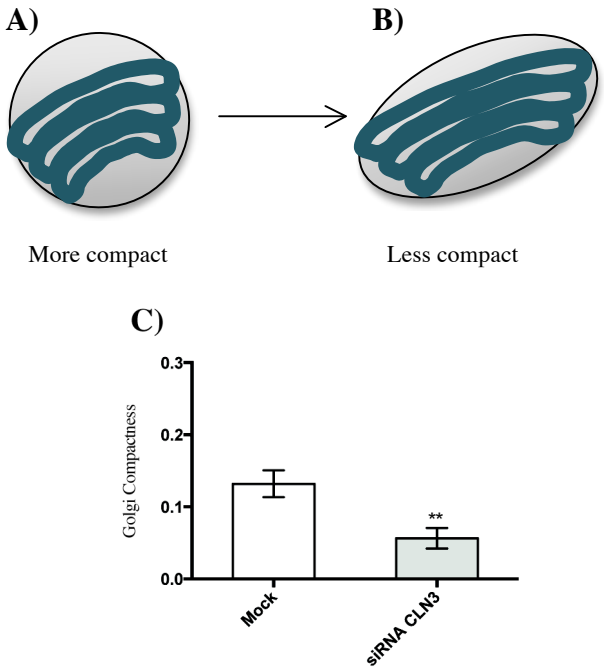

***Figure* 3.1.1.4** – CLN3 depletion affects the Golgi complex compactness. Circularity/compactness is an adimensional number comprised between 1.0 (a perfect circle, **A**) and 0.0 (a less circular, more polygonal geometrical object, **B**). **C)** The graph shows the decrease in Golgi compactness (the *cis*-Golgi compartment) upon CLN3 depletion (The experiment was done in triplicate, and the data shown are mean±SEM shown in *Appendix A*).

3.1.2 Golgi complex morphology in 1-kb patient fibroblast cell lines

The same measurements, described in the previous section, were conducted on the Golgi complex of human fibroblast cell lines generated from skin biopsies taken from patients homozygous for the 1-kb deletion in *CLN3*. For this study 4 different 1-kb patient cell lines and 4 fibroblast cell lines generated from 4 different healthy donors were compared (table 3.1.2.1). Figure 3.1.2.1 shows healthy and patient fibroblasts stained with an antibody against GM130, a marker for *cis*-Golgi.

The 4 different 1-kb patient cell lines show an increase in the Golgi area of ~22% (Figure 3.1.2.1, panel B, graph D) when compared to the 4 different control cell lines (Figure 3.1.2.1, panel A, graph C). The mean of control and 1-kb patients was plotted in the graph E in figure 3.1.2.1. Significantly, the increase in area observed in the 1-kb patient cell lines is consistent with the increase observed in *CLN3* depleted cells (Figure 3.1.1.1, graph B). In addition, the less organised Golgi morphology observed in HeLa cells depleted for *CLN3* was also observed in 1-kb patient fibroblasts (Figure 3.1.2.1, F). The medial and TGN area were also assessed in one of the 1-kb patient cell lines (HF480Pa) and, similar to that observed in HeLa cells, the TGN showed a significant increase in its area (Figure 3.1.2.3) whereas no changes were detected in the *medial* compartment (Figure 3.1.2.2).

Furthermore, the Golgi complex was also analysed in fibroblasts generated from siblings affected by CLN3 disease homozygous for a different mutation in *CLN3*, a larger deletion (exon 9-15) (Figure 3.1.2.4, A). In this cell line, the Golgi complex area was increased (Figure 3.1.2.4, B) and it showed a less compact/organised morphology

(Figure 3.1.2.4, C). This increase in Golgi complex area is similar to the increase observed in the 1-kb patient fibroblast cell lines (Figure 3.1.2.4, D). Moreover, the Golgi complex seems not to be significant affected in other types of NCL. Indeed, a screening conducted in patient fibroblast cells affected by a different subtype of NCL revealed that this organelle is not affected in other NCL subtype. These results show that the Golgi complex is slightly increased in CLN6 patient fibroblast cells (Figure 3.1.2.5).

Together these results clearly demonstrate that a loss or a *CLN3* mutation affects the Golgi morphology.

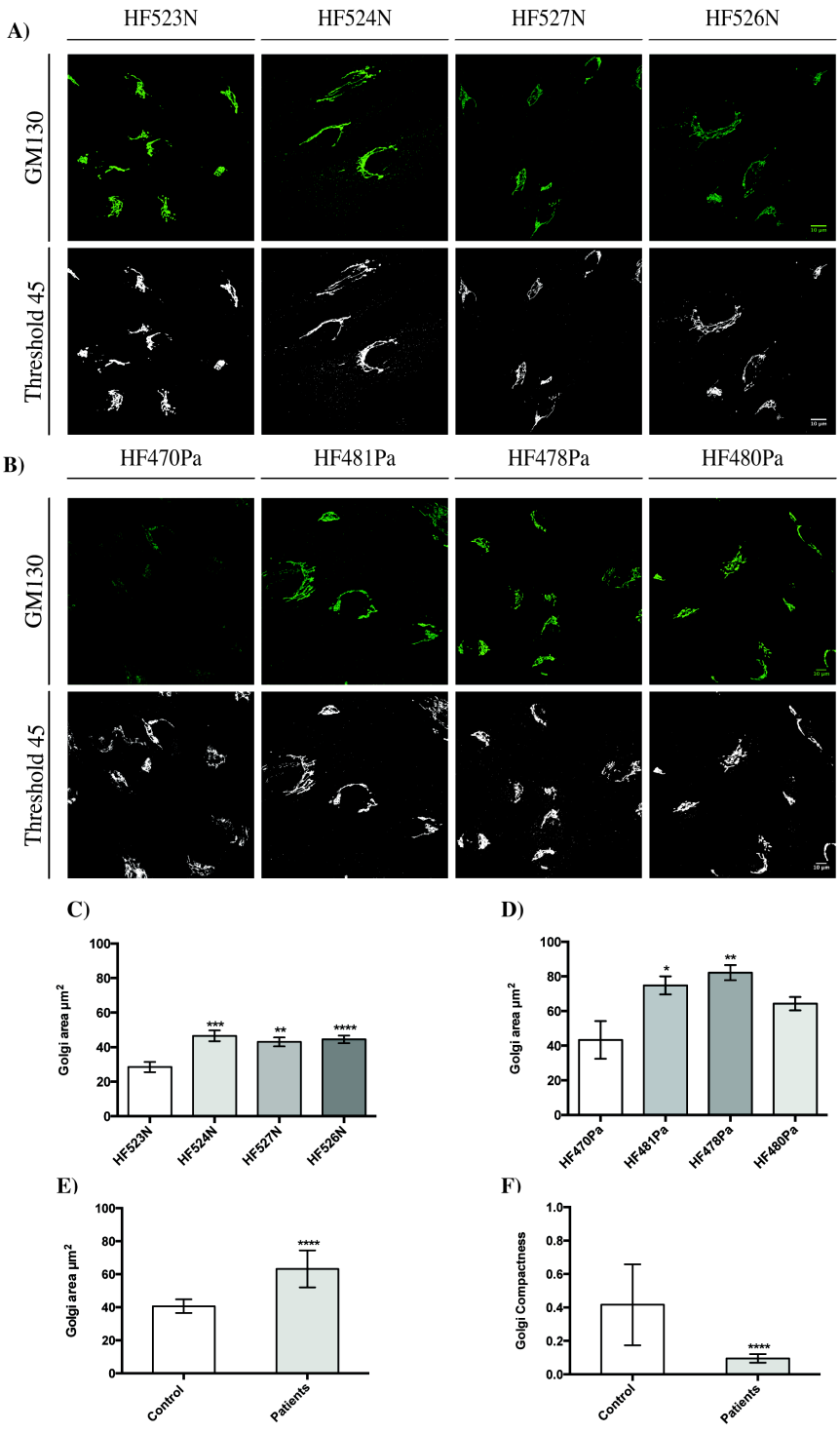

***Figure* 3.1.2.1** - CLN3 1-kb deletion dependent changes in Golgi complex morphology. Immunofluorescence images of human fibroblast cell lines, control (panel **A**) and CLN3 1-kb patient cell lines (panel **B**), stained for GM130. To quantify the Golgi complex area images were set at a threshold of ~45 (**A** and **B**) images were taken using a Leica SPE scanning confocal microscope (Scale Bar 10 µM). **C)** Golgi complex area of the 4 different healthy fibroblast cell lines. **D)** Golgi complex area of 4 different 1-kb fibroblasts. **E)** Mean of the Golgi complex area in both healthy fibroblast and 1-kb patient cell lines. **F)** Compactness of healthy and 1-kb patient fibroblast cell lines. (The experiment was done in triplicate, and the data shown are mean±SEM shown in *Appendix A*).

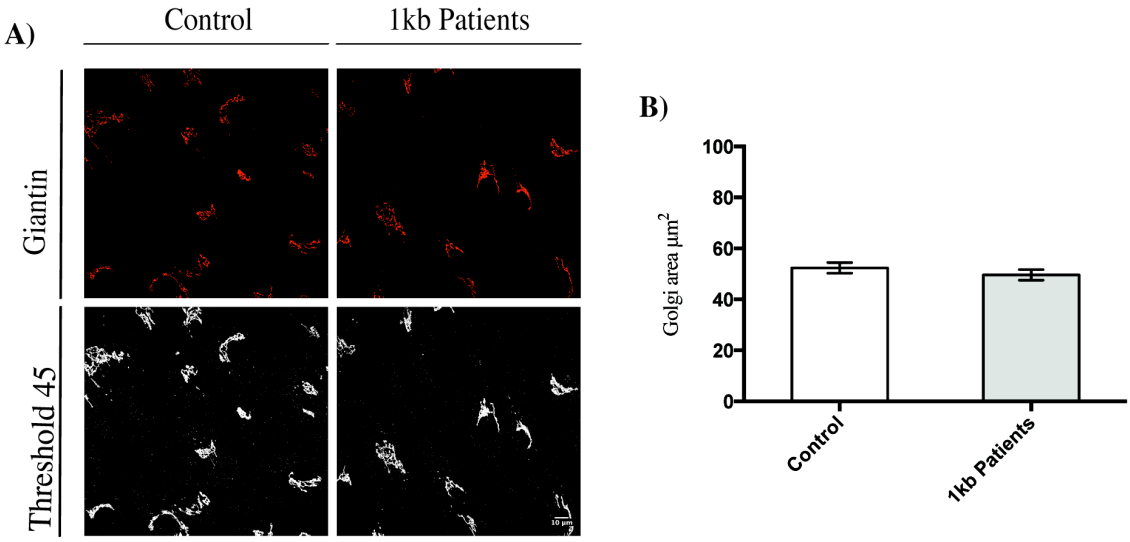

***Figure* 3.1.2.2** - CLN3 1-kb deletion does not affect the *medial*-Golgi area. Immunofluorescence images of 1-kb fibroblast cell lines (panel **A**), stained for Giantin. Images were taken using a Leica SPE scanning confocal microscope (Scale Bar 10 µM). **B)** The graph shows the mean of the *medial*-Golgi area in 1-kb patient cell lines (The experiment was done in triplicate, and the data shown are mean±SEM shown in *Appendix A*).

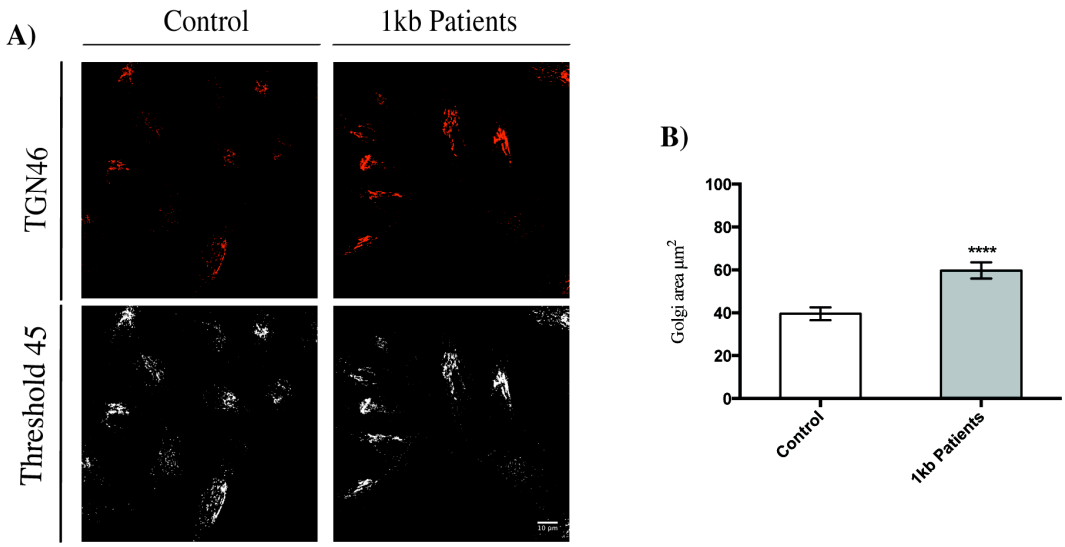

***Figure* 3.1.2.3** - CLN3 1-kb deletion affects the TGN area. Immunofluorescence images of 1-kb fibroblast cell lines (panel **A**), stained for TGN46, images were taken using a Leica SPE scanning confocal microscope (Scale Bar 10 µM). **B)** The graph shows the mean of the TGN area in 1-kb patient cell lines (The experiment was done in triplicate, and the data shown are mean±SEM shown in *Appendix A*).

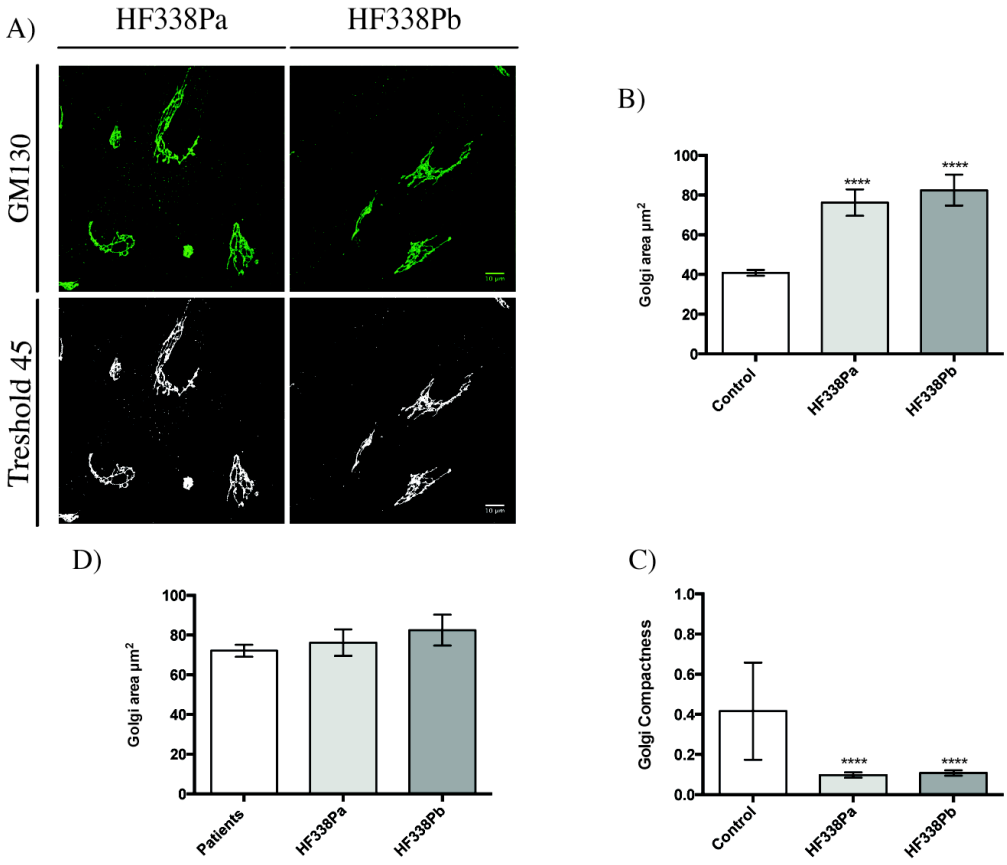

***Figure* 3.1.2.4** - CLN3 exons 9-15 deletion dependent changes in Golgi complex morphology. Immunofluorescence images of 9-15 patient fibroblast cell lines (panel **A**), stained for GM130, images were taken using a Leica SPE scanning confocal microscope (Scale Bar 10 µM). **B)** The graph depicts the Golgi complex area in HF338Pa and HF338Pb. **C)** Compactness of the Golgi complex in CLN3 ex9-15 deletion fibroblast cell lines. **D)** The graph compares the Golgi complex area of the cell lines carrying the ex9-15 deletion vs 1-kb patient cell lines. (The experiment was done in triplicate, and the data shown are mean±SEM shown in *Appendix A*).

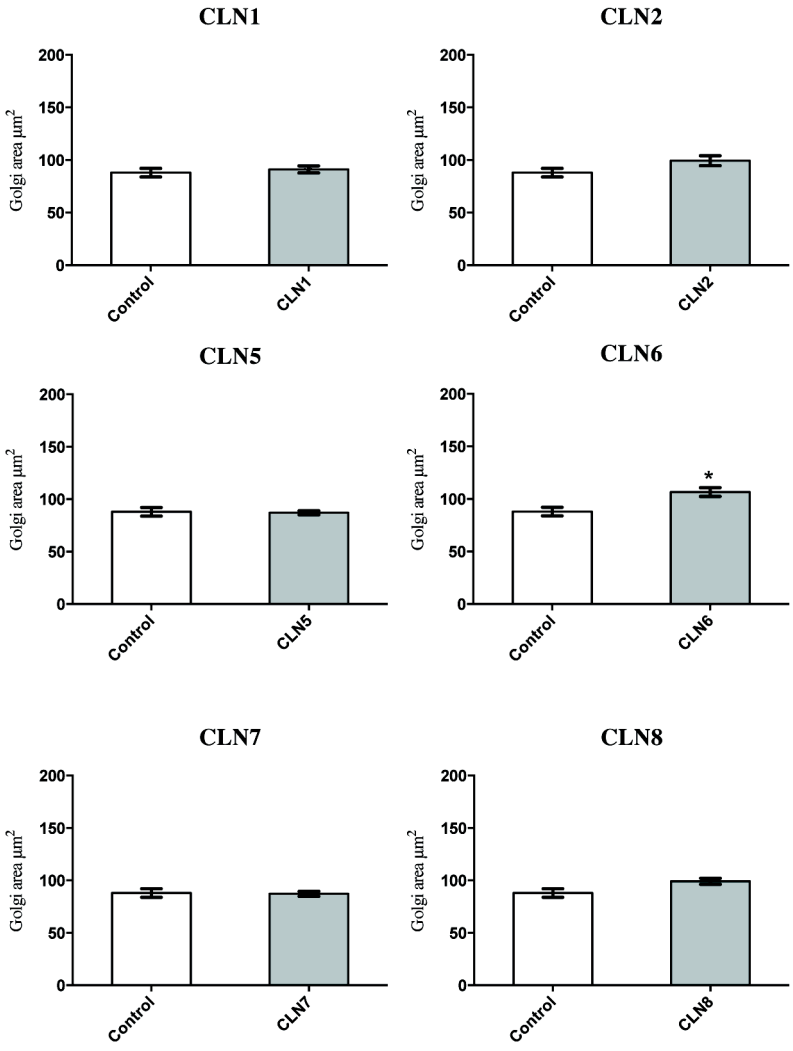

***Figure* 3.1.2.5** – Golgi complex morphology is not affected in other NCLs. A screening conducted in fibroblast cells from patients affected by different subtype of NCL. (The experiment was done in triplicate, and the data shown are mean±SEM shown in *Appendix A*).

3.1.3 Synopsis

Previous work in the lab established a connection between the morphology of the Golgi apparatus and deletion of *btn1*, the yeast orthologue of *CLN3*. In this study mammalian cell lines that were depleted for *CLN3* and fibroblasts from patients homozygous for the 1-kb deletion were analysed to investigate if this phenomenon is conserved in mammalian cells. The observation, that only loss of CLN3 activity is linked to marked morphological changes in the Golgi complex in mammalian cells, supports the hypothesis that defects in the Golgi complex are likely to play a role in the pathology of CLN3 disease. *CLN3* depletion causes an increase in the Golgi complex area, in particular in the cis-Golgi and TGN. Analysis of *CLN3* depleted HeLa cells are consistent with the results obtained from the 1-kb patient fibroblast cell lines, where a 25% increase in Golgi area was observed. Moreover, fibroblast cells generated from siblings affected by CLN3 disease carrying a larger deletion (that removes exons 9-15) also show similar defects in the Golgi area.

The whole Golgi complex is affected in CLN3 disease, with an unusual less compact organisation. These data are consistent with the published data from Codlin et al., (2009) where the lack of *btn1* was shown to affect the Golgi complex morphology and organisation. Moreover, cells from CLN6 patients also have a slight increase in the area of the *cis*- Golgi, but those from patients with other types of NCL do not. This emphasizes the specificity of the changes at the Golgi apparatus in CLN3 disease.

Chapter Four

Chapter Four

Golgi complex morphological changes are accompanied by Mn^{2+} dyshomeostasis in CLN3 disease

4.1 CLN3 depletion/loss affects the Mn^{2+} homeostasis at the Golgi complex in mammalian cell lines

Codlin et al., (2009) showed how the absence of Btn1p causes mis-trafficking and secretion of the vacuolar protein Carboxypeptidase Y, due to the mis-trafficking of its receptor Vps10. However, the cause of this mis-trafficking is not known.

Recently, Dr. Michael Bond showed that fission yeast lacking *btn1* is more sensitive to manganese (Mn^{2+}), with cells less able to survive with increasing concentration (unpublished data). Mn^{2+} homeostasis is finely regulated by the Golgi complex (see introduction, section 1.5.8). However, the molecular mechanism by which this regulation occurs is not completely understood. Moreover, it is unclear what the physiological concentration of Mn^{2+} is inside the organelle, as current commercially available probes are not sensitive enough to detect manganese. Therefore, to date, the best current and commonly used tool to investigate Mn^{2+} in the Golgi is GPP130. GPP130 is a Golgi-resident protein that is sensitive to intra-Golgi Mn^{2+} concentration, which is degraded by the lysosomes when the intra-Golgi Mn^{2+} concentration increases.

4 Golgi complex morphological changes are accompanied by Mn^{2+} dyshomeostasis

This chapter frames the effects of CLN3 on Golgi complex and Mn^{2+} homeostasis. The experiments shown in this section were performed in two complementary cell lines: HeLa cells transiently depleted for *CLN3* and the 1-kb patient fibroblasts. Both cell types show an unusual divalent ionic homeostasis, in particular of Mn^{2+}.

4.1.1 CLN3 depletion affects Mn^{2+} homeostasis at the Golgi complex

The sensitivity of the fission yeast *S. pombe* to different metals was investigated in our lab, by Dr. Michael Bond (unpublished data). Wild-type and *btn1* depleted yeast cells (see tab. 2.1.6.1.1) were plated onto YES+agar (see tab. 2.1.6.2.2) containing different divalent metals (calcium, magnesium and manganese) and growth was assayed by growing at 30°C for 2 to 3 days (Figure 4.1.1.1). Cells lacking *btn1* showed a higher sensitivity to Mn^{2+} (Figure 4.1.1.1).

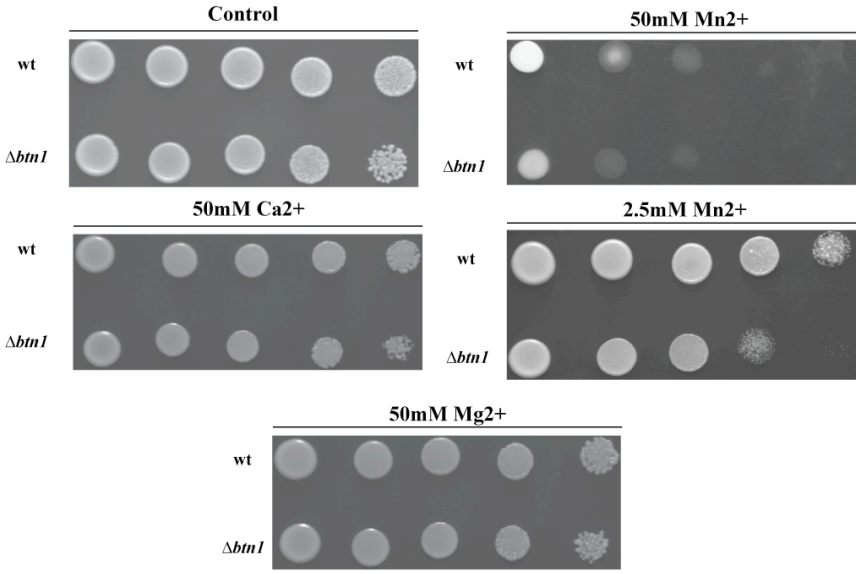

***Figure* 4.1.1.1** - *S. pombe* metal sensitivity assay. Lack of *btn1* confers sensitivity to Mn^{2+} but not to Ca^{2+} and Mg^{2+}. Wild-type and *btn1* deleted strains were grown to mid-log phase at 30°C before serial dilution (10X) and plated by drops onto pre-warmed solid medium (YES+AGAR). Plates were grown for 2 to 3 days at the indicated metal concentration before photodocumentation. (*Images from Dr. Bond, M., unpublished data*).

These results show that fission yeast deleted for *btn1* are sensitive to high Mn^{2+} concentration (Figure 4.1.1.1) and that Btn1 function may be connected with Mn^{2+} homeostasis. The same may be true for mammalian cells. Therefore, in order investigate whether the morphological changes in the Golgi complex caused by *CLN3* are accompanied by changes in Golgi-Mn^{2+} homeostasis, the GPP130 levels were investigated. GPP130 is a Golgi-resident protein that is sensitive to Mn^{2+} concentration. Moreover, its lysosomal-dependent degradation correlates with an increase in the intra-Golgi Mn^{2+} concentration (Mukhopadhyay et al., 2010; Mukhopadhyay and Linstedt 2011; Masuda et al., 2013). Under normal intra-Golgi Mn^{2+} concentration, GPP130 recycles between the Golgi complex and endosomes. However, when the intra-Golgi Mn^{2+} concentration increases, GPP130 is redirected to the lysosomes for degradation (Figure 4.1.1.2). Therefore we investigated GPP130 levels in CLN3 depleted cells after exposure to 500 µM of Mn^{2+} for 0, 1, and 8 hours.

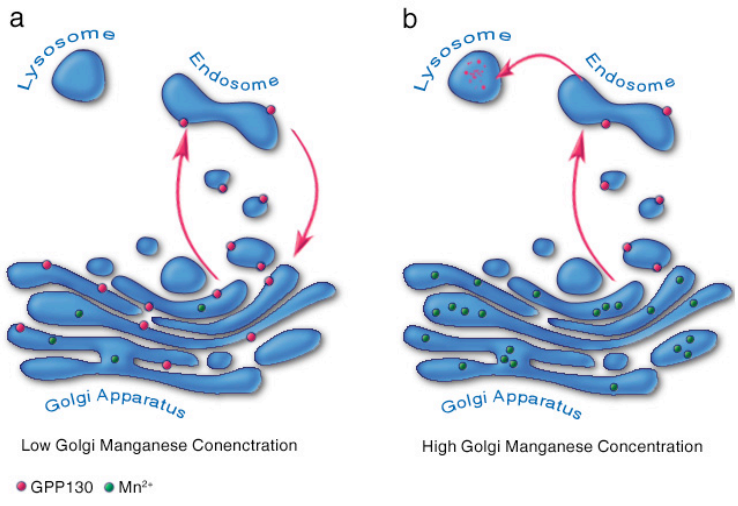

***Figure* 4.1.1.2** - GPP130 as Mn^{2+} sensor. a) At normal intra-Golgi Mn^{2+} concentration GPP130 recycles between Golgi and endosomes. b) At high intra-Golgi Mn^{2+} concentration GPP130 is trafficked to lysosomes and degraded.

In mock-transfected HeLa cells, GPP130 is degraded 8 hours after incubation with Mn^{2+}. However, in *CLN3*-depleted HeLa cells the levels of GPP130, upon Mn^{2+} exposure, do not change (Figure. 4.1.1.3, panel A, i and ii). This suggests that Mn^{2+} intake by the Golgi complex is impaired when CLN3 is absent, or that an increase can no longer be sensed. Many scenarios could be envisaged to explain this result. CLN3 could be directly linked to the transport of manganese or it could regulate its intake by modulating other factors such as SPCA1, the main Golgi Ca^{2+}/Mn^{2+} pump (see introduction, section 1.5.8). In addition, the lack of GPP130 degradation could also be due to aberrant function within lysosomes in this CLN3 disease model, given that CLN3 disease is a LSD. To test lysosomal function, the lysosomal-dependent degradation of the epidermal growth factor receptor (EGFR) was assessed (Figure 4.1.1.3, panel A, i, iii and iii'). Various agents are able to stimulate EGFR in the absence of ligand binding. The activity of EGFR is, also, dependent on divalent cations, in particular Mn^{2+} is a powerful activator (Mohammadi et al., 1993). The activation of EGFR is followed by its internalization and it is either recycled and/or degraded within lysosomes (Dikic 2003; Herbst 2004). To test the functionality of the lysosomes the EGFR levels were investigated. CLN3-depleted HeLa cells supported degradation of EGF receptor by lysosomes. These results suggest that lysosomes are still functional, at least for this activity, after CLN3 depletion. Indeed, the degradation of EGFR still occurs in CLN3 depleted HeLa cells (Figure 4.1.1.3. panel A, iii'). Moreover, the lysosome function was tested in *CLN3*-depleted HeLa cells using the VIVAprobe™ lysosome assay kit (Methods, section 2.2.8). The kit use the photostable red fluorophore cresyl violet (CV), bi-substituted via amide linkage to the peptide sequence Arg-Arg to give the cathepsin B substrate CV-$(RR)_2$. In CLN3-depleted cells, lysosomes show a significant decrease in this functionality, although this is not abolished (Figure 4.1.1.3, B).

We next investigated the fate of GPP130 levels upon manganese exposure, in patient cell lines. Fibroblasts from 1-kb patients show much increased levels of GPP130 protein compared to control fibroblasts (Figure 4.1.1.4, panel A, i and ii). This relative difference remains after exposure to Mn^{2+} (Figure 4.1.1.4, A and B). Upon manganese exposure, a decrease in GPP130 levels was observed in both control and patient fibroblasts (Figure 4.1.1.4). The initial general increase observed in patient fibroblasts suggests that CLN3 affects GPP130 turnover efficiency and that these patient cells may have decreased manganese sensitivity. Since a decrease in GPP130 levels is still seen upon manganese exposure, we investigated whether trafficking of this protein still occurs allowing degradation in the lysosome. GPP130 degradation is similar in both types of cells, suggesting that trafficking is occurring normally (Figure 4.1.1.4, panel A, ii and iii). In addition, lysosome function of the 1-kb patient fibroblast cell lines was tested. These cells retain cathepsin B function. Lysosome activity of patient cells is affected less than that of CLN3 1-kb deleted, consistent with patient cells retaining residual CLN3 function (Figure 4.1.1.4, graph B).

Patient fibroblasts are not manganese irresponsive, although higher levels of manganese appear to be necessary to achieve a turnover similar to that observed in control cells. If patient cells were irresponsive to manganese concentrations, and not merely insensitive, no changes in GPP130 levels upon manganese exposure would be expected. This may be due to the fact that mutant CLN3, in 1-kb patients, still possesses residual function.

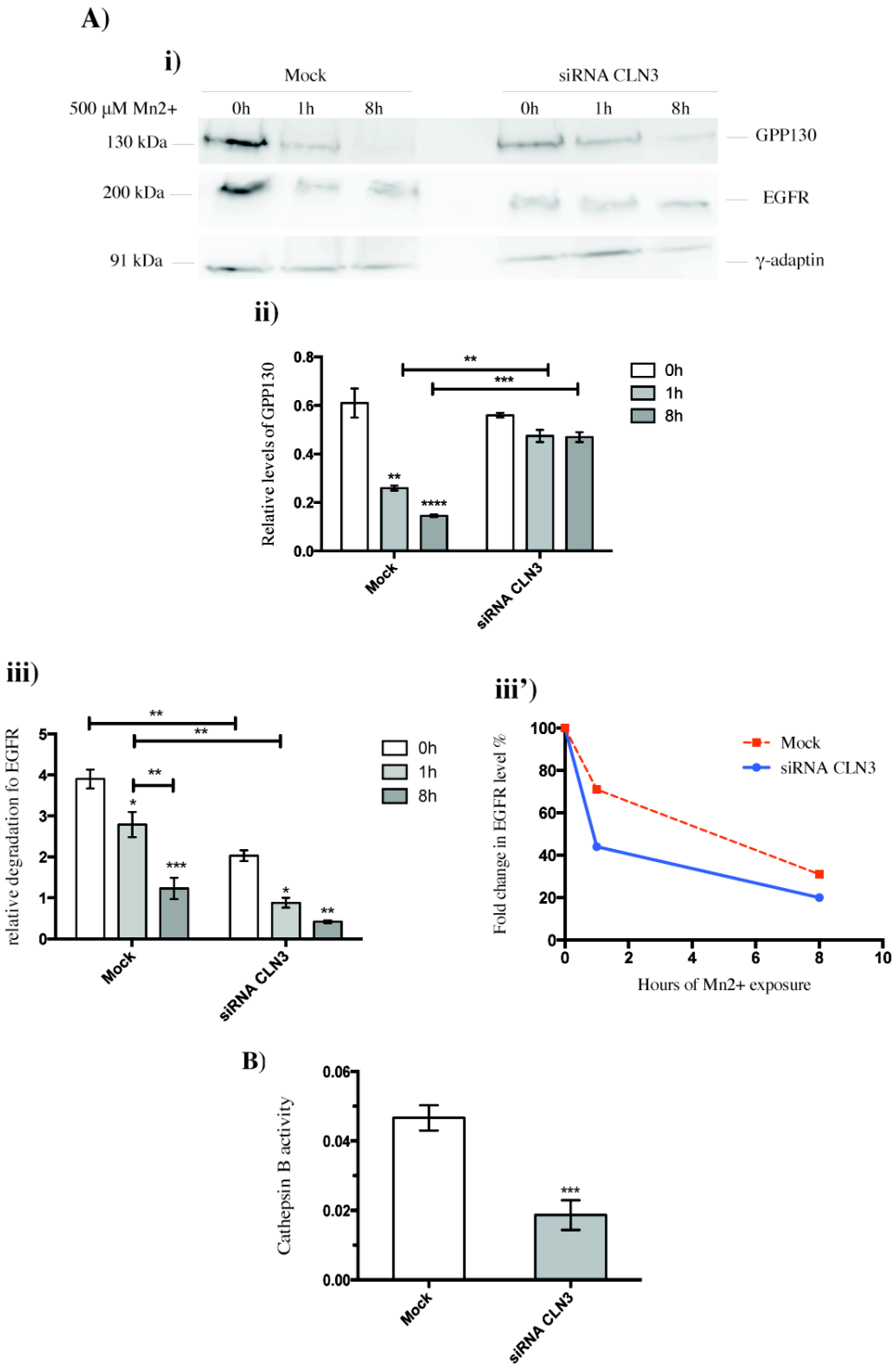

***Figure* 4.1.1.3** - CLN3 depletion affects GPP130 levels. **A) i)** WB analysis of GPP130 in HeLa cells upon Mn^{2+} exposure in CLN3 depleted and Mock-treated cells (upper panel), with γ-adaptin as a loading control (lower panel). **ii)** The degradation ratio of GPP130 on CLN3-depleted and mock-treated cells. **iii and iii')** The lysosomal-dependent degradation of EGFR. **B)** Reduced lysosomal function in HeLa depleted cells (The experiment was done in triplicate, and the data shown are mean±SEM shown in *Appendix B*).

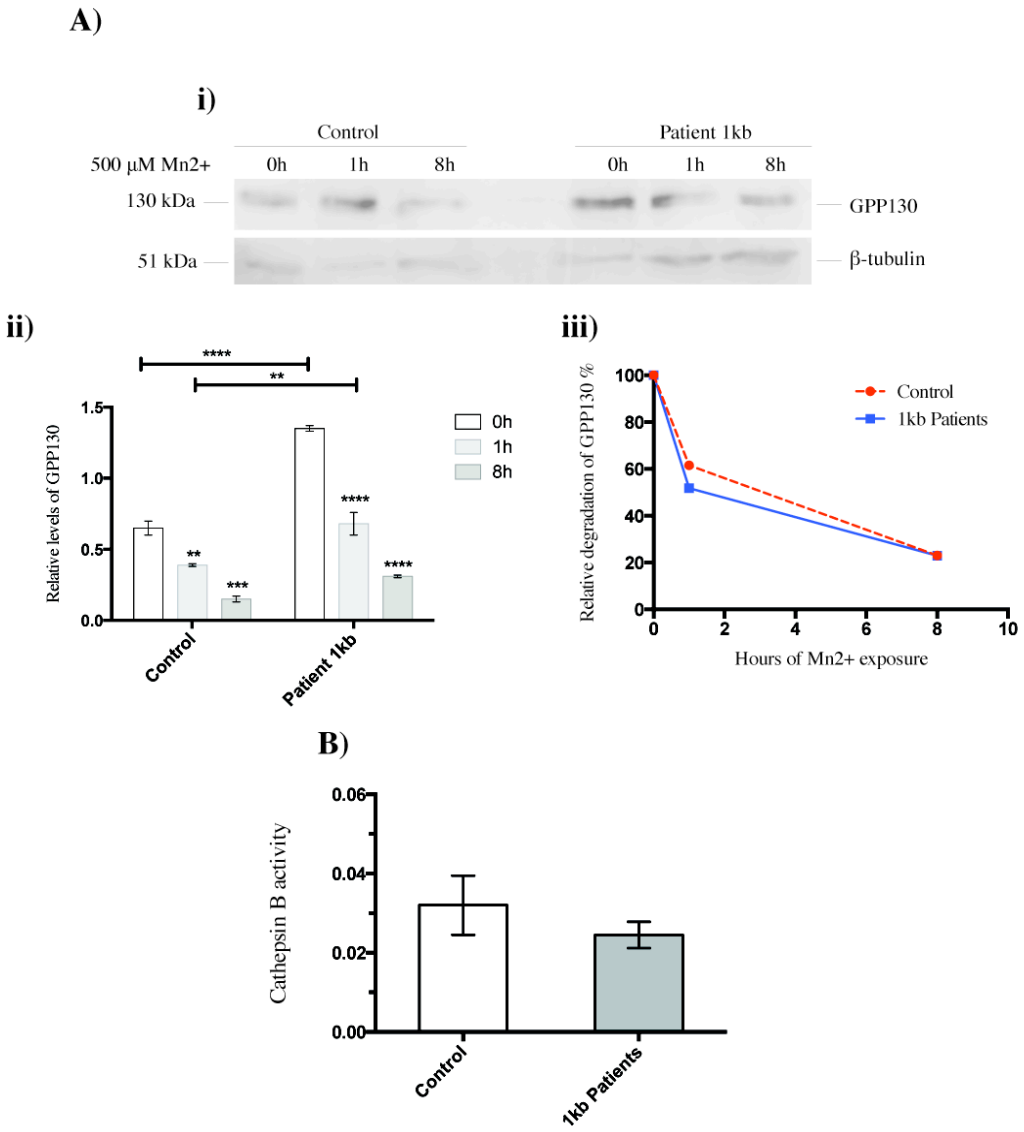

***Figure* 4.1.1.4** - CLN3 1-kb deletion affect GPP130 levels. **A**). **i)** WB analysis of GPP130 upon Mn^{2+} exposure in 1-kb patient fibroblast cell lines and control fibroblast (upper panel) and β-tubulin as a loading control (lower panel). **ii and iii)** The graph shows the degradation ratio of GPP130 on both 1-kb patient cell lines and healthy control. **B**) The graphs show the reduced lysosomal function in 1-kb patient fibroblast cell lines. (The experiment was done in triplicate, and the data shown are mean±SEM shown in *Appendix B*).

4.1.2 Synopsis

In this Chapter, I have shown that *CLN3*-depleted HeLa cells and fibroblast cells from 1-kb patients cannot deal efficiently with high manganese concentrations, using the Golgi-resident protein GPP130 as a marker for intra-Golgi manganese concentrations. The data suggest that the Golgi complex intakes Mn^{2+} less efficiently in 1-kb patient's fibroblast cell lines. It is also clear that in patients homozygous for the 1-kb deletion in *CLN3*, the mutant protein possesses a residual function. Indeed, in these patient cells, the turnover of the GPP130 is reduced. GPP130 is, however, still able to traffic to the lysosomes upon Mn^{2+} exposure, as there are no differences in degradation of the protein in patient fibroblasts. The data here shown suggest that when *CLN3* is depleted by siRNA in HeLa cells, the Golgi complex is not able to sequestrate the Mn^{2+} from the cytoplasm.

The results suggest that CLN3 regulates Mn^{2+} intake by the Golgi complex. This might be achieved either by regulating the main Ca^{2+}/Mn^{2+} pump, SPCA1, or CLN3 might, itself, be a key factor in Mn^{2+} homeostasis, even acting as a channel or transporter for Mn^{2+} in the Golgi complex. In which case, the decrease in GPP130 degradation may be due to inefficient uptake of Mn^{2+} from the cytoplasm into the Golgi. Certainly, lysosomes are still functional in CLN3 depleted cells and so any Mn^{2+}-stimulated trafficked GPP130 could still be degraded. Interestingly, 1-kb patient fibroblast cell lines do not have a significant decrease in lysosomal-activity (Figure 4.1.1.4, B) in contrast to the significant decrease observed in *CLN3* depleted HeLa cells (Figure 4.1.1.3, B). This effect is most likely due to the CLN3 1-kb mutant protein possessing a

residual function that affects lysosomal activity in these cells less than when it is acutely depleted.

Chapter Five

Chapter Five

CLN3 dysfunction triggers ER stress

5.1 Lack of CLN3 triggers ER stress in mammalian cells

In the previous section I showed data that suggested that when CLN3 is depleted or mutated the Golgi complex is not able to uptake Mn^{2+} efficiently. A reduced manganese concentration within the Golgi complex, is known to trigger ER stress leading to unfolded protein response activation (Xu et al., 2010). The early steps of protein maturation take place in the ER, such as: folding of the nascent polypeptide chains and posttranslational modifications important for the correct folding and function of the protein (Harding et al., 1999). When the influx of nascent unfolded polypeptides exceeds the folding and processing capacity of the ER the homeostasis of the ER is perturbed. Under these ER stress conditions a signalling pathway is activated, known as the unfolded protein response (UPR) (Harding et al., 1999). Therefore, the role of the ER in the pathogenesis of CLN3 disease in *CLN3*-depleted HeLa cells and 1-kb patient fibroblast cell lines was investigated.

This chapter shows that loss or depletion of CLN3 triggers ER stress. In particular, when CLN3 is mutated and/or depleted, the membrane system of the ER increase its size in order to overcome the stress stimulus that lead to activation of the UPR, which eventually leads to apoptosis.

5.1.1 ER stress in *CLN3*-depleted HeLa cells and 1-kb patient fibroblast cell lines

As the previous observations of the Golgi complex morphology and manganese dis-homeostasis are consistent in both CLN3-depleted HeLa cells and 1-kb patient fibroblast cell lines, the ER morphology was studied by transmission electron microscope in 1-kb patient fibroblasts only.

Fibroblast cells from 1-kb patients were fixed and embedded for transmission electron microscopy as described in Materials and Methods, section 2.2.13.2. The ER volume was estimated using a stereological approach (Materials and Methods, section 2.2.17).

The increase of the ER size is a clear sign of ER stress (Schuck et al., 2009). It can occur when unfolded proteins build up in the ER causing stress activation. The ER deals with the stress by increasing its volume in order to dilute the increased unfolded protein load and to host more chaperones (Schuck et al., 2009) (see Introduction, section 1.6). EM analysis of 1-kb patient fibroblast cells revealed a striking increase in the volume of the endoplasmic reticulum (ER). The micrographs in figure 5.1.1.1, panel A, clearly demonstrate an enlargement of the ER, which increase its volume 3.5 fold compared to the control fibroblast cells (Figure 5.1.1.1 panel B, graph i). The ER of CLN6 patient fibroblast was also analysed. CLN6 is a transmembrane ER-resident protein (Heine et al., 2004; Mole et al., 2004). Mutations in CLN6 cause vLINCL disease (Sharp et al., 1997). The ER of these CLN6 fibroblast cell lines is increased as in CLN3 1-kb patient fibroblast (Figure 5.1.1.1, panel B, graph ii). This result suggests that ER stress activation is a shared feature between CLN3 and CLN6 disease.

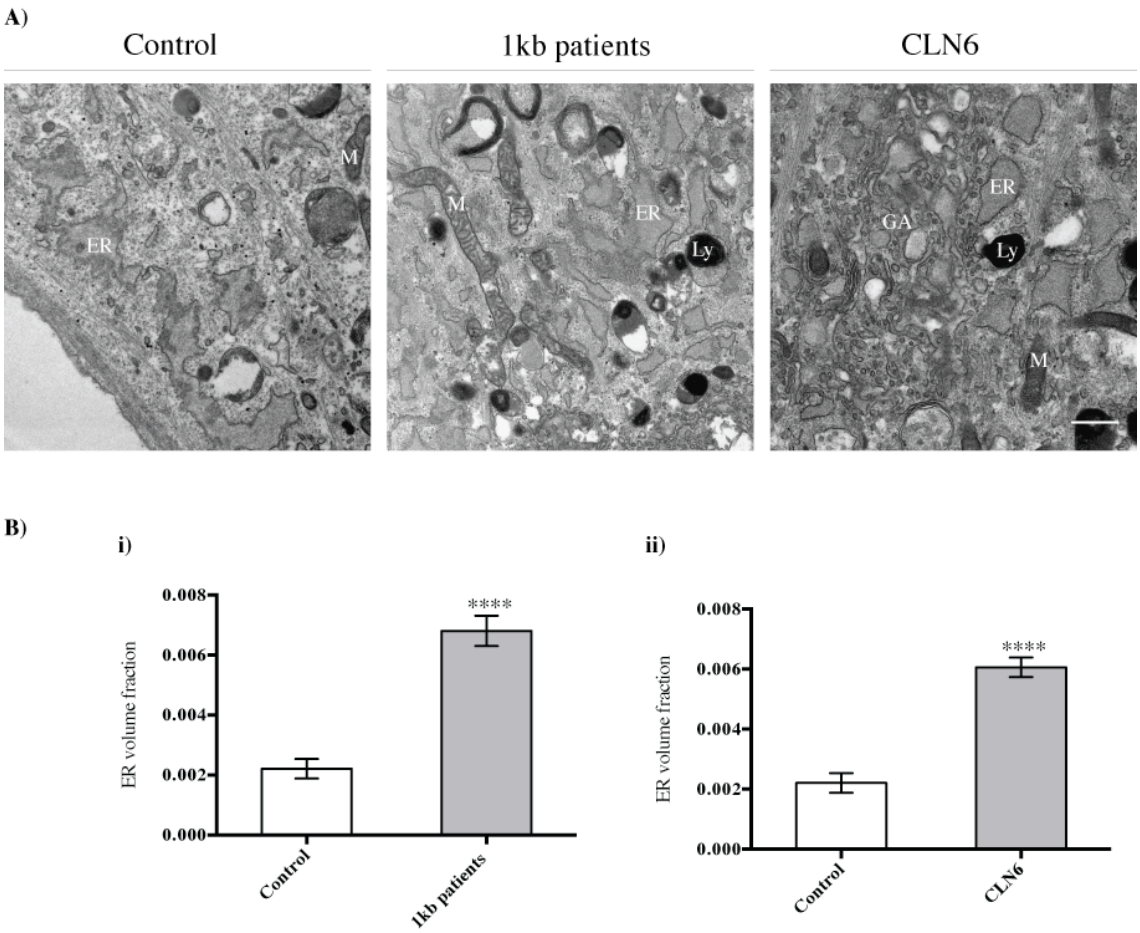

***Figure* 5.1.1.1** - ER membrane size in CLN3 1-kb and CLN6 patient fibroblast cell lines. The ER in these cell lines presents an increased volume fraction. The ER volume increases 3.5 fold in CLN3 fibroblasts and 3 fold in CLN6 fibroblasts compared to the healthy control. Scale bar 500nm. (The experiment was done in triplicate, and the data shown are mean±SEM shown in *Appendix C*).

However, ER expansion alone is not sufficient to determine whether there is an accompanying UPR activation in this cell line. Therefore, the levels of the ER stress markers GRP78/BiP and CHOP/GADD153 were assessed in *CLN3*-depleted HeLa cells upon Mn^{2+} exposure. GRP78 is a key factor for the protein folding processes in the ER. This protein recognises unfolded proteins and by a prolonged interaction with the still-folding protein is able to trigger the UPR. GRP78 expression increases in conjunction with the ER volume expansion (Walter and Ron 2011) (see introduction, section 1.6.2).

GRP78 was detected by western blot after 48 hours of *CLN3* depletion, and again after cells were exposed to 500 μM of Mn^{2+} for the indicated time points (see tab. 2.1.2.3.1). Cells were harvested and the protein extracted (see Material and Methods. Section 2.2.7). GRP78 protein levels were observed to be higher in CLN3 depleted HeLa cells, than those that were mock-treated. Levels are further increased upon Mn^{2+} exposure (Figure 5.1.1.2). This data highlights that after *CLN3* depletion not only is the volume of the ER expanded, as observed in fibroblast from 1-kb patients (Figure 5.1.1.1), but also the expression of GRP78 is enhanced.

Many studies have established that the specific induction of GRP78 is indicative of ER stress (Lee 2001). ER stress can occur under various physiological settings that have significant implications in health and disease (Lee 2001). Recently, it was reported that the levels of GRP78 decrease in *CLN3*-depleted cells exposed to tunicamycin whereas GRP78 levels are increased following overexpression of exogenous CLN3 (Wu et al., 2014). These results are in contradiction with the observations reported here. This apparent difference could be due to tunicamycin and manganese triggering different ER stress pathways.

Loss/depletion of *CLN3* triggers ER stress in both HeLa and 1-kb fibroblast cells. Therefore, I investigated whether the ER stress induced in this acute model of CLN3 disease is followed by UPR activation. As a marker of UPR activation the endogenous levels of CHOP were assessed. CHOP is a proapoptotic protein that is upregulated downstream of the transcription factor ATF4, which is uniquely responsive to ER stress (Welihinda and Kaufman 1996). CHOP is activated in the final step of the UPR and causes downregulation of anti-apoptotic proteins (Zinszner et al., 1998) (see introduction, section 1.5.6).

In *CLN3*-depleted HeLa cells the levels of CHOP increase significantly (more than 2 fold) 56 hours post-transfection (Figure. 5.1.1.3). Moreover, when these *CLN3*-depleted cells are exposed to high manganese concentrations the levels of CHOP have already increased by 1 hour after exposure (Figure. 5.1.1.3). The result obtained upon Mn^{2+} exposure is due to the fact that the lack of Mn^{2+} within the Golgi complex impairs the correct glycosylation process causing mis-folding of the processed proteins (Xu et al., 2010). Furthermore, the Golgi complex is not able to detoxify the excess of Mn^{2+} causing the Mn^{2+} accumulation within the cytoplasm, which is also able to trigger ER stress (Xu et al., 2010). The levels of CHOP were also assessed in 1-kb patient fibroblasts. The fibroblasts from 1-kb patients are less resistant to ER stress, and when these cells are exposed to high manganese concentration, CHOP is further upregulated 1 hour after exposure (Figure 5.1.1.4).

Together these results indicate that loss or depletion of *CLN3* is able to trigger ER stress leading to UPR activation.

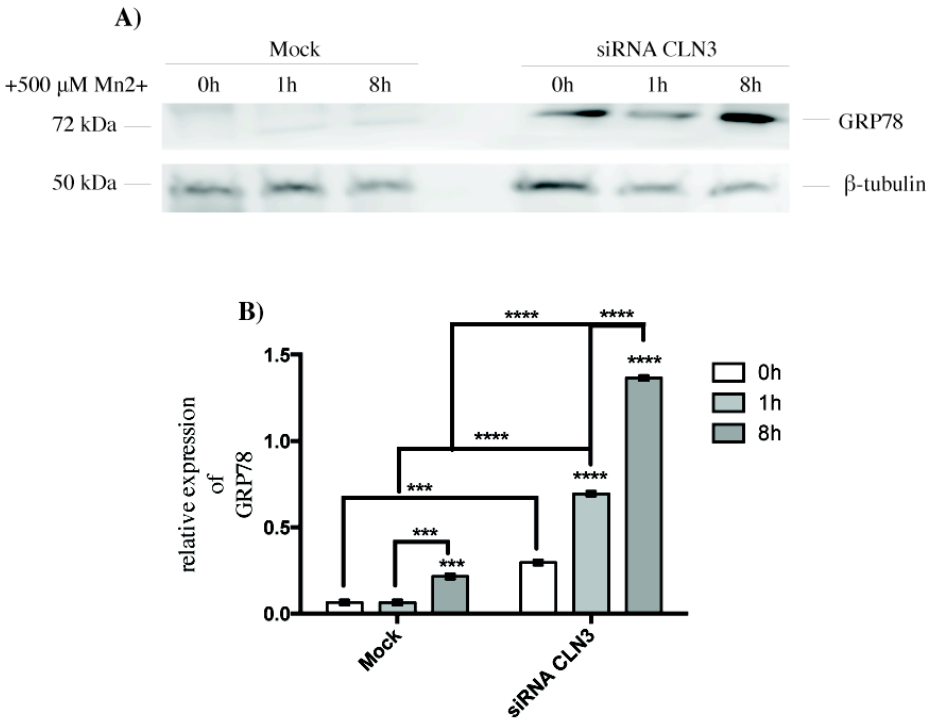

***Figure* 5.1.1.2** - CLN3 depletion enhances GRP78/BiP levels. **A**) WB analysis of GRP78 (upper panel) with β-tubulin as a loading control (lower panel). **B**) The bar chart shows the significant increase of GRP78 in CLN3-depleted HeLa cells and a further increase when exposed to Mn^{2+} (The experiment was done in triplicate, and the data shown are mean±SEM shown in *Appendix C*).

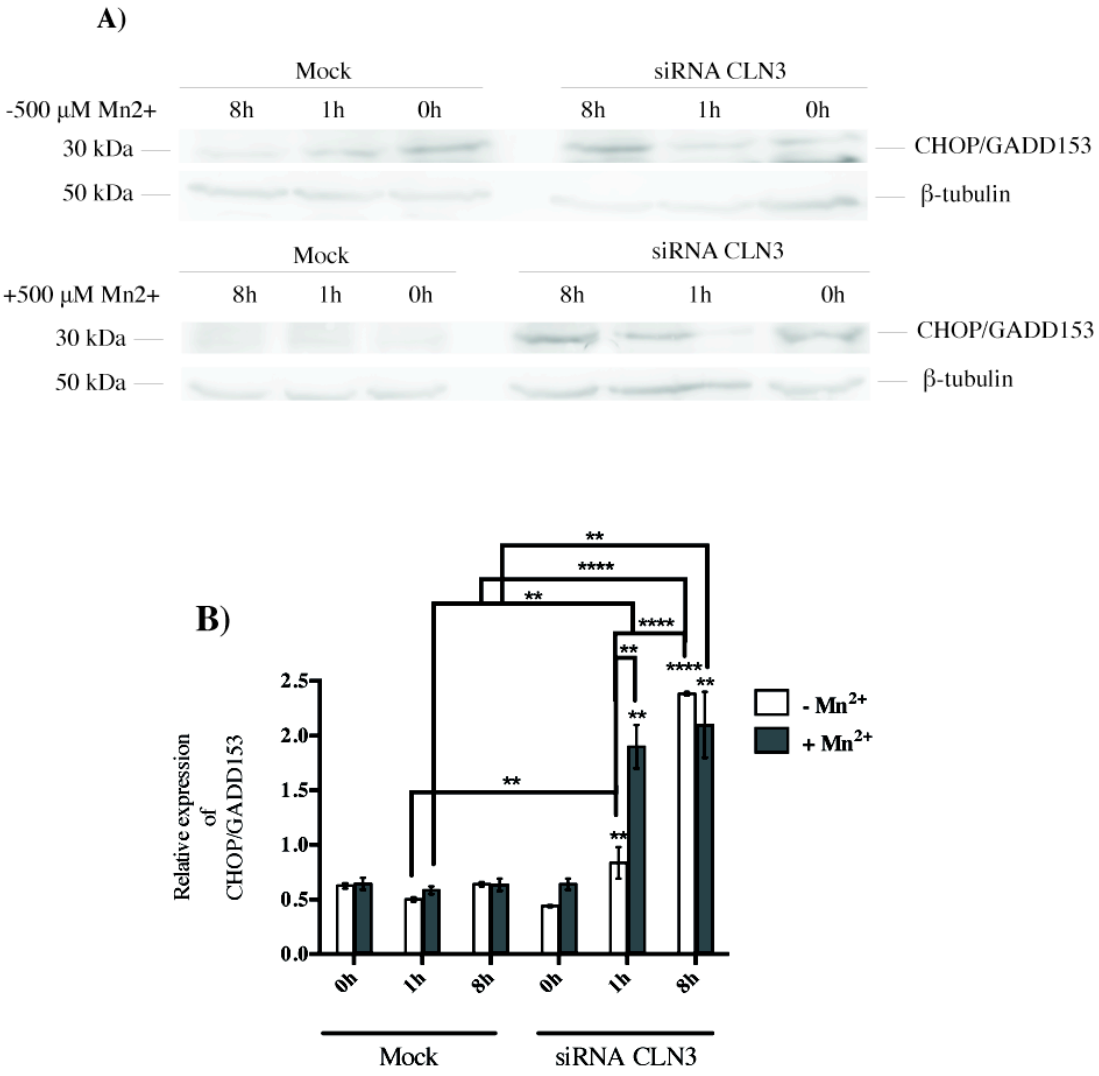

***Figure* 5.1.1.3** - CLN3 depletion enhances CHOP/GADD153 levels. **A**) WB analysis of CHOP with and without exposure to Mn^{2+} with β-tubulin as a loading control. **B**) The bar chart shows a significant increase of CHOP in CLN3-depleted HeLa cells exposed and not to Mn^{2+}. (The experiment was done in triplicate, and the data shown are mean±SEM shown in *Appendix C*).

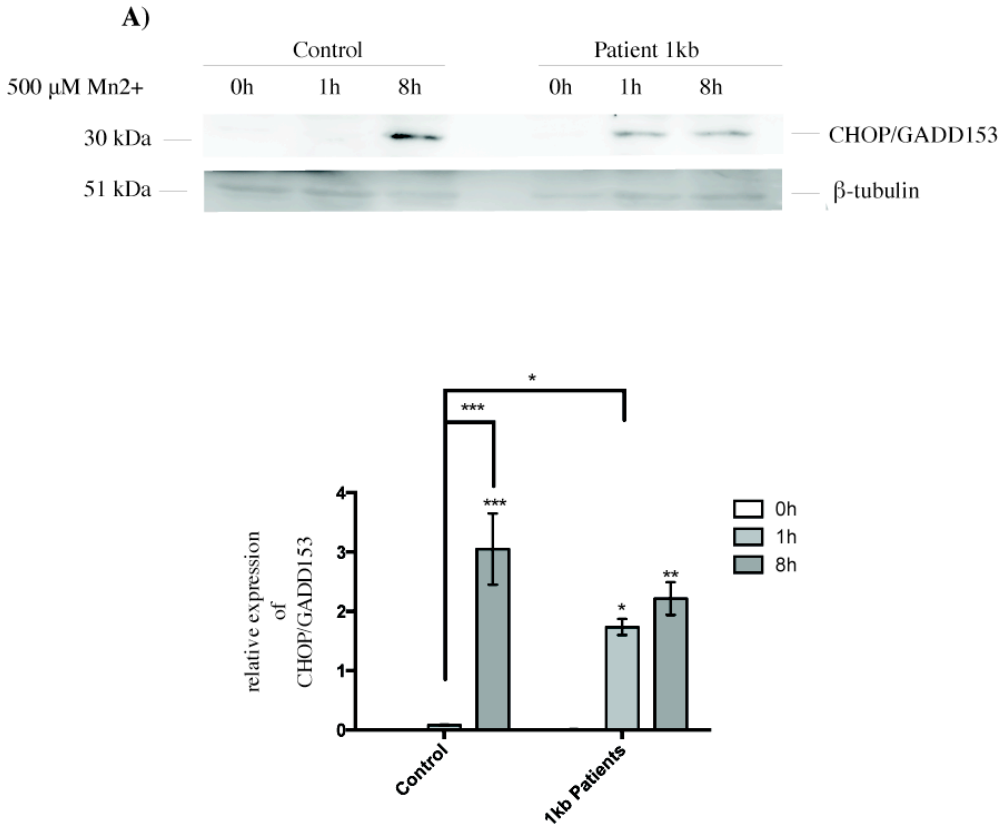

***Figure* 5.1.1.4** – 1-kb CLN3 fibroblast are less resistant to ER stress. **A**) WB analysis of CHOP upon Mn^{2+} exposure with β-tubulin as a loading control. **B**) The bar chart shows the significant increase of CHOP in 1-kb patient fibroblast cells upon Mn^{2+} exposure (The experiment was done in triplicate, and the data shown are mean±SEM shown in *Appendix C*)

5.1.2 Depletion of CLN3 causes activation of the caspase 2

In the previous sections of this chapter we have shown that deletion/depletion of *CLN3* affect Mn^{2+}- Golgi complex intake, which in turn can lead to ER stress and UPR activation. The ER membrane expansion along with the enhanced levels of both GRP78 and CHOP confirm that ER stress and UPR activation is occurring in *CLN3* depleted HeLa cells and 1-kb patient fibroblasts. CHOP expression, as mentioned, increases in the final step of the UPR, in particular, by promoting ER stress-induced apoptosis (Zinszner et al., 1998) (see introduction, section 1.6.2). In order to investigate whether apoptosis is activated in *CLN3* depleted HeLa cells, the activation of caspase 2 was pursued.

Apoptosis is an evolutionarily conserved programmed cell death pathway designed to remove extraneous or damaged cells (Ferri and Kroemer 2001; Reed et al., 2004). Caspases are the central mediators of apoptotic cell death (Riedl and Shi 2004). Caspases are cysteine proteases that cleave after aspartate residues within specific proteins, irreversibly modifying target protein function. Caspases are synthesized as zymogens with low intrinsic activity but are fully activated by cleavage, releasing an inhibitory prodomain and separating the protease subunits.

Caspase 2 activation occurs during both intrinsic and extrinsic apoptotic signalling (Kumar 2009). Caspase 2 is activated by ER stress stimulus and the activated form of caspase 2 leads to apoptosis through activation of caspase cascade and pro-apoptotic factors (Kumar 2009). The discovery of a pool of caspase-2 localized to the cytoplasmic face of the Golgi complex indicates that caspase-2 may play a key role in

apoptotic signalling at the Golgi complex (Mancini et al., 2000). The Golgi localization of caspase-2 implies that it is positioned to interact with upstream apoptotic regulators at the Golgi, resulting in the cleavage of substrates enriched at the Golgi, such as golgin-160 (Mancini et al., 2000). Caspase cleavage was monitored following CLN3-depletion and activation of ER stress. In *CLN3* depleted HeLa cells exposed to Mn^{2+}, caspase 2 is cleaved (Figure 5.1.2.1). These results suggest that depletion of CLN3 is able to trigger apoptosis through ER stress activation.

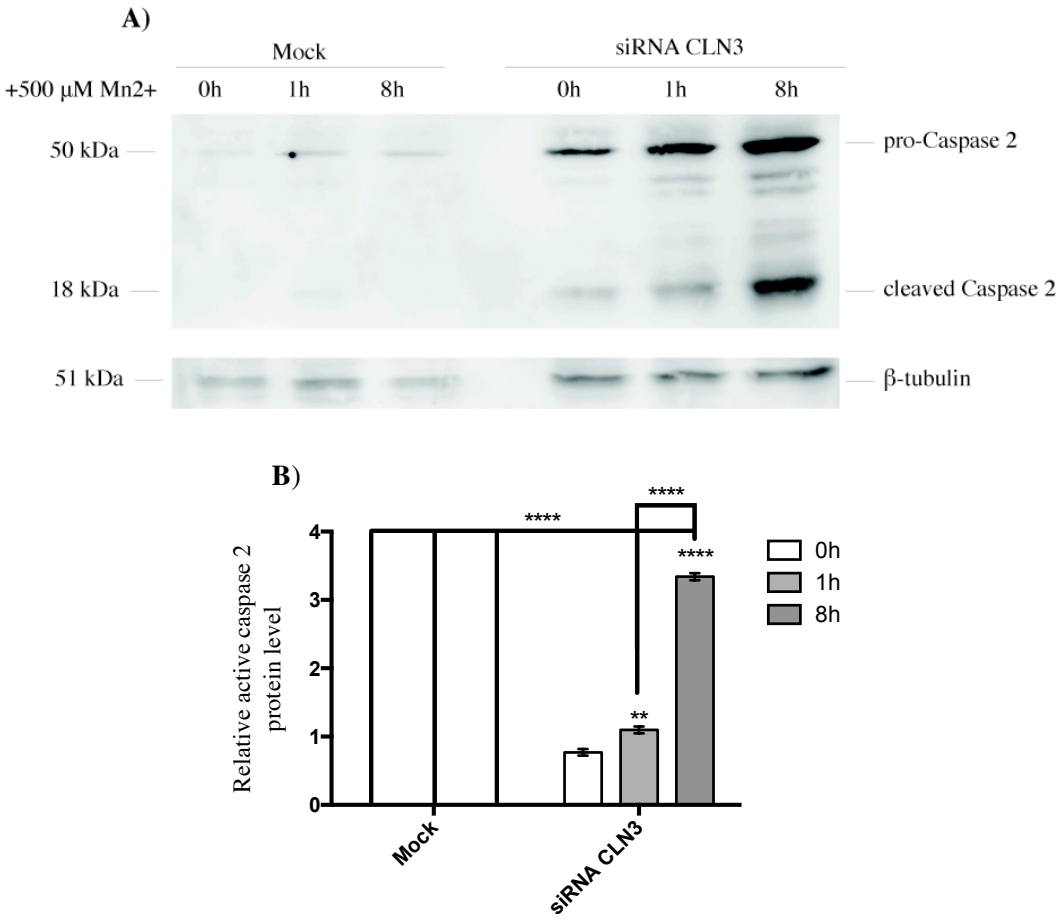

***Figure* 5.1.2.1** - CLN3 depletion causes activation of caspase 2. **A**) WB analysis of caspase 2 (pro-caspase 2 and the active caspase 2 cleaved forms) upon Mn^{2+} exposure (upper panel) with β-tubulin as a loading control (lower panel). **B**) The bar chart shows the increase of the active caspase 2 cleaved 18kDa fragment following CLN3 depletion and Mn^{2+} exposure. (The experiment was done in triplicate, and the data shown are mean±SEM shown in *Appendix C*)

5.1.3 Synopsis

The ER increases the size of its membrane to alleviate stress. Consequently, its incresed volume creates more space for the unfolded proteins, increase in chaperones and folding machineries. Doing so is an attempt to overcome the state of emergency, eventually, leading to activation of the UPR. In this chapter fibroblast cell lines from 1-kb patients, were shown to possess an ER increased in size, which is a clear sign of stress. Consistent with this observation, *CLN3* depleted HeLa cells also showed an ER enlarged, and an increase in GRP78 protein levels. Moreover, the ER stress in *CLN3*-depleted HeLa cells leads to the activation of the UPR, as demonstrated by the increase in CHOP levels. In these cells, CHOP increases even more significantly when the cells are exposed to high manganese concentration. This effect could be due to an inability of the Golgi complex to detoxify the excess manganese, with the ion accumulation in the cytoplasm generating stress. Another possibility is that there is a lack of Mn^{2+} in the Golgi lumen that affects protein glycosylation. Improper protein glycosylation itself triggers ER stress since proteins cannot fold properly and accumulate in the ER (Xu et al., 2010). Indeed, this bivalent cation is the main cofactor of Golgi-resident glycoysyltransferases (Gastinel et al., 2001; Persson et al., 2001; Lobsanov et al., 2004). In addition, CLN3 depleted HeLa cells cannot overcome the UPR, leading to activation of the apoptotic pathway as indicated by caspase 2 cleavage.

These results show that CLN3 is involved in Golgi Mn^{2+} homeostasis and deregulation of this process leads to a very stressful event for the cells. Therefore, as a result of the incapacity of the ER to overcome this deregulation, the persistent stress conditions activate the UPR, leading to the activation of the apoptotic pathway.

Furthermore, the ER of CLN6 fibroblast cell lines is also increased in the same way as CLN3 1-kb patient fibroblast. This result suggests that the ER stress activation may be a shared feature between CLN3 and CLN6 disease. However, further studies are needed to establish the role of the ER stress in CLN6 disease and to elucidate the source of the stress in these CLN6 patients' fibroblast cell lines and in *CLN6* depleted HeLa cell lines.

Chapter Six

Chapter Six

Deletion of *btn1* in *S. pombe* affects Golgi complex morphology and causes expansion of the ER

6.1 Absence of *btn1* in *S. pombe* causes morphological changes in the Golgi

This chapter shows that lack of *btn1*, the CLN3 orthologue in fission yeast, causes an enlargement of both the Golgi complex and the ER. Those results are concordant with the results observed in mammalian cell lines.

6.1.1 Golgi complex morphology in the *S. pombe* model for Batten disease

The morphological changes of the Golgi complex observed in mammalian cell lines are also present in fission yeast *btn1*Δ. New mutant strains, created by Dr. Michael Bond and Mariana Vieira (Methods, section 2.2.10) were used for this study. The observation previously made by Codlin *et al.,* (2009) used a fission yeast strain with a different genetic background from that used in this study. The observations made using the electron microscope gave us more information about Golgi complex and ER stress in CLN3 disease. The volume fraction of the Golgi complex in fission yeast, for this study, has been quantified by stereological approach (Materials and Methods, section 2.2.17). The *S. pombe* cells were inoculated in minimal medium, grown and prepared for TEM (Methods, section 2.2.12.1). The Golgi complex in the *btn1*-deleted strain shows an increase in volume (Figure 6.1.1.1). This increase observed in fission yeast is consistent with the increase observed in HeLa cells *CLN3* depleted (Results, chapter 3, section 3.1.1) and 1-kb patient fibroblast (Results, chapter 3, section 3.1.2).

In addition, the Golgi complex in *btn1*-deleted cells shows abnormal shapes (Figure 6.1.1.2). For example, the curvilinear shape occurs more in in *btn1*-deleted cells than in the wild type strain whereas the expected linear shape is observed with less frequency. These results suggest that the Golgi complex responds to the lack of Btn1p and, as a result, the organelle change its shape. The changes observed could initiate a stress signal. Indeed, it has been previously reported that the Golgi complex fragmentation is a common characteristic shared by different neurodegenerative disorders (Gonatas et al., 2006).

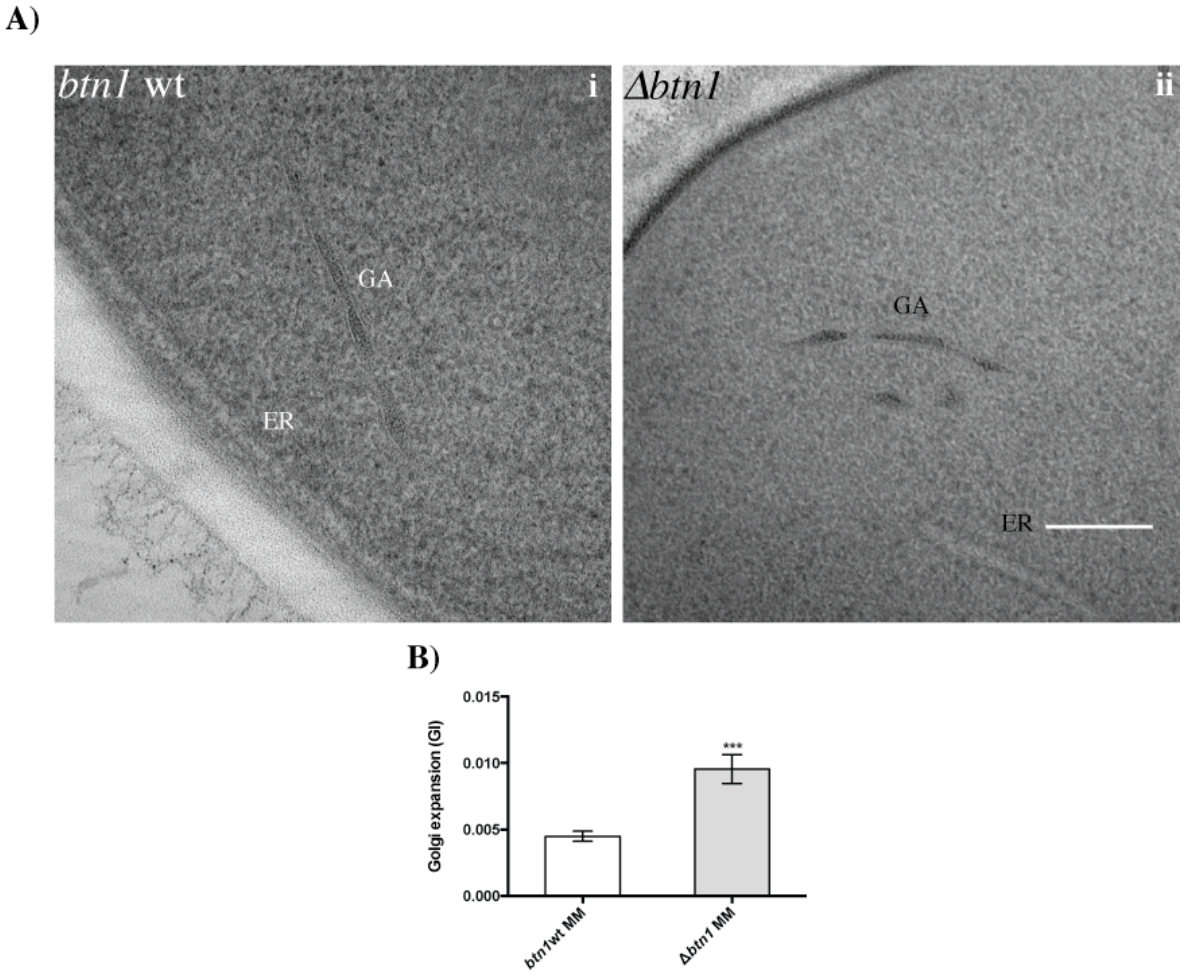

***Figure* 6.1.1.1** – *btn1*Δ exhibits changes in GA morphology. **A**) The micrographs are showing the Golgi complex in fission yeast. i) wild-type cells; ii) *btn1*Δ, (scale bar 200nm). **B**) The bar chart shows an increased area of the Golgi complex in fission yeast, *S. pombe,* lacking *btn1*. GA=Golgi Apparatus; ER= endoplasmic reticulum. (The experiment was done in triplicate, and the data shown are mean±SEM shown in *Appendix D).*

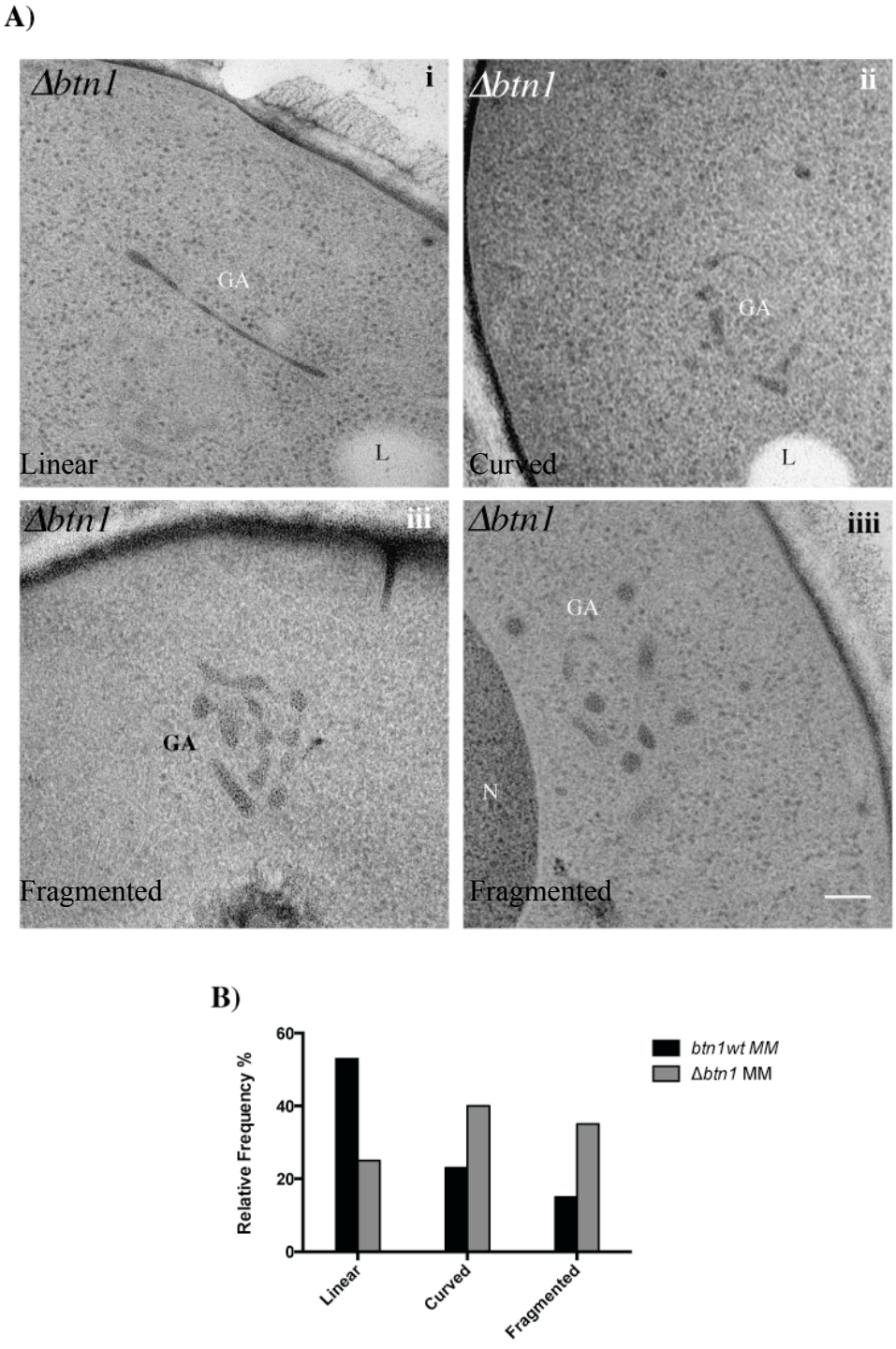

***Figure* 6.1.1.2** – Golgi complex morphology in fission yeast *btn1*Δ. Golgi complex in fission yeast deleted for *btn1* shows abnormal shapes (A and B). Scale bar 200nm. GA=Golgi apparatus; ER=endoplasmic reticulum; L=lipid droplet; N=nucleus. (wt: Linear= 53; curved=23; fragmented=15. *btn1*Δ; Linear=25; curved=40; fragmented=35) (The experiment was done in triplicate).

6.1.2 ER volume fraction in *S. pombe* model for Batten disease

The early steps of the protein maturation process, such as folding of the nascent polypeptide chains and posttranslational modifications important for the correct folding and function of the protein take place within the ER (Harding et al., 1999). If the influx of nascent unfolded polypeptides exceeds the folding and processing capacity of the ER the homeostasis of the ER is be perturbed. Under ER stress conditions, the ER membrane increases its volume (Schuck et al., 2009). The ER deals with the stress by increasing its volume in order to dilute the increased unfolded protein load and host more chaperones (Schuck et al., 2009) (see Introduction, section 1.6).

Therefore, I investigated whether the increase of the ER volume fraction observed in HeLa cells *CLN3* depleted and 1-kb patient fibroblast cell lines also occur in *S. pombe* deleted for *btn1*. The stereological analysis revealed that the ER of *S. pombe* lacking *btn1* is enlarged (Figure 6.1.2.1). The volume fraction of the ER of fission yeast, lacking *btn1,* shows a significant increase compared with the wild type strain (Figure 6.1.2.1).

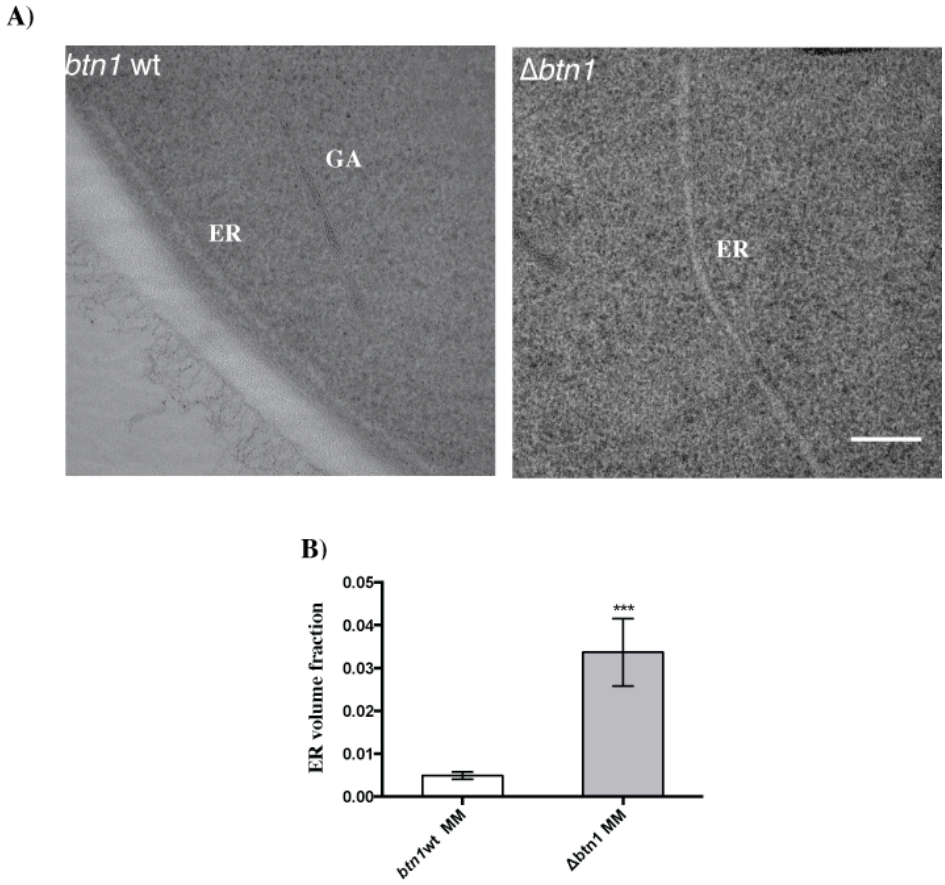

***Figure* 6.1.2.1** – ER volume fraction in fission yeast. The yeast *btn1*Δ shows a significant increase in the ER volume (**A**), which is quantified in bar chart **B**. i) scale bar, 200nm. ii) scale bar 200nm.. GA=Golgi apparatus; ER=endoplasmic reticulum. (The experiment was done in triplicate, and the data shown are mean±SEM shown in *Appendix D)*.

6.2 Synopsis

In this chapter I have shown that both the morphological changes observed at Golgi complex level and the increase of the ER volume in CLN3-depleted HeLa cells and in fibroblast generated form 1-kb patient skin biopsies are also present in fission yeast *S. pombe* lacking *btn1*. Specifically, fission yeast lacking *btn1* show an increased volume fraction of the Golgi complex, which is accompanied by morphological changes. The Golgi complex in fission yeast lacking *btn1* more frequently adopts a curvilinear shape rather than the canonical linear morphology observed in wild-type cells. These results further corroborate the fact that Golgi complex and ER play a pivotal role in the CLN3 disease pathogenesis that is conserved across diverse species (Codlin and Mole 2009).

Chapter Seven

Chapter Seven

Pharmacological rescue of the Golgi complex organisation in juvenile CLN3 disease patient fibroblasts

7.1 Drug rescue of the Golgi compactness in juvenile CLN3 disease patient cell lines

This chapter details the ability of three drugs, Alloxazine, E64 and prochlorperazine dimaleate, to rescue the aberrant Golgi complex organisation in juvenile CLN3 patient fibroblast cell lines homozygous for the 1-kb deletion.

7.1.1 Drug screening in juvenile CLN3 disease patient cell lines

A screen of the LoPAC drug library of pharmacologically active compounds for rescue of cell death in *S. pombe* deleted for btn1 grown in restrictive conditions, by Vieira Mariana, revealed that 3 out of >1000 compounds significantly rescued the phenotype. Those 3 compounds are: Alloxazine an adenosine A(2B)AR receptor antagonist (Liang and Haltiwanger 1995); L-trans-Epoxysuccinyl-leucylamido(4-guanidino)butane (E64), which is a cysteine peptidases inhibitor (Barrett 1982); and prochlorperazine dimaleate a dopamine D_2 receptor antagonist (Lummis and Baker 1997). To test whether these same drugs alleviated the abnormal Golgi morphology of fibroblasts from juvenile CLN3 disease patients, one healthy control and one patient fibroblast line with typical aberrant Golgi morphology (Chapter 3, section 3.1.2) were incubated with different concentrations of alloxazine, E64 and prochlorperazine dimaleate (5, 10 and 20μM) for 24 hours. Afterwards, cells were stained, using GM130 as a marker, and imaged.

The compactness of the Golgi apparatus was measured for all the fibroblasts, with and without drug treatment. A difference in Golgi complex compactness between 1-kb patient and healthy control untreated fibroblasts was observed (Chapter 3, section 3.1.2): 0.08 in control and 0.02 in patient cells.

After incubation with the three compounds at three different concentrations (5, 10 and 20μM), all except alloxazine significantly rescue the low compactness of the Golgi apparatus in the fibroblasts with the 1-kb deletion (Figure 7.1.1.1, D; E and F). E64 restores the compactness value to 0.08 at 5 and 10μM and to 0.1 at the higher concentration of 20μM (Figure 7.1.1.1, E). Prochlorperazine dimaleate also restores the

value to 0.09 and 0.08 at 5 and 10 µM respectively (Figure 7.1.1.1, F). At a higher concentration (20µM), it seems that this compound kills the cells, since no cells remained in any of the two experiments (Figure 7.1.1.1, C and F). With the exception of prochlorperazine dimaleate at 20µM, none of the compounds at any concentration altered the Golgi compactness of the healthy control fibroblasts (Figure 7.1.1.1, A; B; C).

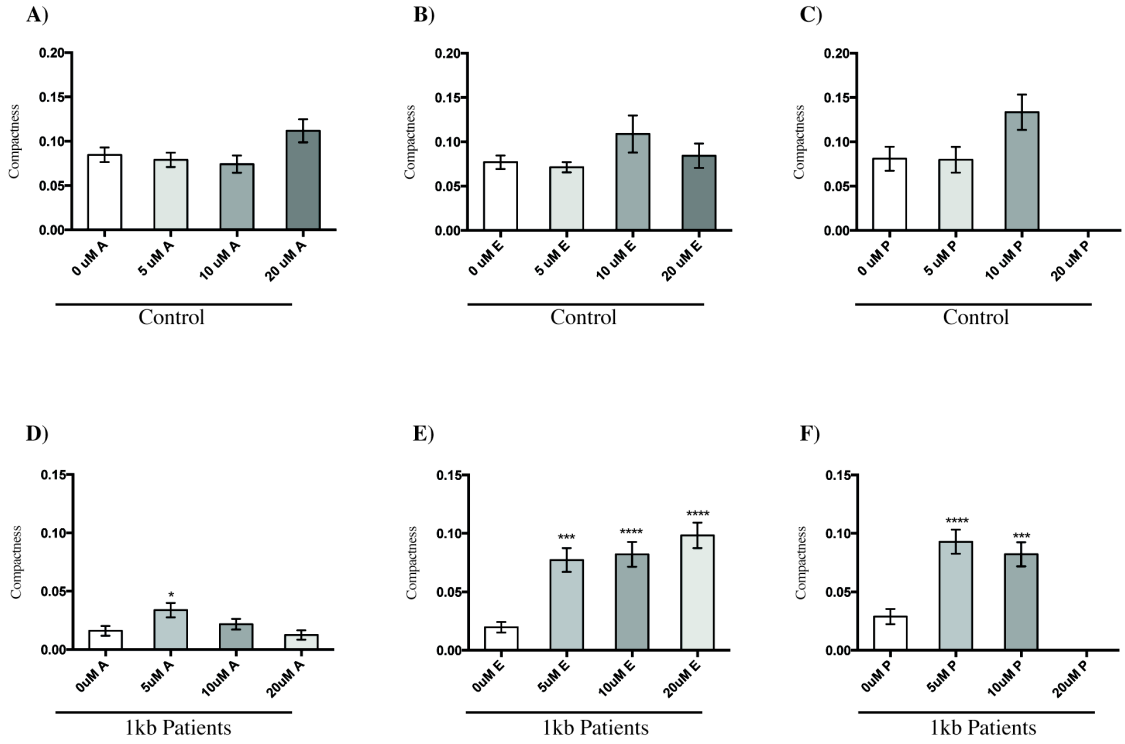

***Figure* 7.1.1.1** - Effect of alloxazine, E64 and prochlorperazine dimaleate on Golgi complex compactness of 1-kb patient fibroblast cell lines. **A; B** and **C**) Control HF527N 24h incubation with Alloxazine (A) E64 (B) and prochlorperazine dimaleate (C). **D**; **E** and **F**) 1-kb Patient fibroblast cell lines, HF480Pa 24h incubation with Alloxazine (A) E64 (B) and prochlorperazine dimaleate (C). After incubation with the three compounds at three different concentrations (5, 10 and 20µM) (The experiment was done in triplicate, and the data shown are mean±SEM shown in *Appendix E*).

In conclusion, E64 and prochlorperazine dimaleate used in this study can rescue significantly the altered Golgi compactness of juvenile CLN3 disease. The 5µM drug concentration is enough to rescue the phenotype as it is shown in Figure 7.1.1.2.

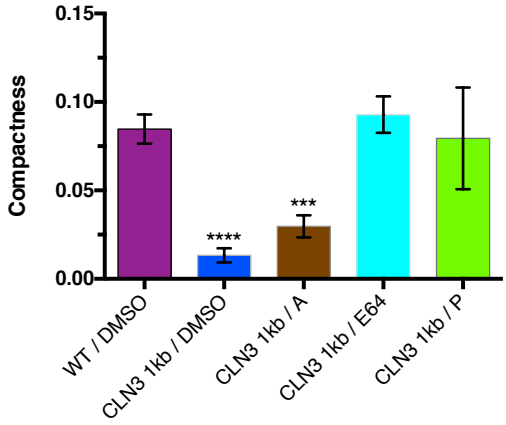

***Figure* 7.1.1.2** – Rescue of the Golgi complex compactness in 1-kb patient fibroblast. The Graph is showing the effect of the drugs on the Golgi complex compactness. In the graph **A**= alloxazine and **P**= prochlorperazine dimaleate. The values plotted in this graph are those deriving from the 5µM drug concentration (The experiment was done in triplicate, and the data shown are mean±SEM shown in *Appendix E*).

6.1.2 Synopsis

In this chapter we have shown the ability of three drugs, Alloxazine, E64 and prochlorperazine dimaleate, to rescue the Golgi complex organisation in 1-kb patient fibroblast cell lines. The drug that more efficiently rescues the Golgi compactness is E64. The promising results obtained from the drug screening are encouraging further investigations.

Chapter eight

Discussion

8.1 Discussion

Defects in *CLN3* lead to the juvenile form of neuronal ceroid lipofuscinosis (juvenile CLN3 disease, JNCL or Batten Disease). CLN3 is a multi-pass trans-membrane protein that is highly conserved in single-celled eukaryotes such as the fission yeast *S. pombe*, suggesting a fundamental role for this protein. CLN3 has been linked to many different cellular processes including autophagy, lipid synthesis and/or modification, lysosomal homeostasis, cytoskeleton organisation and trafficking. Despite these endeavours, the function of CLN3 remains elusive. Overexpression of GFP-tagged CLN3 in mammalian cells shows a consensus localisation at the lysosomal membrane. However, Codlin *et al*., (2009) showed that a GFP-tagged fission yeast orthologous protein, Btn1p, localises at steady state to the Golgi complex as well as later trafficking to the vacuole membrane (the equivalent organelle to the mammalian lysosome). A Golgi location for Btn1 was later reported in budding yeast. In addition, loss of Btn1 function in *S. pombe* affects Golgi homeostasis, including both number and morphology, and trafficking of the hydrolase carboxypeptidase Y, Cpy1p, to the vacuole, probably by retarding the trafficking of its receptor, vacuole protein sorting 10 (Vps10) from the endoplasmic reticulum through the Golgi to the trans-Golgi network (TGN) (Codlin and Mole 2009). The results presented in this study indicate the importance of CLN3 at the Golgi complex and in disease pathogenesis. Moreover, the evidences depicted in this study highlight the role of the Golgi complex in sensing and transducing stress. This lays the basis for further work to determine both the exact mechanism of CLN3 activity and the stress-transducing pathways affected.

8.1.1 CLN3 and Golgi complex

Both mutation and depletion of *CLN3* in mammalian cells affects the Golgi complex morphology. In *CLN3* depleted HeLa cells the area of the Golgi complex is increased, with the *cis*-Golgi and TGN the most affected compartments. The same increase in *cis*-Golgi and TGN was observed in fibroblast cell lines generated from CLN3 patients' biopsies. Moreover, it is not only the size of the Golgi complex that is affected in these cell lines. The organisation of this organelle is also affected as demonstrated by the compactness studies. Significantly, the Golgi complex morphological changes observed in CLN3 depleted cells and/or fibroblast cell lines generated from patients with the 1-kb mutation are not present in fibroblast cell lines generated from patients affected by the other forms of NCLs.

Furthermore, the same morphological changes were observed in *S. pombe* deleted for *btn1*. In these fission yeast cells the fractional area of the Golgi complex increases, and there are changes in the organisation of the Golgi complex. We observed, more curvilinear shaped and less linear Golgi complex in *btn1* deleted cells.

These results suggest that the Golgi complex is affected by the catastrophic events triggered by loss of CLN3/Btn1 function. The Golgi responds to the loss of CLN3/Btn1 function by changing its shape that could originate some kind of stress signals. Importantly, this change is specific to CLN3 and is conserved across diverse species, suggesting that it is fundamentally connected with loss of CLN3/Btn1 function.

8.1.2 CLN3 and manganese

The morphological changes of the Golgi complex are accompanied by evidence that the Golgi cannot efficiently take manganese in from the cytoplasmic milieu upon depletion of *CLN3* or when *CLN3* is mutated, as in patient fibroblast. The Golgi-resident protein GPP130, which senses a rise in the concentration of the intra-Golgi Mn^{2+} levels and is degraded, is not degraded when CLN3 is either depleted or mutated, suggesting that Mn^{2+} is not being taken up by the Golgi, even when exposed to high concentrations. GPP130 degradation is strictly correlated with manganese concentration (Mukhopadhyay et al., 2010; Mukhopadhyay and Linstedt 2011; Masuda et al., 2013) within the Golgi complex. This failure in degradation is not a result of aberrant trafficking of GPP130 or lysosomal-dependent degradation upon the loss/depletion of CLN3. A normal EGFR degradation pattern was observed in *CLN3* depleted HeLa cells, supporting functional trafficking and degradation by lysosomes in these cells. Moreover, the lysosomal activity, of both *CLN3* depleted HeLa cells and 1-kb patient fibroblast cell lines, was assessed by measuring the Cathepsin B activity. Interestingly, and consistent with partial retention of function by the 1-kb mutant CLN3 protein, the reduction of the lysosomal activity of the 1-kb patient cell lines is less than that observed in *CLN3* depleted HeLa cells.

It is not easy to study Mn^{2+} homeostasis within the Golgi complex. To date, there are no commercially available probes that efficiently measure intra-Golgi manganese level. Some probes were tested but none were satisfactory. The failure of these probes is probably due to the much higher Ca^{2+} concentration compared to the manganese concentration within this organelle. As Mn^{2+} and Ca^{2+} are ions that share the same

divalent charge and are of similar size, probes supposed to detect Mn^{2+} may actually instead detect intra-Golgi Ca^{2+} concentrations (Liang and Canary 2010). Alternatively, the intra-Golgi calcium concentration is also affected, and this interferes with the use of these probes.

The most powerful tool available to indicate manganese concentration in the Golgi is therefore the protein GPP130, which is sensitive and specific. However, little it is known about the relation between GPP130 and manganese. Manganese could exist in various chemical forms including oxidation states (Mn^{2+}, Mn^{3+}, Mn^{4+}, Mn^{6+}, Mn^{7+}), salts (sulfate and gluconate), and chelates (aspartate, fumarate, succinate). It is not known whether one of the manganese chemical forms blocks and/or decrease the degradation ratio of GPP130.

In order to answer this question a key experiment would be the isolation of the Golgi complex by subcellular fractionation. The purified fraction of Golgi complexes exposed to high manganese concentration could be then analysed using inductively coupled plasma mass spectrometry (ICP-MS). In particular, ICP-MS is able to detect and count the number of ions present within the Golgi complex.

8.1.3 CLN3 and ER stress

In both 1-kb patient fibroblast cell lines and fission yeast, significant increase in the volume of the ER is detected and the protein levels of GRP78 are also enhanced in the mammalian cell model for CLN3 disease. The CLN3 1-kb mutated likely affects the Golgi complex intake of Mn^{2+}. A lack of Mn^{2+} within the Golgi complex can compromise the correct protein glycosylation steps (Butterworth 1986; Hurley 1987; Erikson and Aschner 2003). It is well known that incorrect protein glycosylation leads to accumulation of unfolded and misfolded protein within the ER (Xu et al., 2010). Such proteins building up in the ER can trigger the stress on the reticulum.

The ER stress leads to the activation of the unfolded protein response. The *CLN3* HeLa cells depleted and 1-kb patient fibroblast cell lines also show an increase in CHOP protein levels. CHOP is activated in the final step of the UPR and causes downregulation of the anti-apoptotic proteins (Zinszner et al., 1998). I also showed that loss/depletion of CLN3 leads to apoptosis, via caspase 2 cleavage and activation. Caspase 2 activation occurs during both intrinsic and extrinsic apoptotic signaling and leads to apoptosis through activation of caspase cascade and pro-apoptotic factors (Kumar 2009).

8.1.4 Model for cellular dysfunction

Experimental evidences suggest that several organelles are capable of sensing and relaying pro-apoptotic signals, culminating in the proteolytic activation of caspases and cell death (Reed et al., 2004). Each organelle is likely to be uniquely poised and equipped to sense specific stimuli related to their function and structure. For example, the ER is a major site for folding, modification and assembly of newly synthesized transmembrane and secretory proteins and has evolved a stress response pathway, the unfolded protein response, to cope with the accumulation of unfolded or misfolded proteins (Rutkowski and Kaufman 2004). Activation of the UPR has been shown to induce the expression of chaperones, attenuate translation, and degrade misfolded proteins in an attempt to alleviate the stress. Prolonged ER stress resulting in irreparable damage leads to apoptosis. Due to its central function in protein folding, the ER has evolved a unique ability to monitor the folding state of proteins and respond to improperly folded proteins by first adapting or, if the damage is too severe, causing cell death (Zinszner et al., 1998).

Evidence suggests that there is also a post-ER quality control system that operates at the Golgi complex to eliminate mutant or misfolded proteins that escape the ER (Arvan et al., 2002; Ramos-Castaneda et al., 2005). It is also likely that the Golgi complex can sense and transduce unique stress signals. Similar to ER stress signalling, the Golgi complex may initiate stress signaling through components of Golgi-localized machinery. Apoptosis would result if the stress cannot be alleviated. The discovery of a pool of caspase-2 localized to the cytoplasmic face of the Golgi complex suggests that caspase 2 may play a key role in apoptotic signaling at the Golgi complex (Mancini et

al., 2000).

Changes in both Golgi cisternae structure, including unstacking or swelling, and Golgi ion content, could also lead to transduction of a stress signal (Mancini et al., 2000). For example, changes in membrane curvature, as we observed in fission yeast, induced by swelling could result in either the recruitment or release of specific proteins allowing the activation of a proapoptotic-signalling cascade.

The results in *CLN3* depleted cells suggest that CLN3 regulates or influences the Mn^{2+} intake by the Golgi complex. This might be achieved either by regulating the main Ca^{2+}/Mn^{2+} pump, SPCA1, or CLN3 itself might be a key factor in the Mn^{2+} homeostasis at the Golgi complex. In addition, I observed that Mn^{2+} dyshomeostasis could be one of the initiating stress signals at Golgi complex. The Mn^{2+} dyshomeostasis along with the Golgi cisternae morphological changes presented in this study seem to transduce stress signals from Golgi. In CLN3 disease activation of the ER stress and UPR could be either a downstream effect of the Golgi stress activation or a parallel pathway. Activation of caspase 2 is consistent with both hypotheses.

Golgi-localized caspase 2 may be the best key to unlocking the role of the Golgi complex in apoptotic signalling. Understanding the mechanism by which stresses are sensed at the Golgi complex leading to activation of caspase 2 may shed some light on the role of Golgi structure in stress signalling. In addition, it will be important to determine whether or not the Golgi complex initiates a stress repair response analogous to the UPR prior to initiating apoptosis. Once Golgi-specific stimuli are identified, it will be interesting to determine the gene expression profile of Golgi and other secretory

pathway proteins during apoptosis. In assessing the role of Golgi structure in stress signalling, it will be important to determine if the structural changes observed in yeast and mammalian models of CLN3 disease are clear signs of stress.

Accumulation of biometals, in particular manganese, has been detected for other NCL subtypes such as CLN6 and CLN12/*ATP13A2* (Bras et al., 2012). This latter protein, also known as PARK9 more usually underlies Kufor-Rakeb syndrome (KRS), a rare parkinsonian phenotype with juvenile onset, and is a putative P-type transmembrane that acts as a shuttle for cations, including Mn, across the cell and blood brain barrier (Ramirez et al., 2006; Gitler et al., 2009). The expression level and activity of the manganese-dependent superoxide dismutase (MnSOD) were increased in the sheep CLN6 model as well as human affected by CLN6 disease (Heine et al., 2003). Recently, studies conducted on this ovine CLN6 model revealed an increase in Zn and Mn concentrations in the brain. The regions most affected are those where neuroinflammation and neurodegeneration occur. In addition, synaptic proteins, the metal-binding protein metallothionein, and the AKT/GSK3 and ERK/MAPK cellular signaling pathways were also altered (Kanninen et al., 2013a). Metals accumulation has also been detected in the CLN6 mouse model. Increased expression of the ER/Golgi-localized cation transporter protein, Zip7, was detected in cerebellar Purkinje cells and whole brain fractions and analysis revealed biometal accumulation in CLN6 brain fractions expressing markers for ER, Golgi, endosomes and lysosomes. These data link CLN6 expression and biometal homeostasis in CLN6 disease, and support altered cation homeostasis regulation as a key factor in NCL pathogenesis (Kanninen et al., 2013b).

This work may therefore also be relevant to understanding the molecular basis of NCL caused by mutations in CLN6 protein, which is located upstream of the Golgi apparatus, in the endoplasmic reticulum. However, mutated CLN6 does not affect the morphology of the Golgi complex, but it does cause ER membrane expansion in fibroblast cell lines from CLN6 patients.

8.1.5 Proposed model for CLN3 disease

The Golgi complex changes shape and increase its dimensions when CLN3 is mutated and does not efficiently take Mn^{2+} in. In addition, the depletion/mutation of *CLN3* causes ER stress with UPR activation. Furthermore, in CLN3 mammalian cells model there is activation of apoptotic pathway (Figure 8.1.5.1).

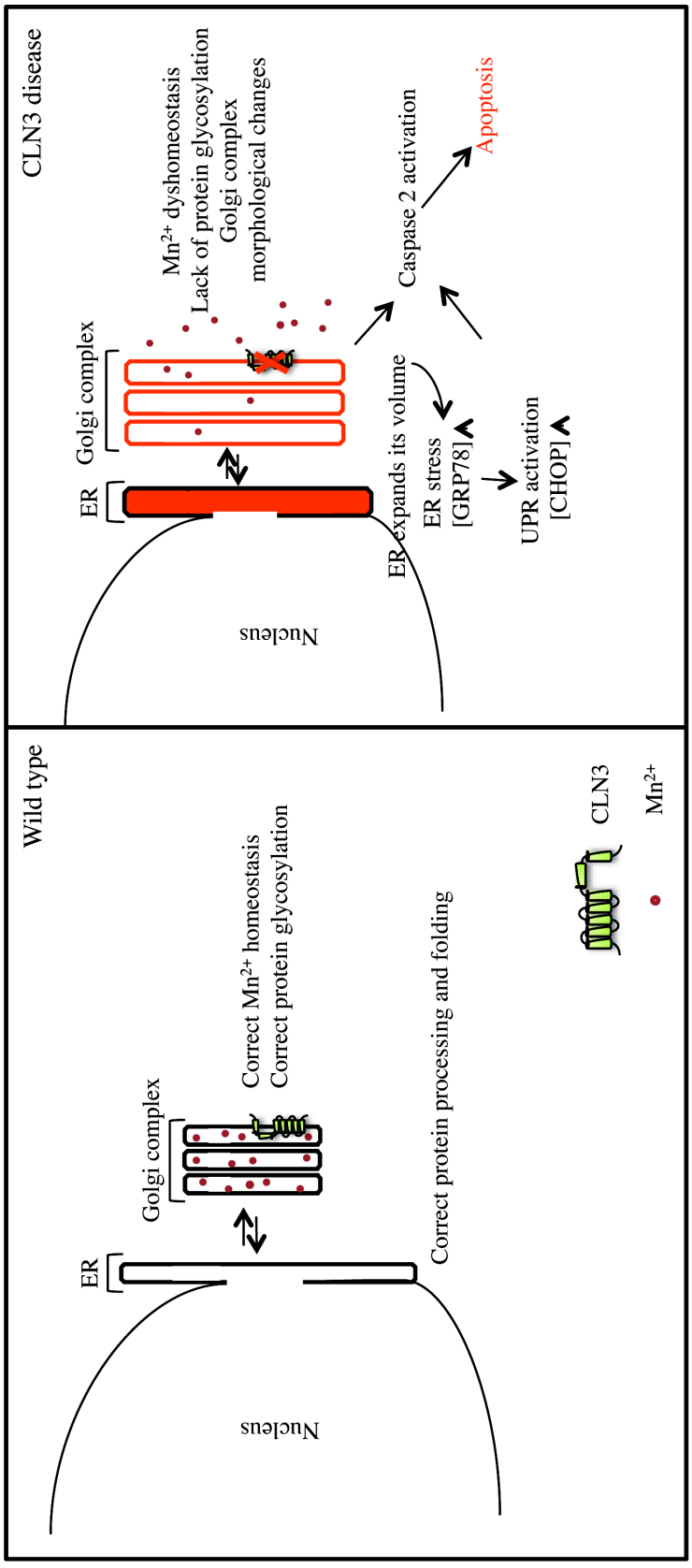

***Figure* 8.1.5.1** – A proposed model for CLN3 disease. When CLN3 is mutated Golgi complex changes morphology and increase its dimensions. These morphological changes are accompanied by Mn^{2+} dyshomeostasis. The Golgi complex, in the CLN3 disease model, does not efficiently take Mn^{2+} in. In addition, the depletion/mutation of *CLN3* cause ER stress with UPR activation. Both Golgi complex modifications and ER stress/UPR activation are able to trigger the apoptosis through caspase 2 cleavage.

8.1.6 Conclusions and future perspectives

Here, we provide evidence that CLN3, is involved in Golgi complex homeostasis and both *CLN3* depletion and 1-kb mutated form is able to trigger stress pathways in mammalian cells as well as deletion of *btn1* in fission yeast *S. pombe*. However, we previously showed that a GFP-tagged Btn1p localises at steady state to the Golgi complex in fission yeast (Codlin et al., 2009a). Moreover, I have shown that loss of Btn1p affects both number and morphology of the Golgi complex as well as trafficking. The Cpy1p is secreted in cells lacking Btn1, due to the mis-trafficking of its receptor vacuolar protein sorting 10 (Vps10) (Codlin and Mole 2009a). Here it is reported a newly identified mechanism, suggesting a potential role for CLN3 in Mn^{2+} homeostasis. This role for CLN3 would explain most of the phenotypes so far observed in the CLN3 disease models, which we believe to be, all, downstream effect of loss of Golgi complex homeostasis.

The findings presented in this study do not necessarily contradict previous work using CLN3 disease models. Early work in mammalian systems concluded that the functional location for CLN3 was the lysosome. However, endogenous levels of CLN3, like Btn1p, are low; hence the need for overexpression of CLN3, which might have affected its subcellular distribution. Nevertheless, a recent study (Storch et al., 2007) concluded that, like Btn1p in *S. pombe*, trafficking of wild type CLN3 to lysosomes was considerably slower than lysosome membrane-resident proteins, and that CLN3 remains in the Golgi compartment for a significant time. Indeed, a location of CLN3 in the Golgi has been noted previously (Haskell et al., 2000; Kremmidiotis et al., 1999).

Evidences suggest that several organelles are capable of sensing and relaying proapoptotic signals; culminating in the caspase activation and cell death (Fava et al., 2012) and Golgi complex could play a role in stress sensing. The Golgi complex shape undergoes to a fine regulation, which is controlled and maintained by many factors (Sengupta and Linstedt 2011). In particular, the glycosyltransferases play a very important role in maintaining the structure and function of the Golgi complex (Nilsson et al., 1994; Hassinen et al., 2010). Indeed, acting in trans those enzymes keep the Golgi cisternae flat (Nilsson et al., 1994; Hassinen et al., 2010). Moreover, those enzymes are responsible for the protein glycosylation, which ensure a correct protein folding. Those enzymes use Mn^{2+} as cofactor and the disturbance of Mn^{2+} concentration within both the cell and the Golgi complex compromises the protein glycosylation steps, which lead to accumulation of unfolded/misfolded proteins (Butterworth 1986; Hurley 1987; Erikson and Aschner 2003). Here, we have shown that CLN3 depletion mutation cause morphological and size changes of the Golgi complex. We believe that these changes are caused by Mn^{2+} dyshomeostasis within the Golgi. When CLN3 is mutated or deleted The Golgi complex cannot efficiently take Mn^{2+} in and the reduced intra-Golgi manganese concentration trigger stress events. First of all in absence of Mn^{2+} the glycosiltransferases cannot form complexes and act in trans shaping the Golgi, and this would explain the increased size and morphological changes observed in our models. In particular, the curved shape adopted by the Golgi along with ion dyshomeostasis could trigger stress pathways that lead to the activation of the caspase 2. Golgi localised caspase 2 may be the best candidate to unlock the role of the Golgi complex in both stress sensing and apoptotic signaling. The results in CLN3 depleted HeLa cells suggest that CLN3 influence the Mn^{2+} intake, this might be achieved either regulating the main Ca^{2+}/ Mn^{2+} pump, SPCA1, or CLN3 itself may play a role as transporter. Indeed, the

CLN3 depleted HeLa cells are irresponsive to Mn^{2+}. Patient fibroblasts are not manganese irresponsive, although higher levels of manganese appear to be necessary to achieve a turnover similar to that observed in control cells. If patient cells were irresponsive to manganese concentrations, and not merely insensitive, no changes in GPP130 levels upon manganese exposure would be expected. This may be due to the fact that mutant CLN3, in 1-kb patients, still possesses residual function. However, is not easy to investigate Mn^{2+} concentration in Golgi. To date there are no commercially available probes that efficiently measure the intra-Golgi Mn^{2+} concentration. Some probes have been tested but all of them failed. The failure of these probes is due to the fact that in Golgi the Ca^{2+} concentration is highly superior to the manganese concentration. Moreover, Mn^{2+} and Ca^{2+} are ions that are sharing the same divalent charge and similar size. Therefore, the probes made to detect Mn^{2+} truly sense and detect the intra-Golgi Ca^{2+} concentrations (Liang and Canary 2010). The most powerful tool available is the protein GPP130, which is sensitive and specific to intra-Golgi divalent manganese concentration. However, little it is known about the relation between GPP130 and manganese. The manganese could exist in various chemical forms including oxidation states (Mn^{2+}, Mn^{3+}, Mn^{4+}, Mn^{6+}, Mn^{7+}), salts (sulfate and gluconate), and chelates (aspartate, fumarate, succinate). It is not know whether the increase of one of the manganese chemical forms could block and/or decrease the degradation ratio of GPP130. In order to answer to this question a key experiment would be the isolation of the Golgi complex. The purified fraction of the Golgi complex exposed to high manganese concentration could be then analysed using the inductively coupled plasma mass spectrometry (ICP-MS). In particular, the ICP-MS is able to detect and count the number of ions present within the Golgi complex. Moreover, it has been shown that lack of Mn^{2+} impairs the correct protein glycosylation, which could

trigger ER stress. In our model we observed ER stress and UPR activation. Whether the Golgi stress occurs earlier than ER stress is still unknown but for sure they act in an orchestral manner to keep constant the cellular homeostasis. In particular, it seems to be confirmed by the fact that the caspase 2 is activated, as well, by ER stress stimulus and the activated form of caspase 2 leads to apoptosis through activation of caspase cascade and pro-apoptotic factors activation (Kumar 2009). The discovery of a pool of caspase-2 localized to the cytoplasmic face of the Golgi complex indicates that caspase-2 may play a key role in apoptotic signalling at the Golgi complex (Mancini et al., 2000). The Golgi localization of caspase-2 implies that it is positioned to interact with upstream apoptotic regulators at the Golgi, resulting in the cleavage of substrates enriched at the Golgi, such as golgin-160 (Mancini et al., 2000). In summary this work points to a role for CLN3 in the regulation of Golgi complex homeostasis. In particular, we propose a new role for CLN3 in the regulation of the Mn^{2+} homeostasis within the Golgi complex. The new phenotypes presented here open new horizons in term of therapy development. In addition, the insight on CLN3 could help to understand the molecular basis of NCLs caused by mutations in CLN6 and CLN8 proteins, which are located upstream of the Golgi complex, in the endoplasmic reticulum.

References

References

Adachi, Y., K. Yamamoto, et al. (2008). "ATF6 is a transcription factor specializing in the regulation of quality control proteins in the endoplasmic reticulum." Cell structure and function **33**: 75-89.

Andrews, N. C. (2000). "Iron homeostasis: insights from genetics and animal models." Nature reviews. Genetics **1**: 208-217.

Antebi, A. and G. R. Fink (1992). "The yeast Ca(2+)-ATPase homologue, PMR1, is required for normal Golgi function and localizes in a novel Golgi-like distribution." Molecular biology of the cell **3**: 633-654.

Antonny, B., D. Madden, et al. (2001). "Dynamics of the COPII coat with GTP and stable analogues." Nature cell biology **3**: 531-537.

Argon, Y. and B. B. Simen (1999). "GRP94, an ER chaperone with protein and peptide binding properties." Seminars in cell & developmental biology **10**: 495-505.

Arsov, T., K. R. Smith, et al. (2011). "Kufs disease, the major adult form of neuronal ceroid lipofuscinosis, caused by mutations in CLN6." American journal of human genetics **88**: 566-573.

Aschner, M. and M. Gannon (1994). "Manganese (Mn) transport across the rat blood-brain barrier: saturable and transferrin-dependent transport mechanisms." Brain research bulletin **33**: 345-349.

Ash, D. E., J. D. Cox, et al. (2000). "Arginase: a binuclear manganese metalloenzyme." Metal ions in biological systems **37**: 407-428.

Au, C., A. Benedetto, et al. (2008). "Manganese transport in eukaryotes: the role of DMT1." Neurotoxicology **29**: 569-576.

Bachert, C. and A. D. Linstedt (2010). "Dual anchoring of the GRASP membrane tether promotes trans pairing." The Journal of biological chemistry **285**: 16294-16301.

Bähler, J., J.-Q. Wu, et al. (1998). "Heterologous modules for efficient and versatile PCR-based gene targeting in Schizosaccharomyces pombe." Yeast **14**: 943-951.

Baloyannis, S. J., V. Costa, et al. (2004). "Mitochondrial alterations in Alzheimer's disease." American journal of Alzheimer's disease and other dementias **19**: 89-93.

Banfield, D. K., M. J. Lewis, et al. (1994). "Localization of Sed5, a putative vesicle targeting molecule, to the cis-Golgi network involves both its transmembrane and cytoplasmic domains." The Journal of cell biology **127**: 357-371.

Bannykh, S. I., T. Rowe, et al. (1996). "The organization of endoplasmic reticulum export complexes." The Journal of cell biology **135**: 19-35.

Barbeau, A. (1984). "Manganese and extrapyramidal disorders (a critical review and tribute to Dr. George C. Cotzias)." Neurotoxicology **5**: 13-35.

Barceloux, D. G. (1999). "Manganese." Journal of toxicology. Clinical toxicology **37**: 293-307.

Bard, F., L. Mazelin, et al. (2003). "Src regulates Golgi structure and KDEL receptor-dependent retrograde transport to the endoplasmic reticulum." The Journal of biological chemistry **278**: 46601-46606.

Barr, F. A., N. Nakamura, et al. (1998). "Mapping the interaction between GRASP65 and GM130, components of a protein complex involved in the stacking of Golgi cisternae." The EMBO journal **17**: 3258-3268.

Barr, F. A., M. Puype, et al. (1997). "GRASP65, a protein involved in the stacking of Golgi cisternae." Cell **91**: 253-262.

Behnia, R., F. A. Barr, et al. (2007). "The yeast orthologue of GRASP65 forms a complex with a coiled-coil protein that contributes to ER to Golgi traffic." The Journal of cell biology **176**: 255-261.

Bensaoula, T., H. Shibuya, et al. (2000). "Histopathologic and immunocytochemical analysis of the retina and ocular tissues in Batten disease." Ophthalmology **107**: 1746-1753.

Bertolotti, A., X. Wang, et al. (2001). "Increased sensitivity to dextran sodium sulfate colitis in IRE1beta-deficient mice." The Journal of clinical investigation **107**: 585-593.

Bevis, B. J., A. T. Hammond, et al. (2002). "De novo formation of transitional ER sites and Golgi structures in Pichia pastoris." Nature cell biology **4**: 750-756.

Boevink, P., K. Oparka, et al. (1998). "Stacks on tracks: the plant Golgi apparatus traffics on an actin/ER network." The Plant journal : for cell and molecular biology **15**: 441-447.

Boisrame, A., M. Kabani, et al. (1998). "Interaction of Kar2p and Sls1p is required for efficient co-translational translocation of secreted proteins in the yeast Yarrowia lipolytica." The Journal of biological chemistry **273**: 30903-30908.

Bonifacino, J. S. and B. S. Glick (2004). "The mechanisms of vesicle budding and fusion." Cell **116**: 153-166.

Bonifacino, J. S. and J. Lippincott-Schwartz (2003). "Coat proteins: shaping membrane transport." Nature reviews. Molecular cell biology **4**: 409-414.

Bowman, A. B., Erikson, K.M., Aschner, M. (2010). Manganese-the two faces of essentiality and neurotoxicity. Kerala, India, Research Signpost.

Bras, J., A. Verloes, et al. (2012). "Mutation of the parkinsonism gene ATP13A2 causes neuronal ceroid-lipofuscinosis." Human molecular genetics **21**: 2646-2650.

Brewer, J. W. (2014). "Regulatory crosstalk within the mammalian unfolded protein response." Cellular and molecular life sciences : CMLS **71**: 1067-1079.

Burkhardt, J. K. (1998). "The role of microtubule-based motor proteins in maintaining the structure and function of the Golgi complex." Biochimica et biophysica acta **1404**: 113-126.

Burman, J. L., J. N. Hamlin, et al. (2010). "Scyl1 regulates Golgi morphology." PloS one **5**: e9537.

Burton, B. K. (1998). "Inborn errors of metabolism in infancy: a guide to diagnosis." Pediatrics **102**: E69.

Butterworth, J. (1986). "Changes in nine enzyme markers for neurons, glia, and endothelial cells in agonal state and Huntington's disease caudate nucleus." Journal of neurochemistry **47**: 583-587.

Callen, D. F., E. Baker, et al. (1991). "Regional mapping of the Batten disease locus (CLN3) to human chromosome 16p12." American journal of human genetics **49**: 1372-1377.

Canonne-Hergaux, F., S. Gruenheid, et al. (1999). "Cellular and subcellular localization of the Nramp2 iron transporter in the intestinal brush border and regulation by dietary iron." Blood **93**: 4406-4417.

Casanova, J. E. (2007). "Regulation of Arf activation: the Sec7 family of guanine nucleotide exchange factors." Traffic **8**: 1476-1485.

Cellier, M., G. Prive, et al. (1995). "Nramp defines a family of membrane proteins." Proceedings of the National Academy of Sciences of the United States of America **92**: 10089-10093.

Chabin-Brion, K., J. Marceiller, et al. (2001). "The Golgi complex is a microtubule-organizing organelle." Molecular biology of the cell **12**: 2047-2060.

Charbaut, E., S. Chauvin, et al. (2005). "Two separate motifs cooperate to target stathmin-related proteins to the Golgi complex." Journal of cell science **118**: 2313-2323.

Chiu, R., L. Novikov, et al. (2002). "A caspase cleavage fragment of p115 induces fragmentation of the Golgi apparatus and apoptosis." The Journal of cell biology **159**: 637-648.

Christianson, D. W. (1997). "Structural chemistry and biology of manganese metalloenzymes." Progress in biophysics and molecular biology **67**: 217-252.

Codlin, S., R. L. Haines, et al. (2008a). "Btn1 affects cytokinesis and cell-wall deposition by independent mechanisms, one of which is linked to dysregulation of vacuole pH." Journal of cell science **121**: 2860-2870.

Codlin, S., R. L. Haines, et al. (2008b). "btn1 affects endocytosis, polarization of sterol-rich membrane domains and polarized growth in Schizosaccharomyces pombe." Traffic **9**: 936-950.

Codlin, S. and S. E. Mole (2009). "S. pombe btn1, the orthologue of the Batten disease gene CLN3, is required for vacuole protein sorting of Cpy1p and Golgi exit of Vps10p." Journal of cell science **122**: 1163-1173.

Connerly, P. L., M. Esaki, et al. (2005). "Sec16 is a determinant of transitional ER organization." Current biology : CB **15**: 1439-1447.

Consortium, T. I. B. D. (1995). "Isolation of a novel gene underlying Batten disease, CLN3. The International Batten Disease Consortium." Cell **82**: 949-957.

Cosson, P., C. Demolliere, et al. (1996). "Delta- and zeta-COP, two coatomer subunits homologous to clathrin-associated proteins, are involved in ER retrieval." The EMBO journal **15**: 1792-1798.

Cox, J. S., C. E. Shamu, et al. (1993). "Transcriptional induction of genes encoding endoplasmic reticulum resident proteins requires a transmembrane protein kinase." Cell **73**: 1197-1206.

Cox, J. S. and P. Walter (1996). "A novel mechanism for regulating activity of a transcription factor that controls the unfolded protein response." Cell **87**: 391-404.

Croisier, E. and M. B. Graeber (2006). "Glial degeneration and reactive gliosis in alpha-synucleinopathies: the emerging concept of primary gliodegeneration." Acta neuropathologica **112**: 517-530.

Croopnick, J. B., H. C. Choi, et al. (1998). "The subcellular location of the yeast Saccharomyces cerevisiae homologue of the protein defective in the juvenile form of Batten disease." Biochemical and biophysical research communications **250**: 335-341.

Crowley, J. A., Traynor, D.A., Weatherburn, D.C (1999). Enzymes and proteins containing manganese: an overview. In A. Sigel and H. Sigel (ed.), Manganese and its role in biological processes. Metal ions in biological systems. New York, Marcel Dekker.

Curmi, P. A., O. Gavet, et al. (1999). "Stathmin and its phosphoprotein family:general properties, biochemical and functional interaction with tubulin." Cell structure and function **24**: 345-357.

D'Angelo, G., L. Prencipe, et al. (2009). "GRASP65 and GRASP55 sequentially promote the transport of C-terminal valine-bearing cargos to and through the Golgi complex." The Journal of biological chemistry **284**: 34849-34860.

Danial, N. N. and S. J. Korsmeyer (2004). "Cell death: critical control points." Cell **116**: 205-219.

de Graffenried, C. L. and C. R. Bertozzi (2004). "The roles of enzyme localisation and complex formation in glycan assembly within the Golgi apparatus." Current opinion in cell biology **16**: 356-363.

Degterev, A., M. Boyce, et al. (2003). "A decade of caspases." Oncogene **22**: 8543-8567.

Dikic, I. (2003). "Mechanisms controlling EGF receptor endocytosis and degradation." Biochemical Society transactions **31**: 1178-1181.

Dippold, H. C., M. M. Ng, et al. (2009). "GOLPH3 bridges phosphatidylinositol-4-phosphate and actomyosin to stretch and shape the Golgi to promote budding." Cell **139**: 337-351.

Dobson, C. M., A. Šali, et al. (1998). "Protein Folding: A Perspective from Theory and Experiment." Angewandte Chemie International Edition **37**: 868-893.

Dorner, A. J., L. C. Wasley, et al. (1989). "Increased synthesis of secreted proteins induces expression of glucose-regulated proteins in butyrate-treated Chinese hamster ovary cells." The Journal of biological chemistry **264**: 20602-20607.

Dorner, A. J., L. C. Wasley, et al. (1990). "The stress response in Chinese hamster ovary cells. Regulation of ERp72 and protein disulfide isomerase expression and secretion." The Journal of biological chemistry **265**: 22029-22034.

Drack, A. V., J. N. Miller, et al. (2013). "A novel c.1135_1138delCTGT mutation in CLN3 leads to juvenile neuronal ceroid lipofuscinosis." Journal of child neurology **28**: 1112-1116.

Durr, G., J. Strayle, et al. (1998). "The medial-Golgi ion pump Pmr1 supplies the yeast secretory pathway with Ca2+ and Mn2+ required for glycosylation, sorting, and endoplasmic reticulum-associated protein degradation." Molecular biology of the cell **9**: 1149-1162.

Dyer, R. B. and C. T. McMurray (2001). "Mutant protein in Huntington disease is resistant to proteolysis in affected brain." Nature genetics **29**: 270-278.

Edwards, J. A. and J. E. Hoke (1975). "Red cell iron uptake in hereditary microcytic anemia." Blood **46**: 381-388.

Efimov, A., A. Kharitonov, et al. (2007). "Asymmetric CLASP-dependent nucleation of noncentrosomal microtubules at the trans-Golgi network." Developmental cell **12**: 917-930.

Egea, G., F. Lazaro-Dieguez, et al. (2006). "Actin dynamics at the Golgi complex in mammalian cells." Current opinion in cell biology **18**: 168-178.

Eid, T., A. Williamson, et al. (2008). "Glutamate and astrocytes--key players in human mesial temporal lobe epilepsy?" Epilepsia **49 Suppl 2**: 42-52.

Erikson, K. M. and M. Aschner (2003). "Manganese neurotoxicity and glutamate-GABA interaction." Neurochemistry international **43**: 475-480.

Erikson, K. M., T. Syversen, et al. (2005). "Interactions between excessive manganese exposures and dietary iron-deficiency in neurodegeneration." Environmental toxicology and pharmacology **19**: 415-421.

Estevez, A. G., M. A. Sahawneh, et al. (2006). "Arginase 1 regulation of nitric oxide production is key to survival of trophic factor-deprived motor neurons." The Journal of neuroscience : the official journal of the Society for Neuroscience **26**: 8512-8516.

Ezaki, J., M. Takeda-Ezaki, et al. (2003). "Characterization of Cln3p, the gene product responsible for juvenile neuronal ceroid lipofuscinosis, as a lysosomal integral membrane glycoprotein." Journal of neurochemistry **87**: 1296-1308.

Fairclough, R. J., L. Dode, et al. (2003). "Effect of Hailey-Hailey Disease mutations on the function of a new variant of human secretory pathway Ca2+/Mn2+-ATPase (hSPCA1)." The Journal of biological chemistry **278**: 24721-24730.

Fanchiotti, S., F. Fernandez, et al. (1998). "The UDP-Glc:Glycoprotein glucosyltransferase is essential for Schizosaccharomyces pombe viability under conditions of extreme endoplasmic reticulum stress." The Journal of cell biology **143**: 625-635.

Farquhar, M. G. and G. E. Palade (1981). "The Golgi apparatus (complex)-(1954-1981)-from artifact to center stage." The Journal of cell biology **91**: 77s-103s.

Faso, C., A. Boulaflous, et al. (2009). "The plant Golgi apparatus: last 10 years of answered and open questions." FEBS letters **583**: 3752-3757.

Fava, L. L., F. J. Bock, S. Geley and A. Villunger (2012). "Caspase-2 at a glance." J Cell Sci **125**: 5911-15.10.1242/jcs.115105:

Feinstein, T. N. and A. D. Linstedt (2008). "GRASP55 regulates Golgi ribbon formation." Molecular biology of the cell **19**: 2696-2707.

Feldheim, D., J. Rothblatt, et al. (1992). "Topology and functional domains of Sec63p, an endoplasmic reticulum membrane protein required for secretory protein translocation." Molecular and cellular biology **12**: 3288-3296.

Folsch, H., P. E. Mattila, et al. (2009). "Taking the scenic route: biosynthetic traffic to the plasma membrane in polarized epithelial cells." Traffic **10**: 972-981.

Forbes, J. R. and P. Gros (2003). "Iron, manganese, and cobalt transport by Nramp1 (Slc11a1) and Nramp2 (Slc11a2) expressed at the plasma membrane." Blood **102**: 1884-1892.

Franke, W. W., J. Kartenbeck, et al. (1972). "Inter- and intracisternal elements of the Golgi apparatus. A system of membrane-to-membrane cross-links." Zeitschrift fur Zellforschung und mikroskopische Anatomie **132**: 365-380.

Frost, A., M. G. Elgort, et al. (2012). "Functional repurposing revealed by comparing S. pombe and S. cerevisiae genetic interactions." Cell **149**: 1339-1352.

Fujita, Y., E. Ohama, et al. (2006). "Fragmentation of Golgi apparatus of nigral neurons with alpha-synuclein-positive inclusions in patients with Parkinson's disease." Acta neuropathologica **112**: 261-265.

Fujita, Y., K. Okamoto, et al. (2000). "Fragmentation of the Golgi apparatus of the anterior horn cells in patients with familial amyotrophic lateral sclerosis with SOD1 mutations and posterior column involvement." Journal of the neurological sciences **174**: 137-140.

Futai, E., S. Hamamoto, et al. (2004). "GTP/GDP exchange by Sec12p enables COPII vesicle bud formation on synthetic liposomes." The EMBO journal **23**: 4146-4155.

Futerman, A. H. and G. van Meer (2004). "The cell biology of lysosomal storage disorders." Nature reviews. Molecular cell biology **5**: 554-565.

Gachet, Y., S. Codlin, et al. (2005). "btn1, the Schizosaccharomyces pombe homologue of the human Batten disease gene CLN3, regulates vacuole homeostasis." Journal of cell science **118**: 5525-5536.

Galizzi, G., D. Russo, et al. (2011). "Different early ER-stress responses in the CLN8(mnd) mouse model of neuronal ceroid lipofuscinosis." Neuroscience letters **488**: 258-262.

Garrick, M. D., K. G. Dolan, et al. (2003). "DMT1: a mammalian transporter for multiple metals." Biometals : an international journal on the role of metal ions in biology, biochemistry, and medicine **16**: 41-54.

Gastinel, L. N., C. Bignon, et al. (2001). "Bovine alpha1,3-galactosyltransferase catalytic domain structure and its relationship with ABO histo-blood group and glycosphingolipid glycosyltransferases." The EMBO journal **20**: 638-649.

Gauthier, N. C., O. M. Rossier, et al. (2009). "Plasma membrane area increases with spread area by exocytosis of a GPI-anchored protein compartment." Molecular biology of the cell **20**: 3261-3272.

Gavet, O., S. El Messari, et al. (2002). "Regulation and subcellular localization of the microtubule-destabilizing stathmin family phosphoproteins in cortical neurons." Journal of neuroscience research **68**: 535-550.

Germain, M., J. P. Mathai, et al. (2002). "BH-3-only BIK functions at the endoplasmic reticulum to stimulate cytochrome c release from mitochondria." The Journal of biological chemistry **277**: 18053-18060.

Gething, M. J. (1999). "Role and regulation of the ER chaperone BiP." Seminars in cell & developmental biology **10**: 465-472.

Gilkey, J. C. and L. A. Staehelin (1986). "Advances in ultrarapid freezing for the preservation of cellular ultrastructure." Journal of Electron Microscopy Technique **3**: 177-210.

Gitler, A. D., A. Chesi, et al. (2009). "Alpha-synuclein is part of a diverse and highly conserved interaction network that includes PARK9 and manganese toxicity." Nature genetics **41**: 308-315.

Goebel H.H., M. S. E., Lake B.D. (1999). The neuronal ceroid lipofuscinoses (Batten disease), Amsterdam, IOS press.

Goedert, M. (2001). "Alpha-synuclein and neurodegenerative diseases." Nature reviews. Neuroscience **2**: 492-501.

Golgi, C. (1898a). "Intorno alla struttura della cellula nervosa." Boll Soc Med Chir Pavia 13: 1-14.

Golgi, C. (1898b). "Sur la structure des cellules nerveuses des ganglions spinaux." Arch Ital Biol 30: 60-71.

Gonatas, N. K., A. Stieber and J. O. Gonatas (2006). "Fragmentation of the golgi apparatus in neurodegenerative diseases and cell death." J Neurol Sci **246**: 21-30.10.1016/j.jns.2006.01.019:

Goytain, A., R. M. Hines, et al. (2008). "Huntingtin-interacting proteins, HIP14 and HIP14L, mediate dual functions, palmitoyl acyltransferase and Mg2+ transport." The Journal of biological chemistry **283**: 33365-33374.

Graham, T. R. and M. M. Kozlov (2010). "Interplay of proteins and lipids in generating membrane curvature." Current opinion in cell biology **22**: 430-436.

Griffiths, G., S. Pfeiffer, et al. (1985). "Exit of newly synthesized membrane proteins from the trans cisterna of the Golgi complex to the plasma membrane." The Journal of cell biology **101**: 949-964.

Griffiths, G. and K. Simons (1986). "The trans Golgi network: sorting at the exit site of the Golgi complex." Science **234**: 438-443.

Grimm, C., J. r. Kohli, et al. (1988). "Genetic engineering of Schizosaccharomyces pombe: A system for gene disruption and replacement using the ura4 gene as a selectable marker." Molecular and General Genetics MGG **215**: 81-86.

Gu, F., C. M. Crump, et al. (2001). "Trans-Golgi network sorting." Cellular and molecular life sciences : CMLS **58**: 1067-1084.

Gunshin, H., B. Mackenzie, et al. (1997). "Cloning and characterization of a mammalian proton-coupled metal-ion transporter." Nature **388**: 482-488.

Haines, R. L., S. Codlin, et al. (2009). "The fission yeast model for the lysosomal storage disorder Batten disease predicts disease severity caused by mutations in CLN3." Disease models & mechanisms **2**: 84-92.

Hamanaka, R. B., E. Bobrovnikova-Marjon, et al. (2009). "PERK-dependent regulation of IAP translation during ER stress." Oncogene **28**: 910-920.

Hammond, C. and A. Helenius (1994). "Quality control in the secretory pathway: retention of a misfolded viral membrane glycoprotein involves cycling between the ER, intermediate compartment, and Golgi apparatus." The Journal of cell biology **126**: 41-52.

Harding, H. P., Y. Zhang, et al. (1999). "Protein translation and folding are coupled by an endoplasmic-reticulum-resident kinase." Nature **397**: 271-274.

Haskell, R. E., C. J. Carr, et al. (2000). "Batten disease: evaluation of CLN3 mutations on protein localization and function." Human molecular genetics **9**: 735-744.

Hassinen, A., A. Rivinoja, et al. (2010). "Golgi N-glycosyltransferases form both homo- and heterodimeric enzyme complexes in live cells." The Journal of biological chemistry **285**: 17771-17777.

Hauri, H. P., F. Kappeler, et al. (2000). "ERGIC-53 and traffic in the secretory pathway." Journal of cell science **113 (Pt 4)**: 587-596.

Heine, C., B. Koch, et al. (2004). "Defective endoplasmic reticulum-resident membrane protein CLN6 affects lysosomal degradation of endocytosed arylsulfatase A." The Journal of biological chemistry **279**: 22347-22352.

Heine, C., J. Tyynela, et al. (2003). "Enhanced expression of manganese-dependent superoxide dismutase in human and sheep CLN6 tissues." The Biochemical journal **376**: 369-376.

Herbst, R. S. (2004). "Review of epidermal growth factor receptor biology." International Journal of Radiation Oncology ,Ä¢ Biology ,Ä¢ Physics **59**: S21-S26.

Hicke, L., T. Yoshihisa, et al. (1992). "Purification of yeast Sec23 protein by complementation of mutant cell lysates deficient in endoplasmic reticulum-to-Golgi transport." Methods in enzymology **219**: 338-352.

Hiramatsu, N., C. Messah, et al. (2014). "Translational and posttranslational regulation of XIAP by eIF2alpha and ATF4 promotes ER stress-induced cell death during the unfolded protein response." Molecular biology of the cell **25**: 1411-1420.

Hollien, J., J. H. Lin, et al. (2009). "Regulated Ire1-dependent decay of messenger RNAs in mammalian cells." The Journal of cell biology **186**: 323-331.

Hollien, J. and J. S. Weissman (2006). "Decay of endoplasmic reticulum-localized mRNAs during the unfolded protein response." Science **313**: 104-107.

Holopainen, J. M., J. Saarikoski, et al. (2001). "Elevated lysosomal pH in neuronal ceroid lipofuscinoses (NCLs)." European journal of biochemistry / FEBS **268**: 5851-5856.

Hurley, L. S., Keen, C.L. (1987). Manganese in trace elements in human health and animal nutrition. New York, Academic Press.

Huynh, D. P., H. T. Yang, et al. (2003). "Expansion of the polyQ repeat in ataxin-2 alters its Golgi localization, disrupts the Golgi complex and causes cell death." Human molecular genetics **12**: 1485-1496.

Inoue, H. and P. A. Randazzo (2007). "Arf GAPs and their interacting proteins." Traffic **8**: 1465-1475.

Jalanko, A. and T. Braulke (2009). "Neuronal ceroid lipofuscinoses." Biochimica et biophysica acta **1793**: 697-709.

Janes, R. W., P. B. Munroe, et al. (1996). "A model for Batten disease protein CLN3: functional implications from homology and mutations." FEBS letters **399**: 75-77.

Jarvela, I., M. Sainio, et al. (1998). "Biosynthesis and intracellular targeting of the CLN3 protein defective in Batten disease." Human molecular genetics **7**: 85-90.

Jensen, L. T., M. Ajua-Alemanji, et al. (2003). "The Saccharomyces cerevisiae high affinity phosphate transporter encoded by PHO84 also functions in manganese homeostasis." The Journal of biological chemistry **278**: 42036-42040.

Kaczmarski, W., K. E. Wisniewski, et al. (1999). "Studies of membrane association of CLN3 protein." Molecular genetics and metabolism **66**: 261-264.

Kama, R., V. Kanneganti, et al. (2011). "The yeast Batten disease orthologue Btn1 controls endosome-Golgi retrograde transport via SNARE assembly." The Journal of cell biology **195**: 203-215.

Kanninen, K. M., A. Grubman, et al. (2013b). "Altered biometal homeostasis is associated with CLN6 mRNA loss in mouse neuronal ceroid lipofuscinosis." Biology open **2**: 635-646.

Kanninen, K. M., A. Grubman, et al. (2013a). "Increased zinc and manganese in parallel with neurodegeneration, synaptic protein changes and activation of Akt/GSK3 signaling in ovine CLN6 neuronal ceroid lipofuscinosis." PloS one **8**: e58644.

Karecla, P. I. and T. E. Kreis (1992). "Interaction of membranes of the Golgi complex with microtubules in vitro." European journal of cell biology **57**: 139-146.

Katayama, T., K. Imaizumi, et al. (2004). "Induction of neuronal death by ER stress in Alzheimer's disease." Journal of chemical neuroanatomy **28**: 67-78.

Keller, P. and K. Simons (1997). "Post-Golgi biosynthetic trafficking." Journal of cell science **110 (Pt 24)**: 3001-3009.

Kellokumpu, S., R. Sormunen, et al. (2002). "Abnormal glycosylation and altered Golgi structure in colorectal cancer: dependence on intra-Golgi pH." FEBS letters **516**: 217-224.

Kida, E., W. Kaczmarski, et al. (1999). "Analysis of intracellular distribution and trafficking of the CLN3 protein in fusion with the green fluorescent protein in vitro." Molecular genetics and metabolism **66**: 265-271.

Kim, Y., Chattopadhyay, S., Locke, S., Pearce, D.A. (2005). "Interaction among Btn1p, Btn2p, and Ist2p reveals potential interplay among the vacuole, amino acid levels, and ion homeostasis in the yeast Saccharomyces cerevisiae." Eukaryot Cell. **Feb;4(2):281-8**.

Kim, Y., D. Ramirez-Montealegre, et al. (2003). "A role in vacuolar arginine transport for yeast Btn1p and for human CLN3, the protein defective in Batten disease." Proceedings of the National Academy of Sciences of the United States of America **100**: 15458-15462.

Kimmig, P., M. Diaz, et al. (2012). "The unfolded protein response in fission yeast modulates stability of select mRNAs to maintain protein homeostasis." eLife **1**: e00048.

Kinseth, M. A., C. Anjard, et al. (2007). "The Golgi-associated protein GRASP is required for unconventional protein secretion during development." Cell **130**: 524-534.

Kitzmuller, C., R. L. Haines, et al. (2008). "A function retained by the common mutant CLN3 protein is responsible for the late onset of juvenile neuronal ceroid lipofuscinosis." Human molecular genetics **17**: 303-312.

Klausner, R. D., J. G. Donaldson, et al. (1992). "Brefeldin A: insights into the control of membrane traffic and organelle structure." The Journal of cell biology **116**: 1071-1080.

Kondylis, V., K. M. Spoorendonk, et al. (2005). "dGRASP localization and function in the early exocytic pathway in Drosophila S2 cells." Molecular biology of the cell **16**: 4061-4072.

Kousi, M., A. E. Lehesjoki, et al. (2012). "Update of the mutation spectrum and clinical correlations of over 360 mutations in eight genes that underlie the neuronal ceroid lipofuscinoses." Human mutation **33**: 42-63.

Kozutsumi, Y., M. Segal, et al. (1988). "The presence of malfolded proteins in the endoplasmic reticulum signals the induction of glucose-regulated proteins." Nature **332**: 462-464.

Kremmidiotis, G., I. L. Lensink, et al. (1999). "The Batten disease gene product (CLN3p) is a Golgi integral membrane protein." Human molecular genetics **8**: 523-531.

Kuang, X.-L., F. Liu, et al. (2014). "Reductions of the components of the calreticulin/calnexin quality-control system by proteasome inhibitors and their relevance in a rodent model of Parkinson's disease." Journal of neuroscience research: n/a-n/a.

Kuehn, M. J., J. M. Herrmann, et al. (1998). "COPII-cargo interactions direct protein sorting into ER-derived transport vesicles." Nature **391**: 187-190.

Kuo, A., C. Zhong, et al. (2000). "Transmembrane transforming growth factor-alpha tethers to the PDZ domain-containing, Golgi membrane-associated protein p59/GRASP55." The EMBO journal **19**: 6427-6439.

Kwon, J. M., P. G. Rothberg, et al. (2005). "Novel CLN3 mutation predicted to cause complete loss of protein function does not modify the classical JNCL phenotype." Neuroscience letters **387**: 111-114.

Kyttala, A., G. Ihrke, et al. (2004). "Two motifs target Batten disease protein CLN3 to lysosomes in transfected nonneuronal and neuronal cells." Molecular biology of the cell **15**: 1313-1323.

Kyttala, A., K. Yliannala, et al. (2005). "AP-1 and AP-3 facilitate lysosomal targeting of Batten disease protein CLN3 via its dileucine motif." The Journal of biological chemistry **280**: 10277-10283.

Ladinsky, M. S., D. N. Mastronarde, et al. (1999). "Golgi structure in three dimensions: functional insights from the normal rat kidney cell." The Journal of cell biology **144**: 1135-1149.

LaFerla, F. M. (2002). "Calcium dyshomeostasis and intracellular signalling in Alzheimer's disease." Nature reviews. Neuroscience **3**: 862-872.

Lapinskas, P. J., K. W. Cunningham, et al. (1995). "Mutations in PMR1 suppress oxidative damage in yeast cells lacking superoxide dismutase." Molecular and cellular biology **15**: 1382-1388.

Lauronen, L., P. B. Munroe, et al. (1999). "Delayed classic and protracted phenotypes of compound heterozygous juvenile neuronal ceroid lipofuscinosis." Neurology **52**: 360-365.

Lebrun, A. H., P. Moll-Khosrawi, et al. (2011). "Analysis of potential biomarkers and modifier genes affecting the clinical course of CLN3 disease." Molecular medicine **17**: 1253-1261.

Lederkremer, G. Z., Y. Cheng, et al. (2001). "Structure of the Sec23p/24p and Sec13p/31p complexes of COPII." Proceedings of the National Academy of Sciences of the United States of America **98**: 10704-10709.

Lee, H. J., F. Khoshaghideh, et al. (2006). "Impairment of microtubule-dependent trafficking by overexpression of alpha-synuclein." The European journal of neuroscience **24**: 3153-3162.

Lee, M. C., E. A. Miller, et al. (2004). "Bi-directional protein transport between the ER and Golgi." Annual review of cell and developmental biology **20**: 87-123.

Leman, A. R., D. A. Pearce, et al. (2005). "Gene symbol: CLN3. Disease: Juvenile neuronal ceroid lipofuscinosis (Batten disease)." Human genetics **116**: 544.

Levi, S. K., D. Bhattacharyya, et al. (2010). "The yeast GRASP Grh1 colocalizes with COPII and is dispensable for organizing the secretory pathway." Traffic **11**: 1168-1179.

Lewis, M. J. and H. R. Pelham (1990). "A human homologue of the yeast HDEL receptor." Nature **348**: 162-163.

Liang, J. and J. W. Canary (2010). "Discrimination between hard metals with soft ligand donor atoms: An on-fluorescence probe for manganese(ii)." Angewandte Chemie International Edition **49**: 7710-13.10.1002/anie.201002853:

Lin, H. Y., P. Masso-Welch, et al. (1993). "The 170-kDa glucose-regulated stress protein is an endoplasmic reticulum protein that binds immunoglobulin." Molecular biology of the cell **4**: 1109-1119.

Lin, P., F. Li, et al. (2007). "Calnuc binds to Alzheimer's beta-amyloid precursor protein and affects its biogenesis." Journal of neurochemistry **100**: 1505-1514.

Lisman, Q., T. Pomorski, et al. (2004). "Protein sorting in the late Golgi of Saccharomyces cerevisiae does not require mannosylated sphingolipids." The Journal of biological chemistry **279**: 1020-1029.

Liu, X. F. and V. C. Culotta (1999a). "Mutational analysis of Saccharomyces cerevisiae Smf1p, a member of the Nramp family of metal transporters." Journal of molecular biology **289**: 885-891.

Liu, X. F. and V. C. Culotta (1999b). "Post-translation control of Nramp metal transport in yeast. Role of metal ions and the BSD2 gene." The Journal of biological chemistry **274**: 4863-4868.

Livak, K. J. and T. D. Schmittgen (2001). "Analysis of relative gene expression data using real-time quantitative PCR and the 2(-Delta Delta C(T)) Method." Methods **25**: 402-408.

Lobsanov, Y. D., P. A. Romero, et al. (2004). "Structure of Kre2p/Mnt1p: a yeast alpha1,2-mannosyltransferase involved in mannoprotein biosynthesis." The Journal of biological chemistry **279**: 17921-17931.

Luiro, K., O. Kopra, et al. (2001). "CLN3 protein is targeted to neuronal synapses but excluded from synaptic vesicles: new clues to Batten disease." Human molecular genetics **10**: 2123-2131.

Luk, E. E. and V. C. Culotta (2001). "Manganese superoxide dismutase in Saccharomyces cerevisiae acquires its metal co-factor through a pathway involving the Nramp metal transporter, Smf2p." The Journal of biological chemistry **276**: 47556-47562.

Ma, Y. T., A. Chaudhuri and R. R. Rando (1992). "Substrate specificity of the isoprenylated protein endoprotease." Biochemistry 31: 11772-7

Maag, R. S., M. Mancini, et al. (2005). "Caspase-resistant Golgin-160 disrupts apoptosis induced by secretory pathway stress and ligation of death receptors." Molecular biology of the cell **16**: 3019-3027.

Maciejewski, P. K. and D. L. Rothman (2008). "Proposed cycles for functional glutamate trafficking in synaptic neurotransmission." Neurochemistry international **52**: 809-825.

Mackenzie, B. and M. A. Hediger (2004). "SLC11 family of H+-coupled metal-ion transporters NRAMP1 and DMT1." Pflugers Archiv : European journal of physiology **447**: 571-579.

Maeda, Y. and T. Kinoshita (2008). "Dolichol-phosphate mannose synthase: structure, function and regulation." Biochimica et biophysica acta **1780**: 861-868.

Magistretti, P. J., L. Pellerin, et al. (1999). "Energy on demand." Science **283**: 496-497.

Mancini, M., C. E. Machamer, et al. (2000). "Caspase-2 is localized at the Golgi complex and cleaves golgin-160 during apoptosis." The Journal of cell biology **149**: 603-612.

Mao, Q., B. J. Foster, et al. (2003). "Membrane topology of CLN3, the protein underlying Batten disease." FEBS letters **541**: 40-46.

Marciniak, S. J., C. Y. Yun, et al. (2004). "CHOP induces death by promoting protein synthesis and oxidation in the stressed endoplasmic reticulum." Genes & development **18**: 3066-3077.

Marra, P., T. Maffucci, et al. (2001). "The GM130 and GRASP65 Golgi proteins cycle through and define a subdomain of the intermediate compartment." Nature cell biology **3**: 1101-1113.

Martino, M. B., L. Jones, et al. (2013). "The ER stress transducer IRE1beta is required for airway epithelial mucin production." Mucosal immunology **6**: 639-654.

Masuda, M., M. Braun-Sommargren, et al. (2013). "Golgi phosphoprotein 4 (GPP130) is a sensitive and selective cellular target of manganese exposure." Synapse **67**: 205-215.

Mattson, M. P. (2000). "Apoptosis in neurodegenerative disorders." Nature reviews. Molecular cell biology **1**: 120-129.

Mellman, I. and K. Simons (1992). "The Golgi complex: in vitro veritas?" Cell **68**: 829-840.

Metcalf, D. J., A. A. Calvi, et al. (2008). "Loss of the Batten disease gene CLN3 prevents exit from the TGN of the mannose 6-phosphate receptor." Traffic **9**: 1905-1914.

Mildvan, A. S., M. C. Scrutton, et al. (1966). "Pyruvate carboxylase. VII. A possible role for tightly bound manganese." The Journal of biological chemistry **241**: 3488-3498.

Miller, J. N., C. H. Chan, et al. (2013). "The role of nonsense-mediated decay in neuronal ceroid lipofuscinosis." Human molecular genetics **22**: 2723-2734.

Miller, P. M., A. W. Folkmann, et al. (2009). "Golgi-derived CLASP-dependent microtubules control Golgi organization and polarized trafficking in motile cells." Nature cell biology **11**: 1069-1080.

Mironov, A. A., A. A. Mironov, Jr., et al. (2003). "ER-to-Golgi carriers arise through direct en bloc protrusion and multistage maturation of specialized ER exit domains." Developmental cell **5**: 583-594.

Missiaen, L., L. Dode, et al. (2007). "Calcium in the Golgi apparatus." Cell calcium **41**: 405-416.

Missiaen, L., L. Raeymaekers, et al. (2004). "SPCA1 pumps and Hailey-Hailey disease." Biochemical and biophysical research communications **322**: 1204-1213.

Mogelsvang, S., B. J. Marsh, et al. (2004). "Predicting function from structure: 3D structure studies of the mammalian Golgi complex." Traffic **5**: 338-345.

Mole, S., Williams, R., Goebel, H. (2011). The Neuronal Ceroid Lipofuscinoses (Batten Disease), Oxford University Press (UK).

Mole, S. E., G. Michaux, et al. (2004). "CLN6, which is associated with a lysosomal storage disease, is an endoplasmic reticulum protein." Experimental cell research **298**: 399-406.

Mollenhauer, H. H. (1965). "An Intercisternal Structure in the Golgi Apparatus." The Journal of cell biology **24**: 504-511.

Mori, K., W. Ma, et al. (1993). "A transmembrane protein with a cdc2+/CDC28-related kinase activity is required for signaling from the ER to the nucleus." Cell **74**: 743-756.

Morishima, N., K. Nakanishi, et al. (2004). "Translocation of Bim to the endoplasmic reticulum (ER) mediates ER stress signaling for activation of caspase-12 during ER stress-induced apoptosis." The Journal of biological chemistry **279**: 50375-50381.

Mowbrey, K. and J. B. Dacks (2009). "Evolution and diversity of the Golgi body." FEBS letters **583**: 3738-3745.

Mukherjee, S., R. Chiu, et al. (2007). "Fragmentation of the Golgi apparatus: an early apoptotic event independent of the cytoskeleton." Traffic **8**: 369-378.

Mukhopadhyay, S., C. Bachert, et al. (2010). "Manganese-induced trafficking and turnover of the cis-Golgi glycoprotein GPP130." Molecular biology of the cell **21**: 1282-1292.

Mukhopadhyay, S. and A. D. Linstedt (2011). "Identification of a gain-of-function mutation in a Golgi P-type ATPase that enhances Mn2+ efflux and protects against toxicity." Proceedings of the National Academy of Sciences of the United States of America **108**: 858-863.

Munro, S. and H. R. Pelham (1987). "A C-terminal signal prevents secretion of luminal ER proteins." Cell **48**: 899-907.

Munroe, P. B., H. M. Mitchison, et al. (1997). "Spectrum of mutations in the Batten disease gene, CLN3." American journal of human genetics **61**: 310-316.

Murphy, V. A., K. C. Wadhwani, et al. (1991). "Saturable transport of manganese(II) across the rat blood-brain barrier." Journal of neurochemistry **57**: 948-954.

Murray, S. (2008). Chapter 1 High Pressure Freezing and Freeze Substitution of Schizosaccharomyces pombe and Saccharomyces cerevisiae for TEM. Methods in Cell Biology. D. A. Terence, Academic Press. **Volume 88:** 3-17.

Muzaffar, N. E. and D. A. Pearce (2008). "Analysis of NCL Proteins from an Evolutionary Standpoint." Current genomics **9**: 115-136.

Nakano, A. and M. Muramatsu (1989). "A novel GTP-binding protein, Sar1p, is involved in transport from the endoplasmic reticulum to the Golgi apparatus." The Journal of cell biology **109**: 2677-2691.

Nebenfuhr, A., L. A. Gallagher, et al. (1999). "Stop-and-go movements of plant Golgi stacks are mediated by the acto-myosin system." Plant physiology **121**: 1127-1142.

Nilsson, T., M. H. Hoe, et al. (1994). "Kin recognition between medial Golgi enzymes in HeLa cells." The EMBO journal **13**: 562-574.

Noskova, L., V. Stranecky, et al. (2011). "Mutations in DNAJC5, encoding cysteine-string protein alpha, cause autosomal-dominant adult-onset neuronal ceroid lipofuscinosis." American journal of human genetics **89**: 241-252.

Nugent, T., S. E. Mole, et al. (2008). "The transmembrane topology of Batten disease protein CLN3 determined by consensus computational prediction constrained by experimental data." FEBS letters **582**: 1019-1024.

Ohyama, T., P. Verstreken, et al. (2007). "Huntingtin-interacting protein 14, a palmitoyl transferase required for exocytosis and targeting of CSP to synaptic vesicles." The Journal of cell biology **179**: 1481-1496.

Oka, T. and A. Nakano (1994). "Inhibition of GTP hydrolysis by Sar1p causes accumulation of vesicles that are a functional intermediate of the ER-to-Golgi transport in yeast." The Journal of cell biology **124**: 425-434.

Okada, T., H. Yoshida, et al. (2002). "Distinct roles of activating transcription factor 6 (ATF6) and double-stranded RNA-activated protein kinase-like endoplasmic reticulum kinase (PERK) in transcription during the mammalian unfolded protein response." The Biochemical journal **366**: 585-594.

Okazaki, K., N. Okazaki, et al. (1990). "High-frequency transformation method and library transducing vectors for cloning mammalian cDNAs by trans-complementation of Schizosaccharomyces pombe." Nucleic acids research **18**: 6485-6489.

Olson, M. and S. Kornbluth (2001). "Mitochondria in apoptosis and human disease." Current molecular medicine **1**: 91-122.

Osorio, N. S., A. Carvalho, et al. (2007). "Nitric oxide signaling is disrupted in the yeast model for Batten disease." Molecular biology of the cell **18**: 2755-2767.

Oyama, F., N. Murakami, et al. (1998). "Chloroquine myopathy suggests that tau is degraded in lysosomes: implication for the formation of paired helical filaments in Alzheimer's disease." Neuroscience research **31**: 1-8.

Ozcan, U., Q. Cao, et al. (2004). "Endoplasmic reticulum stress links obesity, insulin action, and type 2 diabetes." Science **306**: 457-461.

Ozon, S., A. Guichet, et al. (2002). "Drosophila stathmin: a microtubule-destabilizing factor involved in nervous system formation." Molecular biology of the cell **13**: 698-710.

Padilla-Lopez, S. and D. A. Pearce (2006). "Saccharomyces cerevisiae lacking Btn1p modulate vacuolar ATPase activity to regulate pH imbalance in the vacuole." The Journal of biological chemistry **281**: 10273-10280.

Pal, P. K., A. Samii, et al. (1999). "Manganese neurotoxicity: a review of clinical features, imaging and pathology." Neurotoxicology **20**: 227-238.

Pao, S. S., I. T. Paulsen, et al. (1998). "Major facilitator superfamily." Microbiology and molecular biology reviews : MMBR **62**: 1-34.

Pearce, D. A., T. Ferea, et al. (1999a). "Action of BTN1, the yeast orthologue of the gene mutated in Batten disease." Nature genetics **22**: 55-58.

Pearce, D. A., S. A. Nosel, et al. (1999b). "Studies of pH regulation by Btn1p, the yeast homolog of human Cln3p." Molecular genetics and metabolism **66**: 320-323.

Pears, M. R., S. Codlin, et al. (2010). "Deletion of btn1, an orthologue of CLN3, increases glycolysis and perturbs amino acid metabolism in the fission yeast model of Batten disease." Molecular bioSystems **6**: 1093-1102.

Pears, M. R., J. D. Cooper, et al. (2005). "High resolution 1H NMR-based metabolomics indicates a neurotransmitter cycling deficit in cerebral tissue from a mouse model of Batten disease." The Journal of biological chemistry **280**: 42508-42514.

Pebrel-Richard, C., A. Debost-Legrand, et al. (2014). "An unusual clinical severity of 16p11.2 deletion syndrome caused by unmasked recessive mutation of CLN3." European journal of human genetics : EJHG **22**: 369-373.

Pelham, H. R., K. G. Hardwick, et al. (1988). "Sorting of soluble ER proteins in yeast." The EMBO journal **7**: 1757-1762.

Perier, C. and M. Vila (2012). "Mitochondrial biology and parkinson's disease." Cold Spring Harb Perspect Med **2**: a009332.10.1101/cshperspect.a009332:

Persson, K., H. D. Ly, et al. (2001). "Crystal structure of the retaining galactosyltransferase LgtC from Neisseria meningitidis in complex with donor and acceptor sugar analogs." Nature structural biology **8**: 166-175.

Polishchuk, R. S. and A. A. Mironov (2004). "Structural aspects of Golgi function." Cellular and molecular life sciences : CMLS **61**: 146-158.

Portnoy, M. E., X. F. Liu, et al. (2000). "Saccharomyces cerevisiae expresses three functionally distinct homologues of the nramp family of metal transporters." Molecular and cellular biology **20**: 7893-7902.

Prescott, A. R., J. M. Lucocq, et al. (1997). "Distinct compartmentalization of TGN46 and beta 1,4-galactosyltransferase in HeLa cells." European journal of cell biology **72**: 238-246.

Pullarkat, R. K. and G. N. Morris (1997). "Farnesylation of Batten disease CLN3 protein." Neuropediatrics **28**: 42-44.

Puthenveedu, M. A., C. Bachert, et al. (2006). "GM130 and GRASP65-dependent lateral cisternal fusion allows uniform Golgi-enzyme distribution." Nature cell biology **8**: 238-248.

Qin, Z. H., Y. Wang, et al. (2004). "Huntingtin bodies sequester vesicle-associated proteins by a polyproline-dependent interaction." The Journal of neuroscience : the official journal of the Society for Neuroscience **24**: 269-281.

Rabin, O., L. Hegedus, et al. (1993). "Rapid brain uptake of manganese(II) across the blood-brain barrier." Journal of neurochemistry **61**: 509-517.

Rabouille, C., N. Hui, et al. (1995). "Mapping the distribution of Golgi enzymes involved in the construction of complex oligosaccharides." Journal of cell science **108 (Pt 4)**: 1617-1627.

Rakheja, D., S. B. Narayan, et al. (2004). "CLN3P, the Batten disease protein, localizes to membrane lipid rafts (detergent-resistant membranes)." Biochemical and biophysical research communications **317**: 988-991.

Rambourg, A., Clermort, Y. (1997). Three-dimensional structure of the Golgi apparatus in mammalian cells., In Roth&Berger (eds) The Golgi apparatus" Birkhauser, basel, pp37-61.

Ramirez, A., A. Heimbach, et al. (2006). "Hereditary parkinsonism with dementia is caused by mutations in ATP13A2, encoding a lysosomal type 5 P-type ATPase." Nature genetics **38**: 1184-1191.

Ramirez, I. B. and M. Lowe (2009). "Golgins and GRASPs: holding the Golgi together." Seminars in cell & developmental biology **20**: 770-779.

Ratajczak, E., A. Petcherski, et al. (2014). "FRET-Assisted Determination of CLN3 Membrane Topology." PloS one **9**: e102593.

Rivero, S., J. Cardenas, et al. (2009). "Microtubule nucleation at the cis-side of the Golgi apparatus requires AKAP450 and GM130." The EMBO journal **28**: 1016-1028.

Rizzolo, L. J., J. Finidori, et al. (1985). "Biosynthesis and intracellular sorting of growth hormone-viral envelope glycoprotein hybrids." The Journal of cell biology **101**: 1351-1362.

Robison, G., T. Zakharova, S. Fu, W. Jiang, R. Fulper, R. Barrea, M. A. Marcus, W. Zheng and Y. Pushkar (2012). "X-ray fluorescence imaging: A new tool

for studying manganese neurotoxicity." PLoS One 7: e48899.10.1371/journal.pone.0048899:

Rossanese, O. W., J. Soderholm, et al. (1999). "Golgi structure correlates with transitional endoplasmic reticulum organization in Pichia pastoris and Saccharomyces cerevisiae." The Journal of cell biology **145**: 69-81.

Rudell, J. C., L. S. Borges, et al. (2014). "Determinants in the beta and delta subunit cytoplasmic loop regulate Golgi trafficking and surface expression of the muscle acetylcholine receptor." The Journal of biological chemistry **289**: 203-214.

Rudolph, H. K., A. Antebi, et al. (1989). "The yeast secretory pathway is perturbed by mutations in PMR1, a member of a Ca2+ ATPase family." Cell **58**: 133-145.

Rutherford, J. C. and A. J. Bird (2004). "Metal-responsive transcription factors that regulate iron, zinc, and copper homeostasis in eukaryotic cells." Eukaryotic cell **3**: 1-13.

Saini, D. K., M. Chisari, et al. (2009). "Shuttling and translocation of heterotrimeric G proteins and Ras." Trends in pharmacological sciences **30**: 278-286.

Sakurai, A., K. Okamoto, et al. (2000). "Fragmentation of the Golgi apparatus of the ballooned neurons in patients with corticobasal degeneration and Creutzfeldt-Jakob disease." Acta neuropathologica **100**: 270-274.

Sakurai, A., K. Okamoto, et al. (2002). "Pathology of the inferior olivary nucleus in patients with multiple system atrophy." Acta neuropathologica **103**: 550-554.

Salama, N. R., T. Yeung, et al. (1993). "The Sec13p complex and reconstitution of vesicle budding from the ER with purified cytosolic proteins." The EMBO journal **12**: 4073-4082.

Sarpong, A., G. Schottmann, et al. (2009). "Protracted course of juvenile ceroid lipofuscinosis associated with a novel CLN3 mutation (p.Y199X)." Clinical genetics **76**: 38-45.

Schindler, A. J. and R. Schekman (2009). "In vitro reconstitution of ER-stress induced ATF6 transport in COPII vesicles." Proceedings of the National Academy of Sciences of the United States of America **106**: 17775-17780.

Schotman, H., L. Karhinen, et al. (2008). "dGRASP-mediated noncanonical integrin secretion is required for Drosophila epithelial remodeling." Developmental cell **14**: 171-182.

Schuck, S., W. A. Prinz, et al. (2009). "Membrane expansion alleviates endoplasmic reticulum stress independently of the unfolded protein response." The Journal of cell biology **187**: 525-536.

Schuele, S. U., M. Afshari, et al. (2011). "Ictal central apnea as a predictor for sudden unexpected death in epilepsy." Epilepsy & behavior : E&B **22**: 401-403.

Schweizer, A., J. A. Fransen, et al. (1988). "Identification, by a monoclonal antibody, of a 53-kD protein associated with a tubulo-vesicular compartment at the cis-side of the Golgi apparatus." The Journal of cell biology **107**: 1643-1653.

Sengupta, D., S. Truschel, et al. (2009). "Organelle tethering by a homotypic PDZ interaction underlies formation of the Golgi membrane network." The Journal of cell biology **186**: 41-55.

Sengupta, D. and A. D. Linstedt (2011). "Control of organelle size: The golgi complex." Annu Rev Cell Dev Biol **27**: 57-77.10.1146/annurev-cellbio-100109-104003:

Sens, P. and M. Rao (2013). Chapter 18 - (Re)Modeling the Golgi. Methods in Cell Biology. P. Franck and J. S. David, Academic Press. **Volume 118:** 299-310.

Sesso, A., D. T. Fujiwara, et al. (1999). "Structural elements common to mitosis and apoptosis." Tissue & cell **31**: 357-371.

Sevlever, D., P. Jiang, et al. (2008). "Cathepsin D is the main lysosomal enzyme involved in the degradation of alpha-synuclein and generation of its carboxy-terminally truncated species." Biochemistry **47**: 9678-9687.

Shamu, C. E. and P. Walter (1996). "Oligomerization and phosphorylation of the Ire1p kinase during intracellular signaling from the endoplasmic reticulum to the nucleus." The EMBO journal **15**: 3028-3039.

Shewan, A. M., E. M. van Dam, et al. (2003). "GLUT4 recycles via a trans-Golgi network (TGN) subdomain enriched in Syntaxins 6 and 16 but not TGN38: involvement of an acidic targeting motif." Molecular biology of the cell **14**: 973-986.

Shorter, J., R. Watson, et al. (1999). "GRASP55, a second mammalian GRASP protein involved in the stacking of Golgi cisternae in a cell-free system." The EMBO journal **18**: 4949-4960.

Singaraja, R. R., S. Hadano, et al. (2002). "HIP14, a novel ankyrin domain-containing protein, links huntingtin to intracellular trafficking and endocytosis." Human molecular genetics **11**: 2815-2828.

Smith, K. R., H. H. Dahl, et al. (2013). "Cathepsin F mutations cause Type B Kufs disease, an adult-onset neuronal ceroid lipofuscinosis." Human molecular genetics **22**: 1417-1423.

Smith, K. R., J. Damiano, et al. (2012). "Strikingly different clinicopathological phenotypes determined by progranulin-mutation dosage." American journal of human genetics **90**: 1102-1107.

Sorin, A., G. Rosas, et al. (1997). "PMR1, a Ca2+-ATPase in yeast Golgi, has properties distinct from sarco/endoplasmic reticulum and plasma membrane calcium pumps." The Journal of biological chemistry **272**: 9895-9901.

Sousa, M. and A. J. Parodi (1995). "The molecular basis for the recognition of misfolded glycoproteins by the UDP-Glc:glycoprotein glucosyltransferase." The EMBO journal **14**: 4196-4203.

Staehelin, L. A. and B. H. Kang (2008). "Nanoscale architecture of endoplasmic reticulum export sites and of Golgi membranes as determined by electron tomography." Plant physiology **147**: 1454-1468.

Stamer, K., R. Vogel, et al. (2002). "Tau blocks traffic of organelles, neurofilaments, and APP vesicles in neurons and enhances oxidative stress." The Journal of cell biology **156**: 1051-1063.

Staropoli, J. F., A. Karaa, et al. (2012). "A homozygous mutation in KCTD7 links neuronal ceroid lipofuscinosis to the ubiquitin-proteasome system." American journal of human genetics **91**: 202-208.

Steel, G. J., D. M. Fullerton, et al. (2004). "Coordinated activation of Hsp70 chaperones." Science **303**: 98-101.

Steinbrecht, R. and M. Muller (1987). Freeze-Substitution and Freeze-Drying. Cryotechniques in Biological Electron Microscopy. R. Steinbrecht and K. Zierold, Springer Berlin Heidelberg**:** 149-172.

Stengel, O. C. (1826). "Beretning om et mærkeligt Sygdomstilfælde hos fire Sødskende I Nærheden af Roraas." Eyr, 1, 347-352.

Stengel, O. C. (1982). "Account of a singular illness among four siblings in the vicinity of Roraas. Reprinted in Armstrong D., Koppang N., and Rider JA (eds) Ceroid lipofuscinoses (Batten's Disease)." pp 17-19. Amsterdam Elsevier/North Holland Biomedical press.

Stieber, A., Y. Chen, et al. (1998). "The fragmented neuronal Golgi apparatus in amyotrophic lateral sclerosis includes the trans-Golgi-network: functional implications." Acta neuropathologica **95**: 245-253.

Stieber, A., J. O. Gonatas, et al. (2004). "Disruption of the structure of the Golgi apparatus and the function of the secretory pathway by mutants G93A and G85R of Cu, Zn superoxide dismutase (SOD1) of familial amyotrophic lateral sclerosis." Journal of the neurological sciences **219**: 45-53.

Storch, S., S. Pohl, et al. (2004). "A dileucine motif and a cluster of acidic amino acids in the second cytoplasmic domain of the batten disease-related CLN3 protein are required for efficient lysosomal targeting." The Journal of biological chemistry **279**: 53625-53634.

Storch, S., S. Pohl, et al. (2007). "C-terminal prenylation of the CLN3 membrane glycoprotein is required for efficient endosomal sorting to lysosomes." Traffic **8**: 431-444.

Stowers, R. S. and E. Y. Isacoff (2007). "Drosophila huntingtin-interacting protein 14 is a presynaptic protein required for photoreceptor synaptic transmission and expression of the palmitoylated proteins synaptosome-associated protein 25 and cysteine string protein." The Journal of neuroscience : the official journal of the Society for Neuroscience **27**: 12874-12883.

Sutterlin, C., R. Polishchuk, et al. (2005). "The Golgi-associated protein GRASP65 regulates spindle dynamics and is essential for cell division." Molecular biology of the cell **16**: 3211-3222.

Szegezdi, E., D. C. Macdonald, et al. (2009). "Bcl-2 family on guard at the ER." American journal of physiology. Cell physiology **296**: C941-953.

Tamas, M. J., S. K. Sharma, S. Ibstedt, T. Jacobson and P. Christen (2014). "Heavy metals and metalloids as a cause for protein misfolding and aggregation." Biomolecules **4**: 252-67.10.3390/biom4010252:

Takamine, K., K. Okamoto, et al. (2000). "The involvement of the neuronal Golgi apparatus and trans-Golgi network in the human olivary hypertrophy." Journal of the neurological sciences **182**: 45-50.

Takeda, A. (2003). "Manganese action in brain function." Brain research. Brain research reviews **41**: 79-87.

Takeuchi, M., T. Ueda, et al. (2000). "A dominant negative mutant of sar1 GTPase inhibits protein transport from the endoplasmic reticulum to the Golgi apparatus in tobacco and Arabidopsis cultured cells." The Plant journal : for cell and molecular biology **23**: 517-525.

Tang, D., H. Yuan, et al. (2010). "The role of GRASP65 in Golgi cisternal stacking and cell cycle progression." Traffic **11**: 827-842.

Tessitore, A., P. M. M. del, et al. (2004). "GM1-ganglioside-mediated activation of the unfolded protein response causes neuronal death in a neurodegenerative gangliosidosis." Molecular cell **15**: 753-766.

Thibault, G., N. Ismail, et al. (2011). "The unfolded protein response supports cellular robustness as a broad-spectrum compensatory pathway." Proceedings of the National Academy of Sciences of the United States of America **108**: 20597-20602.

Thomas, G. (2002). "Furin at the cutting edge: from protein traffic to embryogenesis and disease." Nature reviews. Molecular cell biology **3**: 753-766.

Ton, V. K., D. Mandal, et al. (2002). "Functional expression in yeast of the human secretory pathway Ca(2+), Mn(2+)-ATPase defective in Hailey-Hailey disease." The Journal of biological chemistry **277**: 6422-6427.

Tooze SA, T. J., and Graham Warren (1988). "Site of Addition of N-Acetyl-galactosamine to the E1 Glycoprotein of Mouse Hepatitis Virus-A59."

Travers, K. J., C. K. Patil, et al. (2000). "Functional and genomic analyses reveal an essential coordination between the unfolded protein response and ER-associated degradation." Cell **101**: 249-258.

Tu, L. and D. K. Banfield (2010). "Localization of Golgi-resident glycosyltransferases." Cellular and molecular life sciences : CMLS **67**: 29-41.

Uversky, V. N., J. Li, et al. (2001). "Metal-triggered structural transformations, aggregation, and fibrillation of human alpha-synuclein. A possible molecular NK between Parkinson's disease and heavy metal exposure." The Journal of biological chemistry **276**: 44284-44296.

Velasco, A., J. Hidalgo, et al. (1988). "Detection of glycosaminoglycans in the Golgi complex of chondrocytes." European journal of cell biology **47**: 241-250.

Vellodi, A. (2005). "Lysosomal storage disorders." British journal of haematology **128**: 413-431.

Verkhratsky, A. (2005). "Physiology and pathophysiology of the calcium store in the endoplasmic reticulum of neurons." Physiological reviews **85**: 201-279.

Vitiello, S. P., J. W. Benedict, et al. (2010). "Interaction between Sdo1p and Btn1p in the Saccharomyces cerevisiae model for Batten disease." Human molecular genetics **19**: 931-942.

Walker, A., C. Ward, et al. (2004). "Golgi fragmentation during Fas-mediated apoptosis is associated with the rapid loss of GM130." Biochemical and biophysical research communications **316**: 6-11.

Walter, P. and D. Ron (2011). "The unfolded protein response: from stress pathway to homeostatic regulation." Science **334**: 1081-1086.

Wang, Y., J. Seemann, et al. (2003). "A direct role for GRASP65 as a mitotically regulated Golgi stacking factor." The EMBO journal **22**: 3279-3290.

Warren, G. and V. Malhotra (1998). "The organisation of the Golgi apparatus." Current opinion in cell biology **10**: 493-498.

Wedler, F. C. and R. B. Denman (1984). "Glutamine synthetase: the major Mn(II) enzyme in mammalian brain." Current topics in cellular regulation **24**: 153-169.

Weisz, O. A. and E. Rodriguez-Boulan (2009). "Apical trafficking in epithelial cells: signals, clusters and motors." Journal of cell science **122**: 4253-4266.

Welihinda, A. A. and R. J. Kaufman (1996). "The unfolded protein response pathway in Saccharomyces cerevisiae. Oligomerization and trans-phosphorylation of Ire1p (Ern1p) are required for kinase activation." The Journal of biological chemistry **271**: 18181-18187.

Williams, R. E. and S. E. Mole (2012). "New nomenclature and classification scheme for the neuronal ceroid lipofuscinoses." Neurology **79**: 183-191.

Winchester, B., A. Vellodi, et al. (2000). "The molecular basis of lysosomal storage diseases and their treatment." Biochemical Society transactions **28**: 150-154.

Wisniewski, K. E., E. Kida, et al. (2001). "Neuronal ceroid lipofuscinoses: classification and diagnosis." Advances in genetics **45**: 1-34.

Wolfe, D. M., S. Padilla-Lopez, et al. (2011). "pH-dependent localization of Btn1p in the yeast model for Batten disease." Disease models & mechanisms **4**: 120-125.

Wood, V., R. Gwilliam, et al. (2002). "The genome sequence of Schizosaccharomyces pombe." Nature **415**: 871-880.

Wootz, H., I. Hansson, et al. (2004). "Caspase-12 cleavage and increased oxidative stress during motoneuron degeneration in transgenic mouse model of ALS." Biochemical and biophysical research communications **322**: 281-286.

Wu, D., J. Liu, et al. (2014). "The Batten disease gene CLN3 confers resistance to endoplasmic reticulum stress induced by tunicamycin." Biochemical and biophysical research communications **447**: 115-120.

Wykoff, D. D. and E. K. O'Shea (2001). "Phosphate transport and sensing in Saccharomyces cerevisiae." Genetics **159**: 1491-1499.

Xia, X. G., H. Zhou, et al. (2005). "An RNAi strategy for treatment of amyotrophic lateral sclerosis caused by mutant Cu,Zn superoxide dismutase." Journal of neurochemistry **92**: 362-367.

Xiang, M., D. Mohamalawari, et al. (2005). "A novel isoform of the secretory pathway Ca2+,Mn(2+)-ATPase, hSPCA2, has unusual properties and is expressed in the brain." The Journal of biological chemistry **280**: 11608-11614.

Xiang, Y. and Y. Wang (2010). "GRASP55 and GRASP65 play complementary and essential roles in Golgi cisternal stacking." The Journal of cell biology **188**: 237-251.

Xu, Y. X., L. Liu, et al. (2010). "Inhibition of Golgi apparatus glycosylation causes endoplasmic reticulum stress and decreased protein synthesis." The Journal of biological chemistry **285**: 24600-24608.

Yoshida, H., T. Matsui, et al. (2001). "XBP1 mRNA is induced by ATF6 and spliced by IRE1 in response to ER stress to produce a highly active transcription factor." Cell **107**: 881-891.

Yoshida, H., T. Okada, et al. (2000). "ATF6 activated by proteolysis binds in the presence of NF-Y (CBF) directly to the cis-acting element responsible for the mammalian unfolded protein response." Molecular and cellular biology **20**: 6755-6767.

Yoshihisa, T., C. Barlowe, et al. (1993). "Requirement for a GTPase-activating protein in vesicle budding from the endoplasmic reticulum." Science **259**: 1466-1468.

Young, J., T. Stauber, et al. (2005). "Regulation of microtubule-dependent recycling at the trans-Golgi network by Rab6A and Rab6A'." Molecular biology of the cell **16**: 162-177.

Yu, A. C., J. Drejer, et al. (1983). "Pyruvate carboxylase activity in primary cultures of astrocytes and neurons." Journal of neurochemistry **41**: 1484-1487.

Yuan, J., M. Lipinski, et al. (2003). "Diversity in the mechanisms of neuronal cell death." Neuron **40**: 401-413.

Zeman, W. and P. Dyken (1969). "Neuronal ceroid-lipofuscinosis (Batten's disease): relationship to amaurotic family idiocy?" Pediatrics **44**: 570-583.

Zhang, F., A. L. Strom, et al. (2007). "Interaction between familial amyotrophic lateral sclerosis (ALS)-linked SOD1 mutants and the dynein complex." The Journal of biological chemistry **282**: 16691-16699.

Zinszner, H., M. Kuroda, et al. (1998). "CHOP is implicated in programmed cell death in response to impaired function of the endoplasmic reticulum." Genes & development **12**: 982-995.

Zwingmann, C., D. Leibfritz, et al. (2003). "Energy metabolism in astrocytes and neurons treated with manganese: relation among cell-specific energy failure, glucose metabolism, and intercellular trafficking using multinuclear NMR-spectroscopic analysis." Journal of cerebral blood flow and metabolism : official journal of the International Society of Cerebral Blood Flow and Metabolism **23**: 756-771.

Appendix

Appendix A

Column B vs. Column A	**siRNA CLN3 vs. Mock**
Unpaired t test	
P value	< 0.0001
P value summary	****
Significantly different? (P < 0.05)	Yes
One- or two-tailed P value?	Two-tailed
t, df	t=6.936 df=80
How big is the difference?	
Mean ± SEM of column A	26.49 ± 1.798 N=41
Mean ± SEM of column B	59.95 ± 4.476 N=41
Difference between means	33.46 ± 4.824
95% confidence interval	23.86 to 43.06
R square	0.3755

3.1.1.1 - CLN3 siRNA dependent changes in *cis*-Golgi morphology. Graph B

Column B vs. Column A	**siRNA CLN6 vs. Mock**
Unpaired t test	
P value	0.0630
P value summary	ns
Significantly different? (P < 0.05)	No
One- or two-tailed P value?	Two-tailed
t, df	t=1.885 df=80
How big is the difference?	
Mean ± SEM of column A	26.49 ± 1.798 N=41
Mean ± SEM of column B	31.66 ± 2.071 N=41
Difference between means	5.170 ± 2.742
95% confidence interval	-0.2874 to 10.63
R square	0.04254

3.1.1.1 - CLN3 siRNA dependent changes in *cis*-Golgi morphology. Graph C

Column A vs. Column B	Mock vs. siRNA CLN3
Unpaired t test	
P value	0.1497
P value summary	ns
Significantly different? (P < 0.05)	No
One- or two-tailed P value?	Two-tailed
t, df	t=1.458 df=64
How big is the difference?	
Mean ± SEM of column A	32.11 ± 2.989 N=33
Mean ± SEM of column B	38.39 ± 3.106 N=33
Difference between means	-6.286 ± 4.311
95% confidence interval	-14.90 to 2.326
R square	0.03216

3.1.1.2 – CLN3 depletion does not affect the *medial*-Golgi area. Graph B

Column A vs. Column B	Mock vs. siRNA CLN3
Unpaired t test	
P value	< 0.0001
P value summary	****
Significantly different? (P < 0.05)	Yes
One- or two-tailed P value?	Two-tailed
t, df	t=4.146 df=80
How big is the difference?	
Mean ± SEM of column A	33.32 ± 2.147 N=41
Mean ± SEM of column B	45.90 ± 2.143 N=41
Difference between means	-12.58 ± 3.034
95% confidence interval	-18.62 to -6.541
R square	0.1769

3.1.1.3 – CLN3 depletion affects the TGN area. Graph B

Column B vs. Column A	siRNA CLN3 vs. Control
Unpaired t test	
P value	0.0017
P value summary	**
Significantly different? (P < 0.05)	Yes
One- or two-tailed P value?	Two-tailed
t, df	t=3.232 df=89
How big is the difference?	
Mean ± SEM of column A	0.1320 ± 0.01856 N=45
Mean ± SEM of column B	0.05644 ± 0.01430 N=46
Difference between means	-0.07552 ± 0.02336
95% confidence interval	-0.1219 to -0.02910
R square	0.1051

3.1.1.4 – CLN3 depletion affects the Golgi complex compactness. Graph C

Sidak's multiple comparisons test	Mean Diff.	95% CI of diff.	Significant?	Summary
HF524N vs. HF523N	18.05	7.485 to 28.61	Yes	***
HF527N vs. HF523N	14.56	2.839 to 26.29	Yes	**
HF526N vs. HF523N	16.00	6.881 to 25.11	Yes	****
HF527N vs. HF524N	-3.482	-15.54 to 8.573	No	ns
HF526N vs. HF524N	-2.049	-11.59 to 7.488	No	ns
HF526N vs. HF527N	1.433	-9.379 to 12.25	No	ns

3.1.2.1 - CLN3 1-kb deletion dependent changes in Golgi complex morphology.Graph C

Sidak's multiple comparisons test	Mean Diff.	95% CI of diff.	Significant?	Summary
HF470Pa vs. HF481Pa	-31.49	-61.84 to -1.150	Yes	*
HF470Pa vs. HF478Pa	-38.82	-70.01 to -7.640	Yes	**
HF470Pa vs. HF480Pa	-20.94	-51.27 to 9.386	No	ns

3.1.2.1 - CLN3 1-kb deletion dependent changes in Golgi complex morphology.Graph D

Column B vs. Column A	Patients vs. Control
Unpaired t test	
P value	< 0.0001
P value summary	****
Significantly different? (P < 0.05)	Yes
One- or two-tailed P value?	Two-tailed
t, df	t=2.135 df=5
How big is the difference?	
Mean ± SEM of column A	40.66 ± 4.113 N=4
Mean ± SEM of column B	63.23 ± 11.22 N=4
Difference between means	22.57 ± 10.57
95% confidence interval	-4.606 to 49.75
R square	0.4769

3.1.2.1 - CLN3 1kb deletion dependent changes in Golgi complex morphology.Graph E

Column B vs. Column A	Patients vs. Control
Unpaired t test	
P value	0.2365
P value summary	ns
Significantly different? (P < 0.05)	No
One- or two-tailed P value?	Two-tailed
t, df	t=1.315 df=6
How big is the difference?	
Mean ± SEM of column A	0.4159 ± 0.2423 N=4
Mean ± SEM of column B	0.09543 ± 0.02551 N=4
Difference between means	-0.3205 ± 0.2437
95% confidence interval	-0.9167 to 0.2758
R square	0.2238

3.1.2.1 - CLN3 1kb deletion dependent changes in Golgi complex morphology.Graph F

Column A vs. Column B	Control vs. 1kb Patients
Unpaired t test	
P value	0.3804
P value summary	ns
Significantly different? (P < 0.05)	No
One- or two-tailed P value?	Two-tailed
t, df	t=0.8790 df=209
How big is the difference?	
Mean ± SEM of column A	52.40 ± 2.093 N=78
Mean ± SEM of column B	49.64 ± 2.065 N=133
Difference between means	2.758 ± 3.138
95% confidence interval	-3.428 to 8.945
R square	0.003683

3.1.2.2 - CLN3 1-kb deletion does not affect the *medial*-Golgi area. Graph B

Column B vs. Column A	1kb Patients vs. Control
Unpaired t test	
P value	< 0.0001
P value summary	****
Significantly different? (P < 0.05)	Yes
One- or two-tailed P value?	Two-tailed
t, df	t=4.166 df=80
How big is the difference?	
Mean ± SEM of column A	39.52 ± 3.020 N=41
Mean ± SEM of column B	59.73 ± 3.796 N=41
Difference between means	20.21 ± 4.851
95% confidence interval	10.56 to 29.87
R square	0.1783

3.1.2.3 - CLN3 1-kb deletion affects the TGN area, graph B

Sidak's multiple comparisons test	Mean Diff.	95% CI of diff.	Significant?	Summary	Adjusted P Value
Control vs. HF338Pa	-35.34	-47.06 to -23.62	Yes	****	< 0.0001
Control vs. HF338Pb	-41.63	-54.83 to -28.43	Yes	****	< 0.0001

3.1.2.4 - CLN3 exons 9-15 deletion dependent changes in Golgi complex morphology, graph B.

Sidak's multiple comparisons test	Mean Diff.	95% CI of D	Significant?	Summary
Patients vs. HF338Pa	-4.106	-20.36 to 12.15	No	ns
Patients vs. HF338Pb	-10.39	-28.89 to 8.097	No	ns

3.1.2.4 - CLN3 exons 9-15 deletion dependent changes in Golgi complex morphology, graph C.

Sidak's multiple comparisons test	Mean Diff.	95% CI of diff.	Significant?	Summary	P Value
HF338Pa vs. Control	-0.3178	-0.4719 to -0.1637	Yes	****	< 0.0001
HF338Pb vs. Control	-0.3078	-0.4639 to -0.1518	Yes	****	< 0.0001
HF338Pb vs. HF338Pa	0.009971	-0.05274 to 0.07268	No	ns	0.9241

3.1.2.4 - CLN3 exons 9-15 deletion dependent changes in Golgi complex morphology, graph D.

Column B vs. Column A	CLN1 vs. Control
Unpaired t test	
P value	0.6534
P value summary	ns
Significantly different? (P < 0.05)	No
One- or two-tailed P value?	Two-tailed
t, df	t=0.4495 df=295
How big is the difference?	
Mean ± SEM of column A	88.08 ± 4.084 N=65
Mean ± SEM of column B	91.10 ± 3.367 N=232
Difference between means	3.022 ± 6.722
95% confidence interval	-10.21 to 16.25
R square	0.0006845

3.1.2.5 – Golgi complex morphology is not affected in other NCLs, CLN1.

Column B vs. Column A	CLN2 vs. Control
Unpaired t test	
P value	0.1278
P value summary	ns
Significantly different? (P < 0.05)	No
One- or two-tailed P value?	Two-tailed
t, df	t=1.529 df=197
How big is the difference?	
Mean ± SEM of column A	88.08 ± 4.084 N=65
Mean ± SEM of column B	99.36 ± 4.736 N=134
Difference between means	11.28 ± 7.376
95% confidence interval	-3.266 to 25.83
R square	0.01173

3.1.2.5 – Golgi complex morphology is not affected in other NCLs, CLN2.

Column B vs. Column A	CLN5 vs. Control
Unpaired t test	
P value	0.1030
P value summary	ns
Significantly different? (P < 0.05)	No
One- or two-tailed P value?	Two-tailed
t, df	t=1.634 df=486
How big is the difference?	
Mean ± SEM of column A	86.22 ± 3.695 N=64
Mean ± SEM of column B	79.65 ± 1.460 N=424
Difference between means	-6.570 ± 4.022
95% confidence interval	-14.47 to 1.333
R square	0.005460

3.1.2.5 – Golgi complex morphology is not affected in other NCLs, CLN5.

Column B vs. Column A	CLN6 vs. Control
Unpaired t test	
P value	0.0278
P value summary	*
Significantly different? (P < 0.05)	Yes
One- or two-tailed P value?	Two-tailed
t, df	t=2.210 df=306
How big is the difference?	
Mean ± SEM of column A	88.08 ± 4.084 N=65
Mean ± SEM of column B	106.5 ± 4.177 N=243
Difference between means	18.47 ± 8.355
95% confidence interval	2.025 to 34.91
R square	0.01571

3.1.2.5 – Golgi complex morphology is not affected in other NCLs, CLN6.

Column B vs. Column A	CLN7 vs. Control
Unpaired t test	
P value	0.8796
P value summary	ns
Significantly different? (P < 0.05)	No
One- or two-tailed P value?	Two-tailed
t, df	t=0.1516 df=356
How big is the difference?	
Mean ± SEM of column A	88.08 ± 4.084 N=65
Mean ± SEM of column B	87.26 ± 2.375 N=293
Difference between means	-0.8185 ± 5.399
95% confidence interval	-11.44 to 9.799
R square	6.455e-005

3.1.2.5 – Golgi complex morphology is not affected in other NCLs, CLN7.

Column B vs. Column A	CLN8 vs. Control
Unpaired t test	
P value	0.3875
P value summary	ns
Significantly different? (P < 0.05)	No
One- or two-tailed P value?	Two-tailed
t, df	t=0.8652 df=346
How big is the difference?	
Mean ± SEM of column A	86.22 ± 3.695 N=64
Mean ± SEM of column B	90.09 ± 1.952 N=284
Difference between means	3.869 ± 4.472
95% confidence interval	-4.926 to 12.66
R square	0.002159

3.1.2.5 – Golgi complex morphology is not affected in other NCLs, CLN8.

Appendix B

Sidak's multiple comparisons test	Mean Diff.	95% CI of diff.	Significant ?	Summary
Mock				
0h vs. 1h	0.3500	0.2310 to 0.4690	Yes	***
0h vs. 8h	0.4650	0.3460 to 0.5840	Yes	****
siRNA CLN3				
0h vs. 1h	0.08500	-0.03397 to 0.2040	No	ns
0h vs. 8h	0.0900	-0.02897 to 0.2090	No	ns

Sidak's multiple comparisons test	Mean Diff.	95% CI of diff.	Significant ?	Summary
Mock - siRNA CLN3				
0h	0.05000	-0.08163 to 0.1816	No	ns
1h	-0.2150	-0.3466 to -0.08337	Yes	**
8h	-0.3250	-0.4566 to -0.1934	Yes	***

4.1.1.3 –CLN3 depletion affect GPP130 degradation Panel A, graph ii.

Sidak's multiple comparisons test	Mean Diff.	95% CI of diff.	Significant?	Summary
Mock				
0h vs. 1h	1.110	0.1672 to 2.053	Yes	*
0h vs. 8h	2.670	1.727 to 3.613	Yes	***
1h vs. 8h	1.560	0.6172 to 2.503	Yes	**
siRNA CLN3				
0h vs. 1h	1.150	0.2072 to 2.093	Yes	*
0h vs. 8h	1.610	0.6672 to 2.553	Yes	**
1h vs. 8h	0.4600	-0.4828 to 1.403	No	ns

4.1.1.3 - CLN3 depletion affect GPP130 degradation. Panel A, graph iii.

Sidak's multiple comparisons test	Mean Diff.	95% CI of diff.	Significant?	Summary
Mock - siRNA CLN3				
0h	1.870	0.9272 to 2.813	Yes	**
1h	1.910	0.9672 to 2.853	Yes	**
8h	0.8100	-0.1328 to 1.753	No	ns

4.1.1.3 - CLN3 depletion affect GPP130 degradation Panel A, graph iii.

Sidak's multiple comparisons test	Mean Diff.	95% CI of diff.	Significant?	Summary
Mock - siRNA CLN3				
0h to 1h Mn^{2+}	-0.8700	-2.678 to 0.9384	No	ns
1h to 8h Mn^{2+}	0.1600	-1.648 to 1.968	No	ns
0h to 8h Mn^{2+}	-1.600	-3.408 to 0.2084	No	ns

4.1.1.3 - CLN3 depletion affect GPP130 degradation Panel A, graph iii'.

Column B vs. Column A	**siRNA CLN3 vs. Mock**
Unpaired t test	
P value	0.0005
P value summary	***
Significantly different? (P < 0.05)	Yes
One- or two-tailed P value?	Two-tailed
t, df	t=4.990 df=10
How big is the difference?	
Mean ± SEM of column A	0.04667 ± 0.003639 N=6
Mean ± SEM of column B	0.01867 ± 0.004271 N=6
Difference between means	-0.0280 ± 0.005611
95% confidence interval	-0.04050 to -0.01550
R square	0.7134

4.1.1.3 - CLN3 depletion affect GPP130 degradation Panel B

Sidak's multiple comparisons test	Mean Diff.	95% CI of diff.	Significant?	Summary
Control				
0h vs. 1h	0.2600	0.09003 to 0.4300	Yes	**
0h vs. 8h	0.5000	0.3300 to 0.6700	Yes	***
Patient 1kb				
0h vs. 1h	0.6700	0.5000 to 0.8400	Yes	****
0h vs. 8h	1.040	0.8700 to 1.210	Yes	****

4.1.1.4 - CLN3 1-kb deletion affect GPP130 degradation. Panel A, graph ii

Sidak's multiple comparisons test	Mean Diff.	95% CI of diff.	Significant?	Summary
0h to 1h Mn^{2+} vs. 1h to 8h Mn^{2+}	-1.025	-2.387 to 0.3367	No	ns
0h to 1h Mn^{2+} vs. 0h to 8h Mn^{2+}	-2.775	-4.137 to -1.413	No	ns
1h to 8h Mn^{2+} vs. 0h to 8h Mn^{2+}	-1.750	-4.473 to 0.9734	No	ns

4.1.1.4 - CLN3 1-kb deletion affect GPP130 degradation. Panel A, graph iii

Column B vs. Column A	1kb Patients vs. Control
Unpaired t test	
P value	0.3806
P value summary	ns
Significantly different? (P < 0.05)	No
One- or two-tailed P value?	Two-tailed
t, df	t=0.9173 df=10
How big is the difference?	
Mean ± SEM of column A	0.0320 ± 0.007461 N=6
Mean ± SEM of column B	0.0245 ± 0.003344 N=6
Difference between means	-0.0075 ± 0.008176
95% confidence interval	-0.02572 to 0.01072
R square	0.07761

4.1.1.4 - CLN3 1-kb deletion affect GPP130 degradation Panel B

Appendix C

Column B vs. **Column A**	**1kb patients** vs. **Control**
Unpaired t test	
P value	< 0.0001
P value summary	****
Significantly different? (P < 0.05)	Yes
One- or two-tailed P value?	Two-tailed
t, df	t=5.439 df=168
How big is the difference?	
Mean ± SEM of column A	0.002212 ± 0.0003283 N=47
Mean ± SEM of column B	0.006803 ± 0.0005057 N=123
Difference between means	0.004591 ± 0.0008441
95% confidence interval	0.002925 to 0.006258
R square	0.1497

5.1.1.1 - ER membrane expansion in 1-kb and CLN6 patient fibroblast cell lines, panel B, graph i.

Column B vs. **Column A**	**CLN6** vs. **Control**
Unpaired t test	
P value	< 0.0001
P value summary	****
Significantly different? (P < 0.05)	Yes
One- or two-tailed P value?	Two-tailed
t, df	t=8.325 df=92
How big is the difference?	
Mean ± SEM of column A	0.002212 ± 0.0003283 N=47
Mean ± SEM of column B	0.006064 ± 0.0003261 N=47
Difference between means	0.003852 ± 0.0004627
95% confidence interval	0.002933 to 0.004771
R square	0.4296

5.1.1.1 - ER membrane expansion in 1kb and CLN6 patient fibroblast cell lines, panel B, graph ii.

Tukey's multiple comparisons test	Mean Diff.	95% CI of diff.	Significant ?	Summary
Mock				
0h vs. 1h	0.0	-0.06509 to 0.06509	No	ns
0h vs. 8h	-0.1500	-0.2151 to -0.08491	Yes	***
1h vs. 8h	-0.1500	-0.2151 to -0.08491	Yes	***
siRNA CLN3				
0h vs. 1h	-0.4000	-0.4651 to -0.3349	Yes	****
0h vs. 8h	-1.070	-1.135 to -1.005	Yes	****
1h vs. 8h	-0.6700	-0.7351 to -0.6049	Yes	****

Sidak's multiple comparisons test	Mean Diff.	95% CI of diff.	Significant ?	Summary
Mock - siRNA CLN3				
0h	-0.2300	-0.2994 to -0.1606	Yes	***
1h	-0.6300	-0.6994 to -0.5606	Yes	****
8h	-1.150	-1.219 to -1.081	Yes	****

5.1.1.2 - CLN3 depletion triggers the ER stress with increase of GRP78/Bip levels, graph B.

Tukey's multiple comparisons test	Mean Diff.	95% CI of diff.	Significant ?	Summary
$+Mn^{2+}$				
0h vs. 1h	0.06000	-0.4929 to 0.6129	No	ns
0h vs. 8h	0.01000	-0.5429 to 0.5629	No	ns
0h vs. 0h	0.005000	-0.5479 to 0.5579	No	ns
0h vs. 1h	-1.255	-1.808 to -0.7021	Yes	****
0h vs. 8h	-1.455	-2.008 to -0.9021	Yes	****
1h vs. 8h	-0.05000	-0.6029 to 0.5029	No	ns
1h vs. 0h	-0.05500	-0.6079 to 0.4979	No	ns
1h vs. 1h	-1.315	-1.868 to -0.7621	Yes	****
1h vs. 8h	-1.515	-2.068 to -0.9621	Yes	****

8h vs. 0h	-0.005000	-0.5579 to 0.5479	No	ns
8h vs. 1h	-1.265	-1.818 to -0.7121	Yes	****
8h vs. 8h	-1.465	-2.018 to -0.9121	Yes	****
0h vs. 1h	-1.260	-1.813 to -0.7071	Yes	****
0h vs. 8h	-1.460	-2.013 to -0.9071	Yes	****
1h vs. 8h	-0.2000	-0.7529 to 0.3529	No	ns
-Mn^{2+}				
0h vs. 1h	0.1250	-0.4279 to 0.6779	No	ns
0h vs. 8h	-0.01500	-0.5679 to 0.5379	No	ns
0h vs. 0h	0.1850	-0.3679 to 0.7379	No	ns
0h vs. 1h	-0.2100	-0.7629 to 0.3429	No	ns
0h vs. 8h	-1.760	-2.313 to -1.207	Yes	****
1h vs. 8h	-0.1400	-0.6929 to 0.4129	No	ns
1h vs. 0h	0.06000	-0.4929 to 0.6129	No	ns
1h vs. 1h	-0.3350	-0.8879 to 0.2179	No	ns
1h vs. 8h	-1.885	-2.438 to -1.332	Yes	****
8h vs. 0h	0.2000	-0.3529 to 0.7529	No	ns
8h vs. 1h	-0.1950	-0.7479 to 0.3579	No	ns
8h vs. 8h	-1.745	-2.298 to -1.192	Yes	****
0h vs. 1h	-0.3950	-0.9479 to 0.1579	No	ns
0h vs. 8h	-1.945	-2.498 to -1.392	Yes	****
1h vs. 8h	-1.550	-2.103 to -0.9971	Yes	****

Test details	Mean 1	Mean 2	Mean Diff.	SE of diff.
+Mn^{2+}				
0h vs. 1h	0.6450	0.5850	0.06000	0.1646
0h vs. 8h	0.6450	0.6350	0.01000	0.1646
0h vs. 0h	0.6450	0.6400	0.005000	0.1646
0h vs. 1h	0.6450	1.900	-1.255	0.1646
0h vs. 8h	0.6450	2.100	-1.455	0.1646
1h vs. 8h	0.5850	0.6350	-0.05000	0.1646
1h vs. 0h	0.5850	0.6400	-0.05500	0.1646
1h vs. 1h	0.5850	1.900	-1.315	0.1646
1h vs. 8h	0.5850	2.100	-1.515	0.1646
8h vs. 0h	0.6350	0.6400	-0.005000	0.1646
8h vs. 1h	0.6350	1.900	-1.265	0.1646

8h vs. 8h	0.6350	2.100	-1.465	0.1646
0h vs. 1h	0.6400	1.900	-1.260	0.1646
0h vs. 8h	0.6400	2.100	-1.460	0.1646
1h vs. 8h	1.900	2.100	-0.2000	0.1646
-Mn^{2+}				
0h vs. 1h	0.6250	0.5000	0.1250	0.1646
0h vs. 8h	0.6250	0.6400	-0.01500	0.1646
0h vs. 0h	0.6250	0.4400	0.1850	0.1646
0h vs. 1h	0.6250	0.8350	-0.2100	0.1646
0h vs. 8h	0.6250	2.385	-1.760	0.1646
1h vs. 8h	0.5000	0.6400	-0.1400	0.1646
1h vs. 0h	0.5000	0.4400	0.06000	0.1646
1h vs. 1h	0.5000	0.8350	-0.3350	0.1646
1h vs. 8h	0.5000	2.385	-1.885	0.1646
8h vs. 0h	0.6400	0.4400	0.2000	0.1646
8h vs. 1h	0.6400	0.8350	-0.1950	0.1646
8h vs. 8h	0.6400	2.385	-1.745	0.1646
0h vs. 1h	0.4400	0.8350	-0.3950	0.1646
0h vs. 8h	0.4400	2.385	-1.945	0.1646
1h vs. 8h	0.8350	2.385	-1.550	0.1646

5.1.1.3 - CLN3 depletion enhances CHOP/GADD153 levels, graph B.

Sidak's multiple comparisons test	**Mean Diff.**	**95% CI of diff.**	**Significant ?**	**Summary**
Mock +Mn2+				
0 vs. 1	0.06000	-0.6467 to 0.7667	No	ns
0 vs. 8	0.01000	-0.6967 to 0.7167	No	ns
1 vs. 8	-0.05000	-0.7567 to 0.6567	No	ns
siRNA CLN3 +Mn2+				
0 vs. 1	-1.260	-1.967 to -0.5533	Yes	**
0 vs. 8	-1.460	-2.167 to -0.7533	Yes	**
1 vs. 8	-0.2000	-0.9067 to 0.5067	No	ns
Test details	Mean 1	Mean 2	Mean Diff.	SE of diff.
Mock +Mn2+				
0 vs. 1	0.6450	0.5850	0.06000	0.2159
0 vs. 8	0.6450	0.6350	0.01000	0.2159
1 vs. 8	0.5850	0.6350	-0.05000	0.2159
siRNA CLN3 +Mn2+				
0 vs. 1	0.6400	1.900	-1.260	0.2159
0 vs. 8	0.6400	2.100	-1.460	0.2159

1 vs. 8	1.900	2.100	-0.2000	0.2159

5.1.1.3 - CLN3 depletion enhances CHOP/GADD153 levels, graph B

Tukey's multiple comparisons test	Mean Diff.	95% CI of diff.	Significant?	Summary
Mock -Mn2+				
0 vs. 1	0.1250	-0.1423 to 0.3923	No	ns
0 vs. 8	-0.01500	-0.2823 to 0.2523	No	ns
1 vs. 8	-0.1400	-0.4073 to 0.1273	No	ns
siRNA CLN3 -Mn2+				
0 vs. 1	-0.3950	-0.6623 to -0.1277	Yes	**
0 vs. 8	-1.945	-2.212 to -1.678	Yes	****
1 vs. 8	-1.550	-1.817 to -1.283	Yes	****

5.1.1.3 - CLN3 depletion enhances CHOP/GADD153 levels graph B

Sidak's multiple comparisons test	Mean Diff.	95% CI of diff.	Significant?	Summary
siRNA CLN3 +Mn2+ - siRNA CLN3-Mn2+				
0	0.2000	-0.5414 to 0.9414	No	ns
1	1.065	0.3236 to 1.806	Yes	**
8	-0.2850	-1.026 to 0.4564	No	ns

5.1.1.3 - CLN3 depletion enhances CHOP/GADD153 levels, graph B

Tukey's multiple comparisons test	Mean Diff.	95% CI of diff.	Significant?	Summary
Control				
0h vs. 1h	-0.0760	-1.270 to 1.118	No	ns
0h vs. 8h	-3.045	-4.239 to -1.851	Yes	***
1h vs. 8h	-2.969	-4.163 to -1.775	Yes	***
1kb Patients				
0h vs. 1h	-1.728	-2.921 to -0.5339	Yes	*
0h vs. 8h	-2.208	-3.401 to -1.014	Yes	**
1h vs. 8h	-0.4800	-1.674 to 0.7136	No	ns

5.1.1.4 – 1-kb CLN3 fibroblast are less resistant to ER stress, graph B.

Sidak's multiple comparisons test	Mean Diff.	95% CI of diff.	Significant ?	Summary
Control - 1kb Patients				
0h	-0.0025	-1.276 to 1.271	No	ns
1h	-1.654	-2.928 to -0.3804	Yes	*
8h	0.8350	-0.4386 to 2.109	No	ns

5.1.1.4 – 1kb CLN3 fibroblast are less resistant to ER stress, Graph B

Sidak's multiple comparisons test	Mean Diff.	95% CI of diff.	Significant ?	Summary
Mock				
0h vs. 1h	0.0	-0.1637 to 0.1637	No	ns
0h vs. 8h	0.0	-0.1637 to 0.1637	No	ns
1h vs. 8h	0.0	-0.1637 to 0.1637	No	ns
siRNA CLN3				
0h vs. 1h	-0.3300	-0.4937 to -0.1663	Yes	**
0h vs. 8h	-2.570	-2.734 to -2.406	Yes	****
1h vs. 8h	-2.240	-2.404 to -2.076	Yes	****

Sidak's multiple comparisons test	Mean Diff.	95% CI of diff.	Significant ?	Summary
Mock - siRNA CLN3				
0h	-0.7700	-0.9337 to -0.6063	Yes	****
1h	-1.100	-1.264 to -0.9363	Yes	****
8h	-3.340	-3.504 to -3.176	Yes	****

5.1.2.1 - CLN3 depletion causes activation of caspase 2, graph B

Appendix D

Column B	**Δ*btn1* MM**
vs.	**vs.**
Column A	***btn1*wt MM**
Unpaired t test	
P value	0.0004
P value summary	***
Significantly different? (P < 0.05)	Yes
One- or two-tailed P value?	Two-tailed
t, df	t=3.752 df=52
How big is the difference?	
Mean ± SEM of column A	0.004486 ± 0.0003775 N=22
Mean ± SEM of column B	0.009555 ± 0.001087 N=32
Difference between means	0.005069 ± 0.001351
95% confidence interval	0.002358 to 0.007780
R square	0.2130

6.1.1.1 – *btn1*Δ exhibits changes in GA morphology

Column B	**Δ*btn1* MM**
vs.	**vs.**
Column A	***btn1*wt MM**
Unpaired t test	
P value	0.0009
P value summary	***
Significantly different? (P < 0.05)	Yes
One- or two-tailed P value?	Two-tailed
t, df	t=4.070 df=16
How big is the difference?	
Mean ± SEM of column A	0.004895 ± 0.0008157 N=10
Mean ± SEM of column B	0.03367 ± 0.007902 N=8
Difference between means	0.02878 ± 0.007072
95% confidence interval	0.01379 to 0.04377
R square	0.5086

6.1.2.1 – ER volume expansion in fission yeast

Appendix E

Dunnett's multiple comparisons test	Mean Diff.	95% CI of diff.	Significant?	Summary
0 uM A vs. 5 uM A	0.005721	-0.02791 to 0.03935	No	ns
0 uM A vs. 10 uM A	0.01052	-0.02235 to 0.04338	No	ns
0 uM A vs. 20 uM A	-0.02709	-0.05880 to 0.004627	No	ns

7.1.1.1 - Effect of alloxazine, E64 and prochlorperazine dimaleate on Golgi complex compactness of 1-kb patient fibroblast cell lines (Graph **A**).

Dunnett's multiple comparisons test	Mean Diff.	95% CI of diff.	Significant?	Summary
0 uM E vs. 5 uM E	0.005665	-0.03387 to 0.04520	No	ns
0 uM E vs. 10 uM E	-0.03182	-0.07306 to 0.009428	No	ns
0 uM E vs. 20 uM E	-0.007294	-0.04409 to 0.02951	No	ns

7.1.1.1 - Effect of alloxazine, E64 and prochlorperazine dimaleate on Golgi complex compactness of 1-kb patient fibroblast cell lines (Graph **B**).

Dunnett's multiple comparisons test	Mean Diff.	95% CI of diff.	Significant?	
0 uM P vs. 5 uM P	0.001197	-0.05404 to 0.05643	No	ns
0 uM P vs. 10 uM P	-0.05238	-0.1052 to 0.0004441	No	ns

7.1.1.1 - Effect of alloxazine, E64 and prochlorperazine dimaleate on Golgi complex compactness of 1-kb patient fibroblast cell lines (Graph **C**).

Dunnett's multiple comparisons test	Mean Diff.	95% CI of diff.	Significant?	Summary
0uM vs. 5uM	-0.01774	-0.03357 to -0.001904	Yes	*
0uM vs. 10uM	-0.005723	-0.02020 to 0.008751	No	ns
0uM vs. 20uM	0.003571	-0.01226 to 0.01940	No	ns

7.1.1.1 - Effect of alloxazine, E64 and prochlorperazine dimaleate on Golgi complex compactness of 1-kb patient fibroblast cell lines (Graph **D**).

Dunnett's multiple comparisons test	Mean Diff.	95% CI of diff.	Significant ?	Summary
0uM vs. 5uM	-0.05753	-0.08916 to -0.02590	Yes	****
0uM vs. 10uM	-0.06238	-0.09541 to -0.02936	Yes	****
0uM vs. 20uM	-0.07865	-0.1095 to -0.04776	Yes	****

7.1.1.1 - Effect of alloxazine, E64 and prochlorperazine dimaleate on Golgi complex compactness of 1-kb patient fibroblast cell lines (Graph **E**)

Dunnett's multiple comparisons test	Mean Diff.	95% CI of diff.	Significant ?	Summary
0uM vs. 5uM	-0.06404	-0.09293 to -0.03516	Yes	****
0uM vs. 10uM	-0.05334	-0.08295 to -0.02372	Yes	***

7.1.1.1 - Effect of alloxazine, E64 and prochlorperazine dimaleate on Golgi complex compactness of 1-kb patient fibroblast cell lines (Graph **F**)

Dunnett's multiple comparisons test	Mean Diff.	95% CI of diff.	Significant ?	Summary
WT / DMSO vs. CLN3 1kb / DMSO	0.07139	0.04390 to 0.09888	Yes	****
WT / DMSO vs. CLN3 1kb / A	0.05499	0.02212 to 0.08786	Yes	***
WT / DMSO vs. CLN3 1kb / E64	-0.008181	-0.03585 to 0.01949	No	ns
WT / DMSO vs. CLN3 1kb / P	0.005206	-0.04323 to 0.05364	No	ns

7.1.1.2 – Rescue of the Golgi complex compactness in 1-kb patient fibroblast

Acknowledgements

I would like to thank my supervisor Sara Mole for her help and guidance during this project. I am grateful to all members of the Mole group, Mike, Mariana, Sophia and Rachel for their help and moral support.

This work was made possible by funding from the NCL Stiftung and Batten Disease Family Association (BDFA).

I would like to thank my friends, especially Blerida, Andrea and Cristina. Moreover, I would like to thank Jacob, the best desk mate. They made my time at the LMCB special and unforgettable.

Finally, I am forever grateful to my parents and Gi for his immense and special support. I dedicate this thesis to my beloved mum**.**